

PDE–Based Modelling and Control Strategies for Manufacturing Processes

Dissertation

zur Erlangung des akademischen Grades
Doktor der Ingenieurwissenschaften
(Dr.-Ing.)
der Technischen Fakultät
der Christian-Albrechts-Universität zu Kiel

Vorgelegt von

Khaled Adel Ali Ali Othman

geboren in Kiel

Kiel 2022

Erstgutachter: Prof. Dr.-Ing. Thomas Meurer
Zweitgutachter: Prof. Dr.-Ing. Boris Lohmann
Prüfungsdatum: 29.08.2022

Erklärung

Ich versichere, dass ich die Dissertation

PDE–Based Modelling and Control Strategies for Manufacturing Processes

selbständig und ohne unzulässige fremde Hilfe angefertigt habe und dass ich alle von anderen Autoren wörtlich übernommenen Stellen, wie auch die sich an die Gedankengänge anderer Autoren eng anlehrenden Ausführungen, meiner Arbeit besonders gekennzeichnet und die entsprechenden Quellen angegeben habe.

Mir ist bekannt, dass die unter Anleitung entstandene Dissertation, vorbehaltlich anders lautender Vereinbarungen, eine Gruppenleistung darstellt und in die Gesamtforschung der betreuenden Institution eingebunden ist. Daher darf keiner der Miturheber (z.B. Texturheber, gestaltender Projektmitarbeiter, mitwirkender Betreuer) ohne (schriftliches) Einverständnis aller Beteiligten, aufgrund ihrer Urheberrechte, auch Passagen der Arbeit weder kommerziell nutzen noch Dritten zugänglich machen. Insbesondere ist das Arbeitnehmererfindergesetz zu berücksichtigen, in dem eine Vorveröffentlichung patentrelevanter Inhalte verboten wird.

Die Arbeit ist entstanden unter Einhaltung der Regeln guter wissenschaftlicher Praxis der Deutschen Forschungsgemeinschaft.

Kiel, 20.06.2022

Khaled Adel Ali Ali Othman

Acknowledgement

All praise is due to Almighty God for his guidance and for helping me to bring forth the present study.

First and foremost, I would like to express my sincere appreciation and thanks to my supervisor Prof. Dr.-Ing. Thomas Meurer for his instant guidance and kind supervision at the highest standards during my study. His advice, discussions, and critical comments have shaped this thesis and significantly improved my research and academic skills. I am very thankful for his patience, motivation, enthusiasm and immense knowledge and I considered myself lucky to work under his supervision.

I would like to express my sincere appreciation to the Egyptian Ministry of Higher Education (Cultural Affairs and Missions Sector) in the Arab Republic of Egypt and the Egyptian culture office in Berlin for the financial support and the encouragement for letting my dream come true.

I would like to describe my special thank to PD Dr. Alexander Schaum for providing the encouragement I needed and for his valuable comments and discussions along my journey. I would like to express my thank to Dr. Petro Feketa for always taking the time to meet and for providing useful information during the math discussion.

I also would like to thank the formers and the entire group of the Chair of Automation and Control, especially my colleagues M.Sc. Pascal Jerono, M.Sc. Manuel Amersdorfer, M.Sc. Simon Helling, M.Sc. Folke Rolf, M.Sc. Henry Baumann and M.Sc. Marcel Jiokeng. Many new ideas emerged during our productive discussions, particularly during coffee breaks and lunchtime.

Special thanks to the all staff of Tebbin Institute for Metallurgical Studies and, in particular, the director of the Institute Prof. Dr Taha Mattar. My thanks should go to my colleagues in the Department of Electrical Engineering at the Tebbin Institute for Metallurgical Studies, especially Prof. Dr Samir El-Bardissi, who, although no longer with us, the former chairman of the department, for his help and encouragement. Furthermore, special thanks to Prof. Dr. Yusry F. Barakat, Prof. Dr. Tarek M. Sami, Prof. Dr. Fathy Toughan, Dr Fayrouz Abd-El

Rahman, Dr Marwa Taher and Dr. Abdelrhman Hassan for their support and help. Special thanks to Dr Ayman Hagra, Dr Ayman Farid, Dr Saad Gomma, and Mr Mohamed Mahmoud.

I would like to express my gratitude to my friend Dr. Abdullah Yaqot for his valuable advice, open support, sincere help, and encouragement during my PhD work.

I would like to express my sincere thanks to Dr Mohamed Sobh Emam, Dr. Moheb Abdelaziz, M.Sc. Mostafa Bakry, M.Sc. Rasool Al-Mafrachi, and M.Sc. Ayman Soukieh for their help and encouragement throughout my PhD journey. Moreover, I would like to provide a special appreciation to my friend Mr. Sherif Yehia for his encouragement and support.

Last but not least, I wish to crown my sincere thanks and deepest gratitude to my parents, my brothers. In addition, my wife and my children Razan, Salma and Mohamed for their prayers, continuous encouragement, true help, for being so understanding and putting up with me, patience and support through this tough journey. This thesis is dedicated to them.

Für meine Eltern und meine Kinder

Contents

List of Symbols	X
List of Figures	XII
Abstract	XV
German summary / Deutsche Kurzfassung	XVI
1 Introduction	1
1.1 Goals of the thesis	5
1.2 Structure of the thesis	5
2 Theoretical Background of Manufacturing systems	6
2.1 Conservation of Mass	6
2.2 Little's law in Production Processes	7
2.3 Example on DES-PDE correlation	8
2.4 Summary	13
3 Modelling of Manufacturing systems	14
3.1 Single Flow Line Model	14
3.2 Validation of the PDE Model	20
3.2.1 Validation for Ramp-up Scenario	20
3.2.2 Validation of Ramp-up-down Scenario	23
3.3 Manufacturing System Networks	25
3.3.1 Dispersing Network Design:	25
3.3.2 Merging Network Design:	27
3.4 Summary	31

4	Direct and Indirect Approaches for Optimal Control	32
4.1	General Overview	32
4.2	Background	33
4.3	Demand Tracking Problem	34
4.3.1	Indirect Method	36
4.3.1.1	Discretization Approach for the Numerical Solution	40
4.3.2	Direct Method	42
4.4	Backlog Problem	43
4.4.1	Indirect Method	43
4.4.2	Direct Method	49
4.5	Simulation Results	50
4.5.1	Demand Tracking Problem	50
4.5.1.1	Dispersing Network	50
4.5.1.2	Merging Network	51
4.5.2	Backlog Problem	51
4.5.2.1	Dispersing Network	52
4.5.2.2	Merging Network	53
4.6	Summary	54
5	Model Predictive Control of a Manufacturing Network	55
5.1	Problem Statement	55
5.2	Model Predictive Control	58
5.3	Problems Formulation	59
5.4	Adjoint-based MPC	60
5.4.1	Optimization Phase	61
5.4.2	Discretization Phase	69
5.5	Simulation Results	71
5.5.1	Selection of Prediction Horizon	72
5.5.2	Performance Analysis of AMPC	73
5.6	Summary	76
6	Conclusions and Outlook	78
A	Solving the Single Flow PDE Model	80

B Derivation of OCPs of a Single Flow Line in the Case of the Indirect Method	81
B.1 Demand Tracking Problem:	81
B.2 Backlog Problem:	82
C Derivation of Distribution Models	85
C.1 M/D/1 Model	86
C.2 G/G/1 Model	87
Bibliography	89

List of Symbols

The following list only contains symbols that are used continuously throughout the text. Local symbols are not listed.

Variables

$U(m, t)$	Newell-Curves
$H(t)$	Heaviside step function
$WIP(m, t)$	work in process
$TW(t)$	total work in process
$F(m, t)$	discrete flux or flow in space
$f(x, t)$	continuous flux or flow
$\Psi(t)$	arbitrary smooth test function
$\rho(x, t)$	density of lots
$v(x, t)$	velocity function
$u(t)$	inflow or influx at the inlet of the system
$y(t)$	outflow or outflux at the outlet of the system
$\zeta(x, t)$	arbitrary function
$\varphi(t)$	flow time
$q_v(t)$	buffer load or storage area
$A_v(t)$	fraction function
$B(t)$	backlog function
$\lambda(x, t)$	adjoint state or Lagrange multiplier for the constraints induced by the PDEs
$\phi(x, t)$	adjoint state or Lagrange multiplier for the constraints induced by the ODEs

$\delta_u J(t)$	variational derivative with respect to input u
$\delta_{A_v} J(t)$	variational derivative with respect to fraction function A_v

Scalars

μ	process rate of a machine
T	process time of a machine
M	number of workstations or machines
Γ	machine utilization
C_a^2	coefficient of variation for inter-arrival time
C_p^2	coefficient of variation for process time
CFL	Courant-Friedrichs-Lewy number
a	speed of arbitrary function
P	prediction horizon
C	control horizon

Abbreviations

BC	boundary condition
IBVP	initial-boundary-value problem
MPC	model predictive control
AMPC	adjoint-based model predictive control
DPS	distributed parameter system
OCP	optimal control problem
IC	initial condition
KKT	Karush-Kuhn-Tucker
DES	discrete event system
MOC	method of characteristics
FD	finite difference
ODE	ordinary differential equation

PDE	partial differential equation
DOC	degree of completion
FCFO	first come first out
SQP	sequential quadratic programming
M/M/1	inter-arrival time and process time are exponentially distributed
M/D/1	inter-arrival time is exponentially distributed and process time is deterministic distributed
G/G/1	inter-arrival time and process time are generally distributed

List of Figures

2.1	Mass flux across a surface S with control volume V	7
2.2	Little's law for a pipeline manufacturing system.	8
2.3	Construction of simple workstation.	9
2.4	Production line with lot n moving through the system.	9
3.1	Ramp-up simulation, $u = 1$ lots/h with $n_x = 11$	17
3.2	Density over space and time for ramp-up, $u = 1$ lots/h with $n_x = 11$	17
3.3	Ramp-up simulation for total WIP, flow time, throughput, and density where $u = 1.5$ lots/h with $n_x = 11$	18
3.4	Density over space and time for ramp-up, $u = 1.5$ lots/h with $n_x = 11$	18
3.5	Ramp-down simulation, u from 1 lots/h to 0.5 lots/h, $n_x = 11$	19
3.6	Density over space and time for ramp-down, from $u = 1$ lots/h to $u = 0.5$ lots/h with $n_x = 11$	20
3.7	Outflow, flow time and total work in process with $M = 10$, $u = 0.5$ lots/h, $\mu = 2$ lots/h and $\Gamma = 25\%$	21
3.8	Outflow, flow time and total work in process with $M = 10$, $u = 1$ lots/h, $\mu = 2$ lots/h and $\Gamma = 50\%$	22
3.9	Outflow, flow time and total work in process with $M = 10$, $u = 1.5$ lots/h, $\mu = 2$ lots/h and $\Gamma = 75\%$	23
3.10	Outflow, flow time and total work in process with $M = 10$, from $u = 1.5$ lots/h to $u = 0.5$ lots/h, $\mu = 2$ lots/h and $\Gamma = 25\%$	24
3.11	Outflow, flow time and total work in process with $M = 10$, from $u = 1.5$ lots/h to $u = 1$ lots/h, $\mu = 2$ lots/h and $\Gamma = 50\%$	25
3.12	Configuration of dispersing network.	26
3.13	In the top, the flow goes through from area e_1 to area e_2 . In the bottom, the flow direction from area e_1 to area e_3	28
3.14	The flow state in each flow line e_1 , e_2 and e_3	28

3.15	Configuration of merging network.	29
3.16	In the top, the flow evolution path from area e_1 to area e_3 . In the bottom, the flow evolution path from area e_2 to area e_3	30
3.17	The flow state in each flow line e_1 , e_2 and e_3	30
4.1	Input $u^*(t)$ (left) and comparison of the desired demand trajectory $f^*(t)$ and $y(t) = f^{e_3}(1, t)$ (right) in case of direct and indirect method.	50
4.2	Direct and indirect approaches used for demand tracking in the merging network.	51
4.3	Inflows in the dispersing network for the backlog problem (top-left), outflows (top-right), $A_v^{e_3^*}(t)$ (bottom-left) and $B(t)$ (bottom-right).	52
4.4	Inflows at arc e_1 in merging network for the backlog problem (top-left), the inflow at arc e_2 (top-right), the fraction $A_v^*(t)$ (bottom-left) and the outflows (bottom-right).	53
4.5	Backlog $B(t)$ of the merging network.	53
5.1	The structure of the complex network.	56
5.2	MPC and the receding horizon mechanism.	58
5.3	Scheme of the AMPC framework.	60
5.4	AMPC performance for different prediction horizons.	72
5.5	The complex network for the demand tracking problem using both AMPC and traditional MPC.	74
5.6	The complex network for the demand tracking problem with disturbance.	74
5.7	The complex network for the backlog problem using MPC.	76
5.8	The complex network for the backlog problem with disturbance.	76

Abstract

Manufacturing or production systems, respectively, might become enormously complex involving a large number of objects, hundreds of processing stages, and many types of machinery showing stochastic behaviour. The application of existing mathematical modelling methodologies to control production processes is complicated due to this complexity. There are many ways for production optimization, but production control is one of the most important components that allows decision-makers to get closer to the efficiency threshold.

Partial differential equations models are computationally feasible and express the whole behaviour of the dynamic system. Therefore, a continuum model based on first-order hyperbolic partial differential equations coupled with ordinary differential equations is addressed to represent a network of production systems. Different interconnection topologies that correspond to dispersing and merging networks are used to model the system network. Boundary optimal control strategies for PDE constrained optimization are employed to solve demand tracking and backlog control problems. The control strategies are based on discretize-then-optimize and optimize-then-discretize mechanisms.

Furthermore, an extensive investigation of a novel approach from late lumping using an adjoint method combined with model predictive control is derived to find the adjoint equations in the case of a complex network. These equations are used to obtain the gradient information of the cost functional as a powerful tool to handle the constraint optimization problems by evaluating the necessary optimality conditions. Besides, the model predictive control can tackle the control problems by suppressing disturbances with an appropriate prediction horizon.

In summary, the numerical results show that the control strategies are capable to solve the control problems with satisfactory results. The results analysis reveals distinct characteristics for each strategy. High precision and low computational load characterize the indirect method of the optimal control. The direct approach of the optimal control stands out for its simplicity and flexibility to any problem. Finally, the traditional MPC is characterised by its robustness in terms of perturbation effects as well as the adjoint-based MPC. In addition the latter can significantly reduce the computational load compared to the traditional MPC.

Deutsche Kurzfassung

Fertigungs- bzw. Produktionssysteme können enorm komplex sein und eine große Anzahl von Objekten, Hunderte von Verarbeitungsstufen und viele Arten von Maschinen mit stochastischem Verhalten umfassen. Die Anwendung bestehender mathematischer Modellierungsmethoden zur Steuerung von Produktionsprozessen wird durch diese Komplexität erschwert. Es gibt viele Möglichkeiten der Produktionsoptimierung, aber die Produktionssteuerung ist eine der wichtigsten Komponenten, die es den Entscheidungsträgern ermöglicht, sich der Effizienzschwelle zu nähern.

Modelle mit partiellen Differentialgleichungen (pDGLn) sind rechnerisch machbar und drücken das gesamte Verhalten des dynamischen Systems aus. Daher wird ein Kontinuumsmodell auf der Grundlage hyperbolischer partieller Differentialgleichungen erster Ordnung, die mit gewöhnlichen Differentialgleichungen gekoppelt sind, zur Darstellung eines Netzwerks von Produktionsprozessen herangezogen. Zur Modellierung des Systemnetzwerks werden verschiedene Verbindungstopologien verwendet, die sich ausbreitenden und zusammenführenden Netzwerken entsprechen. Optimale Kontrollstrategien für die pDGL-beschränkte Optimierung werden eingesetzt, um Probleme der Nachfragesteuerung und der Rückstandskontrolle zu lösen. Die Kontrollstrategien basieren auf den Mechanismen „Diskretisieren-dann-Optimieren“ und „Optimieren-dann-Diskretisieren“.

Darüber hinaus wird eine adjungierte Methode in Kombination mit modellprädiktiver Regelung (MPC) abgeleitet und untersucht. Die adjungierten Gleichungen werden verwendet, um die Gradienteninformation des Kostenfunctionals als ein leistungsfähiges Werkzeug für die Behandlung von Optimierungsproblemen mit Einschränkungen zu erhalten, indem die erforderlichen Optimalitätsbedingungen bewertet werden. Außerdem kann die modellprädiktive Regelung die Produktionskontrolle durch Unterdrückung von Störungen mit einem geeigneten Vorhersagehorizont angehen.

Zusammenfassend zeigen die numerischen Ergebnisse, dass die Kontrollstrategien in der Lage sind, die Kontrollprobleme mit zufriedenstellenden Ergebnissen zu lösen. Die Analyse der Ergebnisse zeigt deutliche Merkmale für jede Strategie. Hohe Genauigkeit und geringer Rechenaufwand kennzeichnen die indirekte Methode der optimalen Steuerung. Der direkte Ansatz der optimalen Steuerung zeichnet sich durch seine Einfachheit und Flexibilität für jedes

Problem aus. Die traditionelle MPC schließlich zeichnet sich durch ihre Robustheit gegenüber Störeffekten aus, ebenso wie die adjungiertenbasierte MPC. Darüber hinaus kann letztere den Rechenaufwand im Vergleich zur traditionellen MPC erheblich reduzieren.

Chapter 1

Introduction

Manufacturing is vital for the economic sector. For the time being, manufacturing brings wealth to many countries. For this purpose, the development of the manufacturing industry has become one of the remarkable governmental plans. Developing and developed countries recognize these opportunities.

In recent years, providing superiority in the industrial field has demanded an efficient production flow. There are numerous strategies for production optimization, but one of the essential components that allow decision-makers to get closer to the efficiency threshold is production control. Production control is a procedure in manufacturing that involves monitoring a production operation and taking steps to control processes [9]. Demand planning, capacity planning, scheduling, work centre assignment, inventory control, costing, and shop floor monitoring, among other things, are all examples of this. The objective of developing an adequate production control system is to improve workflow consistency, which can save money and time [10]. Here are a few aspects and advantages of establishing production control:

- **Reducing Waste:** Project managers are typically faced with the task of reducing waste. The system may identify waste locations and create a strategy to reduce the amount of waste produced through production control. Production control can also account for downtime or maintenance, ensuring a consistent flow of output and removing any regions of lost productivity, see, e.g., [21, 28].
- **Capabilities for Making Decisions:** Accurate data and information enable the process to support optimal production scheduling and control decisions using an integrated system. Project managers benefit from these decision-making capabilities because of the better information in their supply chain and manufacturing process, see, e.g., [15, 71]
- **Cost Minimization:** One of, if not the most important, cost related to manufacturing operations is operating cost. Running the facility, hiring staff, and other elements are expensive, especially when production is not reaching its full potential. Production control can effectively lower costs by enhancing inefficient sections of the operation. The analysis of the main elements inside the process improves productivity, see, e.g., [67, 83, 79]

In the increasingly competitive global marketplace, effective production management is becoming crucial. As a result, enterprises are now focusing on improving production management and treating its evaluation as a strategic decision. There have been several reports that many enterprises have suffered significant losses as a result of production or supply chain issues. Problematic stories include the following:

- In early 1997, twenty Toyota factories were forced to shut down due to a shortage of brake fluid valves [47].
- Recently, many automotive industries worldwide have had to halt operations at their assembly plants due to a shortage of semiconductors. The main cause of these shortages was an unexpected spike in demand at automotive manufacturers that had recovered from the Covid-19 pandemic shock, at the time when they had shortened semiconductor orders due to lower demand for cars and trucks [51].

On the other hand, companies such as Dell Computers, Wal-Mart, and 7-Eleven Japan have regularly surpassed the competition because of their superior production control abilities. All these examples and many more show the importance of the effective production management. Decision-makers face a challenging problem in managing production systems. Therefore, incorporating appropriate control mechanisms to manage resources may lead to profit maximization.

For the modelling of manufacturing systems in general three main approaches are available for manufacturing systems: discrete event models, see, e.g., [61], fluid models, see, e.g., [82], and queuing models, see, e.g., [84]. Typically, discrete event models are stochastic models to describe the dynamics of manufacturing systems. However, the main drawback, as declared in [33], is that it is difficult to design a controller in case of a large or complex system that contains a large amount of information (states). Fluid models are flux oriented and are typically represented by ordinary differential equations (ODEs). The main shortcoming of fluid models is that these models do not express flow times which means that the flux can be produced using zero inventory [106]. Besides, these models are not suitable for modeling the complete dynamic behaviour (transient and steady state) of a manufacturing system. Queuing models show the connection between throughput and flow time only in steady-state which is not applicable for control theory.

At present, partial differential equations (PDEs) are considered one of the principal mathematical modeling elements of many technical processes. In general, the success story of PDE models entering domains of practical research is reinforced by vast progress, particularly in computational mathematics. Meurer [73] summarizes some of the most common PDE applications below:

- Chemical or biochemical reactors [52].

-
- Thermal systems [7] or the reheating and cooling of metal slabs during the steel processing to achieve desired metallurgical changes [101].
 - Electrochemical systems such as fuel cells [97] and Li-ion or Li-polymer battery devices for energy production and storage [40].
 - Smart materials and vibratory systems [86].
 - Flexible structures arising in aerospace and mechanical applications including novel adaptive or flapping wing structures [95].
 - Fluid dynamical systems [1, 13], mixing processes and coupled fluid-structure interactions;
 - Wave propagation in optical fibers [93] and traffic congestion [43].
 - Energy production in fusion reactors [3, 98].

Recently, partial differential equations (PDEs) have been utilized for modeling of manufacturing systems. The main idea comes from the continuum theory of highway traffic [64, 88]. Distributed parameter system (DPS) models based on PDEs have been employed for, e.g., fabrication of semiconductors [42], supply chain management [26] or additive manufacturing [56]. Unver et al. [102] applied diffusive PDE model using observer which achieved the data from discrete event system to improve the behaviour of the model. The PDE models for numerous recycled products in manufacturing systems are utilized [6], and these models are modified in [30]. Hence, adopting PDE models with a proper controller design to address new industrial applications remains a challenging research topic. The motivation for using PDE is to design a high-performance controller to handle infinite-dimensional systems where the lots are produced continuously on large-scale manufacturing systems. Also, PDE models are computationally feasible and express the complete behaviour of the dynamic system by incorporating the system characteristics of both throughputs and flow times. Therefore, PDE models are adopted in the present work.

In the field of manufacturing, control is an important issue, which appears at various operation levels. At the tool level, for example, control is necessary in order to assure a properly working tool that processes a product in the desired way, see, e.g. [38]. At an intermediate level, sequencing and scheduling rules are used to decide which of the products that are waiting in front of a machine, should be processed first, see, e.g. [34, 110]. At the top level of a manufacturing system, the input of the system and the flow of the products through the system are controlled in order to satisfy the customer demands, see, e.g. [41]. Modern control designs have started with push and pull strategies like enterprise resource planning, just-in-time, and material requirements planning, see, e.g. [107]. Also, advanced control techniques such as supervisory control theory are used [20]. The main issue with this sort of control is that several state transitions occur on the same event, resulting in rapid passing through intermediate

stages, preventing actions from those states from being implemented, a phenomenon known as the avalanche effect [87]. A single hyperbolic PDE with non-local velocity is modelled for a re-entrant manufacturing system as well as the adjoint state approach was utilized to control the system by La Marca et al. [60]. Coron et al. [23] analyzed the impact of optimal time control in highly re-entrant manufacturing system as well as in semiconductor production. Armbruster et al. [4] used conservation laws to determine the relationship between density and flow in supply chain networks with a large number of lots. This model is improved by using ODEs coupled to PDEs to reduce network bottlenecks by placing queues in front of each supplier [36]. Furthermore, [55] has applied mixed-integer programming to achieve optimal control for this model in a microscopic view. In [44], kinetic equations based on PDEs are used to simulate a production flow on an assembly line. Also, Boltzmann equations based feedback control laws are used to allow supply chain models to deal with priorities [45]. The feedback stabilization for a PDE-ODE production model using a Lyapunov argument was investigated by [12].

Model predictive control (MPC) is a key control concept for nonlinear finite-dimensional systems that relies on the solution of an optimal control problem on a receding horizon [74]. In systems governed by PDEs, the MPC techniques may be attractive. An approach based on controllability properties is used to compute stability and performance bounds for unconstrained nonlinear MPC methods [39]. Shang et al. [92] used the method of characteristics to design MPC for a class of hyperbolic PDEs. Recently, MPC has become a popular optimization method in process control industries, e.g., cold sheet metal forming process [16], cutting process [85], and wire arc additive manufacturing [108]. In [106], several PDE-models are validated in order to choose the most appropriate one for designing MPC for a manufacturing flow line. The core principle behind MPC is to compute an optimal control input by predicting the future behaviour of the controlled system over a finite time horizon. MPC provides many advantages including, the ability to handle nonlinear systems, control process according to a set of constraints, and management of multi-input-multi-output systems. The fundamental disadvantage of the traditional MPC is its high computational cost [31]. Therefore, a novel developed MPC design called adjoint-based MPC (AMPC) has been used to resolve this issue. Although the design of AMPC provides insight into the system structure, it is proven a viable and effective tool in many applications, see, e.g., [96] and [103]. The contribution of this work addresses the challenges of how to handle the concept of the adjoint method to design a proper optimal control in the context of a network of manufacturing systems in terms of ODEs coupled to PDEs to solve optimization problems for demand tracking and backlog. Furthermore, the concept is extended for feedback control in a complex network of ODE-PDE using AMPC to obtain the gradient information that has a vital role in significantly improving the computational load and the performance. The core of this thesis and the main scientific effort developed therein are the two published manuscripts, see, e.g., [80] has explored a demand tracking problem coupled with PDE-ODE limitations and it is extended in [81] to examine a backlog problem employing optimal control and traditional MPC.

1.1 Goals of the thesis

In this work, the main objectives can be classified as follows:

- Investigate the well-known candidate PDE model to describe and analyse the flow line for M/M/1 process in manufacturing system and validate it with discrete event system by ARENA [89] software.
- Design a proper boundary optimal control to address the optimization problems, so-called demand tracking and backlog in terms of conservation laws coupled with ordinary differential equations in different interconnection topologies that correspond to dispersing and merging networks.
- To solve the aforementioned challenges in the complex network of the production system, develop and enhance the adjoint-based model predictive control. Furthermore, the performance is examined while the influence of disturbance is present.

1.2 Structure of the thesis

The framework of the thesis has been organized as follows, **Chapter 2** shows preliminaries and fundamentals of Little's law and conservation laws. In the microscopic view, a transformation from a derived discrete event simulation to a continuum limit of conservation law is also produced. In **Chapter 3**, an aggregated PDE model to describe M/M/1 process is derived. The dynamic behaviour is examined and validated in different scenarios (ramp-up and ramp-up-down). In addition, the PDEs are coupled to ODEs to create dispersing and merging networks, which are two types of network topology. **Chapter 4** states the optimal control problems (OCPs) addressing demand tracking and backlog to minimize the instantaneous or cumulative error between the desired demand and the system output, respectively. The backlog problem, in particular, has a considerable impact during the operational time interval, resulting in either under- or over-production. The problems are optimized with open-loop optimal control using direct and indirect methods, which are based on discretize-then-optimize and optimize-then-discretize procedures. In **Chapter 5**, an advanced MPC mechanism is developed by incorporating the adjoint method in a complex network of manufacturing flow lines which is represented by using PDEs and ODEs for solving OCPs. The optimality conditions are formulated and efficient gradient information are derived. The PDEs are discretized using a finite difference (FD) scheme in the spatial domain and the Euler method in the time domain. Furthermore, the OCPs are successively solved by the forward shifting property of the AMPC. In addition, the computational time and disturbance using AMPC are examined. **Chapter 6** concludes the work and points out potential research activities for future work.

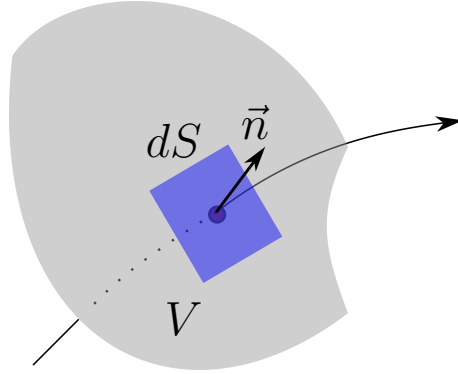
Chapter 2

Theoretical Background of Manufacturing Systems

Production processes are typically stochastic, with non-stationary stochastic input and output processes that vary over time. This stochasticity reflects various random influences such as random machine breakdown and the natural variation in task production links and material flows within the system. A manufacturing system as production line where workstations are connected serially is considered in this work. In this chapter, the essential principles for manufacturing system analysis are described before moving on to analytical models of manufacturing systems. There are two primary principles, Little's law and conservation laws. In general, some of the models for manufacturing systems are based on hyperbolic conservation laws. The goal of this chapter is not to provide a detailed theory of hyperbolic systems of conservation laws. The extensive detail of this theory is found in [18, 19, 24, 48]. The other principle for describing manufacturing systems is Little's law [65], which is considered a core concept in queuing theory [22]. The fundamental concepts will be introduced hereafter. Furthermore, a motivation example demonstrates how the connection between discrete event systems (DESs) and PDEs can be derived since these two models are popular in describing manufacturing systems as described in the literature of the previous chapter.

2.1 Conservation of Mass

The motion of a mass flux is totally governed by conservation laws: mass conservation, momentum conservation, and energy conservation. These conservation laws can be expressed as PDEs or integral equations. The mass conservation law is only taken into account in this work. According to Eulerian approach, consider a control volume V in the space where the mass flux occurs. The normal unit vector (outward-pointing) at each point on the surface is indicated as \vec{n} , and the differential surface element is written as dS as shown in Fig. 2.1. As stated by the law of conservation of mass, the change of mass in the volume must be entirely due to mass inflow or outflow through V :

Figure 2.1: Mass flux across a surface S with control volume V .

$$\frac{\partial}{\partial t} \int_V \rho dV = - \int_S \rho \vec{v} \cdot \vec{n} dS, \quad (2.1)$$

where ρ is the density and \vec{v} is the velocity of the particle. Using the divergence theorem, equation (2.1) can be written as

$$\frac{\partial}{\partial t} \int_V \rho dV = - \int_V \nabla \cdot (\rho \vec{v}) dV. \quad (2.2)$$

Hence, the equation (2.2) can be reformulated as

$$\int_V \left(\frac{\partial}{\partial t} \rho + \nabla \cdot (\rho \vec{v}) \right) dV = 0. \quad (2.3)$$

Since it is true for any arbitrary volume, the conservation of mass is stated in term of PDE as

$$\frac{\partial}{\partial t} \rho + \nabla \cdot (\rho \vec{v}) = 0 \quad (2.4)$$

with $\rho \vec{v}$ denoting the mass flux if V reduces to a line segment, then (2.4) reduces to

$$\frac{\partial}{\partial t} \rho + \frac{\partial}{\partial x} (\rho v) = 0, \quad (2.5)$$

The mass conservation law (2.5) is defined in [5], to consider the PDE model for manufacturing systems. The dependent variables are ρ and $f = \rho v$, which describe density and flow, respectively. These variables are influenced by the independent variables t and x , which describe time and place, respectively.

2.2 Little's law in Production Processes

Little's law is the other production system principle. Significant parameters as shown in Fig. 2.2 describing the properties of a manufacturing system are flow time φ and throughput σ . Flow

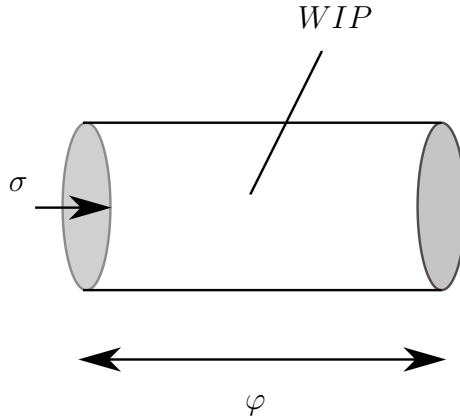


Figure 2.2: Little's law for a pipeline manufacturing system.

time is the amount of time that a lot spends in a system from beginning to end. Throughput is defined as the number of lots per unit time that depart the machine or the system. The sum of lots that is present in the system at a definite moment is expressed by the work in process *WIP* level. These parameters are mathematically represented by Little's law for steady-state

$$\overline{WIP} = \bar{\varphi} \bar{\sigma}, \quad (2.6)$$

which states that the mean work in process \overline{WIP} of a system equals the product of the mean flow time $\bar{\varphi}$ and mean throughput $\bar{\sigma}$ of that system. For example, a production system is depicted as a pipeline in Fig. 2.2. The flow rate in $[m^3/s]$ multiplied the time it takes a fluid element to travel through the pipe in $[s]$ equals the total amount of fluid in the pipeline in $[m^3]$. Little's law is generally valuable because it may be applied to a single station, a line, or a complete system. The underlying relationship will maintain throughout time as long as the three quantities are measured in consistent units [49].

To clarify the incorporation of the principles of the conservation of mass and Little's law in DES, a motivation example on a serial production line containing buffers and machines explores the system parameters and the mathematical basis to describe the relation between PDE and DES in a simple manufacturing system.

2.3 Example on DES-PDE correlation

To analyse the manufacturing systems from the Lagrangian approach perspective, the approaches of Armbruster et al. [4] and d'Apice et al. [25] are summarized. The starting point is to introduce some preliminary fundamentals of how DES work by taking into account the time evolution of each lot from the system entrance to the exit. As shown in Fig. 2.3, a single workstation consists of a single machine m with queue q . The arrival time a_n^m for lot number n is computed at the beginning of the workstation from the machine m . The total number

of lots is denoted by N while the total number of workstations (machines) is identified by M since each workstation contains a single machine. The release time b_n^m is the time when lot n is delivered to the machine m . The leaving time e_n^m is the time that a lot n departs from the machine m and arrives at the machine $m + 1$ at the same moment (transportation time between two successive workstations assumed to be zero) as declared in Figure 2.4. Some hypotheses are adopted as follows

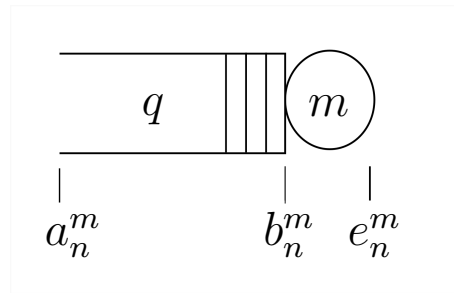


Figure 2.3: Construction of simple workstation.

- 1- The lots are always conserved i.e., their number is preserved inside the system.
- 2- Queues have an infinite buffer.
- 3- Initially no lots are in the system.
- 4- For the sake of simplicity, the lot is traveling downstream and passes each machine once, i.e., no re-entrant system.

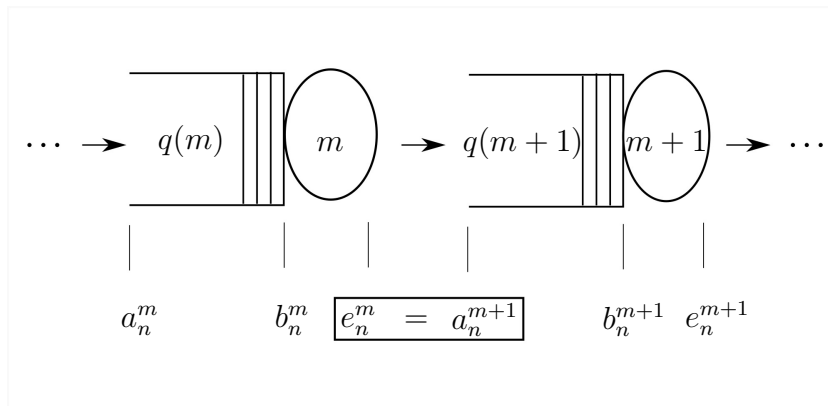


Figure 2.4: Production line with lot n moving through the system.

Each machine has its own configuration parameters, which are deterministic and fixed in this context. These parameters are process rate $\mu(m)$ and process time $T(m)$. Process rate (production rate) is the maximum number of lots per unit of time that can be released by one machine and is also known as maximum capacity. Process time is the required time to finish one production step. The total number of lots that the machine m can handle is the product

of process rate $\mu(m)$ and process time $T(m)$. When the machine can handle only one lot per unit of time one has $\mu(m) = \frac{1}{T(m)}$. Herein, lot n enters the machine m due to the status of the queue $q(m)$ if it is empty or not. When it is empty, lot n goes directly to the front of the queue, and then $b_n^m = a_n^m$. On the other hand, the lot n to be in the front of queue needs to wait until the previous lot $n - 1$ to finish by means of $\mu(m)$ to become $b_n^m = b_{n-1}^m + \frac{1}{\mu(m)}$. The release time is governed by

$$b_n^m = \max \left\{ a_n^m, b_{n-1}^m + \frac{1}{\mu(m)} \right\}, \quad (2.7)$$

lot n takes the processing time $T(m)$ after it is fed into a machine m till to leave it, where the leaving time is computed from

$$e_n^m = b_n^m + T(m), \quad (2.8)$$

after plugging equation (2.8) into (2.7) we obtain

$$e_n^m = \max \left\{ a_n^m + T(m), e_{n-1}^m + \frac{1}{\mu(m)} \right\}. \quad (2.9)$$

Note that, the process time $\mu(m)$ is independent of time, which means that all lots have the same process rate at machine m . In case of a stochastic system μ has to be time dependent to express that each lot has its own processing rate. This microscopic approach expresses the behaviour of each individual lot. Therefore, arrival times a_n^m and departure or ending times e_n^m are the events of the interest.

For the serial production line, workstations are denoted W_0, W_1, \dots, W_{M-1} for M workstations. To elaborate a time recursion analysis, the notation for arrival time a and ending time e for lot n in workstation or machine m are formulated to become $\tau(m, n)$ and $\tau(m + 1, n)$, respectively. The equation (2.9) can be expressed as

$$\tau(m + 1, n) = \max \left\{ \tau(m, n) + T(m), \tau(m + 1, n - 1) + \frac{1}{\mu(m)} \right\}, \quad n \geq 1, \quad m = 0, 1, \dots, M - 1. \quad (2.10)$$

The above equation (2.10) is the recursion formula, and it needs both boundary $\tau^A(n)$ and initial $\tau^I(m)$ conditions for a well-defined recursion as follows

$$\tau^A(n) = \tau(0, n), \quad n \geq 0, \quad \tau^I(m) = \tau(m, 0), \quad m = 0, 1, \dots, M.$$

Obviously, the initial condition is the time that the lot $n = 0$ passing through the entire system. The initial condition $\tau^I(m + 1)$ can be computed from the formula (2.10). Hence, these conditions can be used to calculate

$$f^A(\tau^A(n)) = \frac{1}{\tau^A(n + 1) - \tau^A(n)}, \quad n \geq 0. \quad (2.11)$$

$$\tau^I(m+1) = \tau^I(m) + T(m), \quad m = 0, 1, \dots, M. \quad (2.12)$$

The influx f^A can be calculated from the boundary condition at the beginning of the system. It is the inverse of the inter arrival times at the machine $m = 0$.

By introducing Newell-Curves $U(m, t)$, see, e.g., [78], also named N-Curves, which can be used in equation (2.10) to determine the number of lots coming out from workstation W_{m-1} to workstation W_m at time t by

$$U(m, t) = \sum_{n=0}^{\infty} H(t - \tau(m, n)), \quad t > 0, \quad m = 0, 1, \dots, M. \quad (2.13)$$

Herein, $H(t)$ is the Heaviside step function at time $\tau(m, n)$. The difference between two successive N-Curves allows to compute the work in process WIP i.e.,

$$WIP(m, t) = U(m, t) - U(m+1, t), \quad m = 0, 1, \dots, M-1. \quad (2.14)$$

Equation (2.14) computes the number of lots within workstation W_m and the total work in process TW in the entire system can be expressed by

$$TW(t) = U(0, t) - U(M, t). \quad (2.15)$$

The flux or flow $F(m, t)$ from workstation W_{m-1} to workstation W_m is defined by considering the rate of change of $U(m, t)$, i.e.

$$F(m, t) = \frac{d}{dt}U(m, t) = \sum_{n=0}^{\infty} \delta(t - \tau(m, n)), \quad (2.16)$$

Herein $\delta(\cdot)$ denotes the Dirac delta function and the derivative of WIP with respect to t yields

$$\frac{d}{dt}WIP(m, t) = F(m, t) - F(m+1, t), \quad m = 0, 1, \dots, M-1. \quad (2.17)$$

Hence the flux is expressed by a superposition of Dirac distributions. The discontinuous distribution can be eliminated by using a continuous function instead of the dependence on individual lots.

The following steps are taken towards a continuous formulation under the hypothesis of mass conservation. The constitutive relation of the conservation law in (2.17) can be described in terms of partial differential equations. The fluxes $F(m, t)$ and work in processes $WIP(m, t)$ can be reconstructed in the term of a continuous constitutive relation $f(\rho)$. The $WIP(m, t)$ can be replaced by $\rho(x, t)$, which denotes the lot density in terms of the continuous variable x which also known as the degree of completion (DOC). This independent variable has one spatial dimension $x_0 = 0 < x_1 < \dots < x_M = 1$. Each machine is represented in one grid-point x_m , where lots enter the system at $x_0 = 0$ while they leave at $x_M = 1$. By applying $F(x_m, t)$ instead of $F(m, t)$ and multiplying it by arbitrary smooth test function $\Psi(t)$ in integral or weak form and using the shifting property of the Dirac function, the formula becomes

$$\int_{\tau^I(m)}^{\infty} \Psi(t) F(x_m, t) dt = \sum_{n=0}^{\infty} \int_{\tau^I(m)}^{\infty} \Psi(t) \delta(t - \tau(m, n)) = \sum_{n=0}^{\infty} \Psi(\tau(m, n)), \quad (2.18)$$

where τ is monotonically increasing function due to $\tau^I(m) < \tau(m, n)$. This equation can be rewritten in a form of Riemann sum

$$\int_{\tau^I(m)}^{\infty} \Psi(t)F(x_m, t)dt = \sum_{n=0}^{\infty} \Psi(\tau(m, n))f(x_m, \tau(m, n))\Delta_n\tau(m, n), \quad (2.19)$$

where $\Delta_n\tau(m, n)$ describes the inter-arrival time between two successive lots in machine m and it is the inverse of the flux as declared from (2.11), which is reformed by

$$f(x_m, \tau(m, n)) = \frac{1}{\Delta_n\tau(m, n)}, \quad (2.20a)$$

$$\Delta_n\tau(m, n) = \tau(m, n+1) - \tau(m, n). \quad (2.20b)$$

When $\Delta_n\tau(m, n)$ tends to zero equation (2.19) and the inter arrival times between lots $\Delta_n\tau(m, n)$ can be approximated as [4]

$$\int_{\tau^I(m)}^{\infty} \Psi(t)F(x_m, t)dt \approx \int_{\tau^I(m)}^{\infty} \Psi(t)f(x_m, t)dt, \quad (2.21)$$

and the approximate flux $f(x_m, t)$ is given at $x = x_m$ and $t = \tau(m, n)$. Now assuming that the arrival times can be expressed as a continuous distribution $\tau(x, y)$ as in [4] and the approximate flux f from equation (2.20) can be re-written as follows

$$f(x, \tau(x, y)) = \frac{1}{\frac{\partial}{\partial y}\tau(x, y)}. \quad (2.22)$$

By referring to equation (2.14), which can be revised to become $\rho(x, t) = -\frac{\partial}{\partial x}U(x, t)$. Herein *WIP* is changed into the approximate density $\rho(x, t)$. The assumption of mass conservation is only satisfied for a specific choice of the density ρ , according to an analytical solution [25],

$$\frac{d}{dx}f(x, \tau(x, y)) = \frac{\partial}{\partial t}f(x, \tau(x, y))\frac{\partial}{\partial x}\tau(x, y) + \frac{\partial}{\partial x}f(x, \tau(x, y)). \quad (2.23)$$

By imposing that $\frac{d}{dx}f(x, \tau(x, y)) \stackrel{!}{=} 0$, equation (2.23) satisfies mass conservation law

$$\frac{\partial}{\partial t}\rho(x, t) + \frac{\partial}{\partial x}f(x, t) = 0, \quad (2.24)$$

after the comparison between (2.23) and (2.24), a specific density ρ becomes

$$\rho(x, \tau(x, y)) = f(x, \tau(x, y))\frac{\partial}{\partial x}\tau(x, y), \quad (2.25)$$

this equation (2.25) represents Little's law, where $\frac{\partial}{\partial x}\tau$ is the flow time φ and it is the inverse of the velocity $v = \frac{1}{\frac{\partial}{\partial x}\tau}$. By substituting (2.22) into (2.25), the density becomes

$$\rho(x, y) = \frac{\frac{\partial}{\partial x}\tau(x, y)}{\frac{\partial}{\partial y}\tau(x, y)}. \quad (2.26)$$

The approximate density ρ in (2.26) can also be written in discrete event form by

$$\rho(x_m, \tau(m+1, n)) = \frac{\Delta_m \tau(m, n+1)}{h_m \Delta_n \tau(m+1, n)}, \quad n \geq 0, \quad m = 0, 1, \dots, M-1 \quad (2.27a)$$

$$\Delta_m \tau(m, n) = \tau(m+1, n) - \tau(m, n), \quad h_m = x_{m+1} - x_m. \quad (2.27b)$$

To properly work with integrals and derivatives, switching between continuous and discrete variables and functions is required at this level. It is demonstrated that there is a constitutive relationship between flux and density in terms of $f = f(\rho)$ using formulas (2.20) and (2.27).

Theorem 1. Let the arrival times $\tau(n, m)$ satisfy the recursion (2.10) and let the approximate density ρ and flux f be defined by (2.20), (2.27). Then the approximate flux can be written in terms of the approximate density via a constitutive relation of the form

$$f(x_m, \tau(m, n)) = \min \left\{ \mu(m-1), \frac{h_{m-1} \rho(x_{m-1}, \tau(m, n))}{T(m-1)} \right\}, \quad n \geq 0, \quad m = 1, \dots, M. \quad (2.28)$$

For a proof consult [4]). The flux is produced as a minimum function in case of restricted flow capacity $\mu(m)$ for each machine in production line as stated originally in recursion (2.10) from a microscopic point of view. The constitutive relation $f(\rho)$ is the most proper way to describe the flux in terms of density to plug into the conservation law (2.24) as shown above. Simulation of DES can be performed by ARENA software and used for the validation.

2.4 Summary

In this chapter, the principles of describing the production flow of the manufacturing systems are reviewed. The relation between both DES and PDE are mathematically declared since they are preferred for expressing manufacturing systems. The main focus is put on deriving a conservation law from the time recursion formula to establish the constitutive relation $f(\rho)$ and to show how the transformation between continuous and discrete variables and functions takes place. However, this example is appropriate for simple network with no consideration of dispersing or merging topologies. In the upcoming chapter, a proposed PDE model to satisfy the constitutive relation $f(\rho)$ from the aggregation or macroscopic level is addressed. It is convenient to investigate a sufficiently large number of lots as a continuum flow on either a single flow line or manufacturing network.

Chapter 3

Modelling of Manufacturing Systems

The connection to the mathematical models are used to track and measure existing processes and to monitor the cost-effective distribution of parts or lots. According to the literature, the manufacturing system can be analyzed from macroscopic perspective by considering factory level description or microscopic perspective with more detailed analysis such as machine level. Manufacturing models can generally be classified as discrete event or continuous differential equations. The primary distinction between them lies under the description of lots as individuals (i.e., discrete time instances) or as a continuum flow. A manufacturing system can be represented as a PDE model in which a flow line is composed of a large number of machines or workstations. PDE models depict the entire dynamic behaviour of a system through the combination of both throughput and flow time parameters. Therefore, PDE models are adopted in this thesis.

In this chapter, the investigations are concentrated on a PDE model of a single flow line manufacturing system that covers both ramp-up and ramp-down scenarios. After that, a validation for the PDE model is carried out by ARENA software. Finally, in the context of the manufacturing network, the construction of conservation laws coupled with ODEs in different interconnection topologies is illustrated.

3.1 Single Flow Line Model

In the previous chapter, the PDE model describes only one machine with a buffer. In this chapter, the proposed PDE is utilized as an aggregated model, i.e., the PDE can represent many machines connected serially to represent a production flow line.

The idea of approximating the behaviour of highway traffic to characterize its dynamics with a PDE model arose from the inspired traffic theory. Because the cars and 1-dimensional continuum highway are regarded as products and manufacturing systems, these traffic models demonstrate great consistency with manufacturing systems. Before the proposed PDE model

is introduced, a general overview of the transport equation presented first. The simplest form of conservation of mass (2.24) is given by the linear transport (advection) equation

$$\frac{\partial}{\partial t}\zeta(x, t) + a\frac{\partial}{\partial x}\zeta(x, t) = 0, \quad (3.1)$$

where $\zeta(x, t)$ is any arbitrary function and the speed is denoted by a , which is a constant value. If $a > 0$, the function moves from left to right direction, whereas if $a < 0$, they moves from right to left direction. This PDE is linear hyperbolic [46].

The proposed PDE of a flow line containing identical workstations works according to an M/M/1 process, where the first M refers to the exponential distribution of the inter-arrival time, the second M indicates the exponential distribution of the process time, and 1 refers to a single lot being processed per machine. Each workstation consists of an infinite buffer length and a machine. The system is connected serially, i.e. the line is used in assembly processes such as in the automotive industry. Therefore, the system applies the first come, first out (FCFO) policy. For the sake of simplicity, the other configurations are not considered, such as the transportation time between two successive processes being omitted. Furthermore, the processes or the machines are not prone to failure. Moreover, the flow is only in one direction where the direction goes downstream from the lots that enter the system to leave it. Referring to (2.24), these variables depend on the independent coordinates t and x , which describe respectively time and space. The space is defined as the position of a lot in the manufacturing system. At the start of the system, $x = 0$, and at the end, $x = 1$. The equation (2.24) is considered a first-order hyperbolic partial differential equation. The constitutive relation $f(\rho(x, t))$ can be determined by the adiabatic equation, where the flow is the product of velocity $v(x, t)$ and density $\rho(x, t)$

$$f(x, t) = v(x, t)\rho(x, t). \quad (3.2)$$

The flow time in steady-state $\varphi = \frac{M}{\mu - u}$, where M is the number of machines, u is the inflow and μ is the process rate. The velocity in steady-state is the inverse of the flow time. Hence, the velocity v can be expressed as

$$v(x, t) = \frac{\mu - f(x, t)}{M} = \frac{\mu - \rho(x, t)v(x, t)}{M}$$

$$\mu = v(x, t)(M + \rho(x, t)).$$

The velocity is equivalent to

$$v(x, t) = \frac{\mu}{M + \rho(x, t)}. \quad (3.3)$$

Substitution of (3.3) and (3.2) in (2.24) yields

$$\frac{\partial}{\partial t}\rho(x, t) = -\frac{\partial}{\partial x}\left(\frac{\mu\rho(x, t)}{M + \rho(x, t)}\right) = -\left(\frac{\mu M}{(M + \rho(x, t))^2}\right)\frac{\partial}{\partial x}\rho(x, t). \quad (3.4)$$

The initial condition (IC) and the boundary condition (BC) are given by

$$\begin{aligned}\rho(x, 0) &= g(x), \\ \rho(0, t) &= \frac{Mu(t)}{\mu - u(t)}.\end{aligned}\tag{3.5}$$

Also, an extra parameter is required in the description of the production system to measure the degree of machine occupation. This parameter is called system utilization. The utilization factor $\Gamma = \frac{u}{\mu}$ is crucial to be between zero and one. So, the arrival rate must be less than the process rate to avoid the buffer being too large and hence steady state is never reached. The total work in process of the entire system TW can be written from the following expression

$$TW(t) = \int_0^1 \rho(x, t) dx.\tag{3.6}$$

The analytical solution of the PDE model is found in Appendix C by using the method of characteristics (MOC). The MOC, which is based on the implicit function theorem and the existence-uniqueness theorem of ordinary differential equations, is typically used to demonstrate the existence and uniqueness of solutions to first-order hyperbolic PDEs [17]. To analyze the system behaviour, three variables are investigated. These variables are the mean flow time, the mean throughput or flux and the mean total WIP. Two scenarios, i.e. the ramp-up and the ramp-down, are considered for the PDE model. Ramp-up refers to an increase in production rate from one steady-state to another, whereas ramp-down refers to a decrease in production rate. These two realizations describe the complete dynamic behaviour of the system in both transient and steady-state. The model is numerically solved with the full spatial-temporal discretization. The simulations are carried out on the following setup: The total number of identical machines is $M = 10$, and the mean process rate is $\mu = 2$. The number of discretization points in x direction is represented by $n_x = \frac{1}{\Delta x} + 1$, where Δx is the spatial step size.

Ramp-up Scenario

In this simulation, the ramp-up of the system is examined when there are no lots in the system initially, i.e., the initial density is zero $\rho(x, 0) = 0$. The spatial domain or place x is discretized to be the step size Δx equal to 0.1. The arrival rate (influx or inflow) u is chosen for two realizations to be 1 lots/h and 1.5 lots/h or $\Gamma = 50\%$ and $\Gamma = 75\%$ respectively. The left boundary condition $\rho(0, t)$ from equation (3.5) is assigned as 10 and 30 for $u = 1$ lots/h and 1.5 lots/h, respectively. In the case of $u = 1$ lots/h, the time interval begins at 0 h and ends at 60 h, while in the case of $u = 1.5$ lots/h, it begins at 0 h and ends at 250 h.

In the case of $u = 1$ lots/h as shown from Fig. 3.1, the flow time φ , the throughput $f(1, t)$, the total work in process TW , and the density ρ are presented. The flow time can be computed

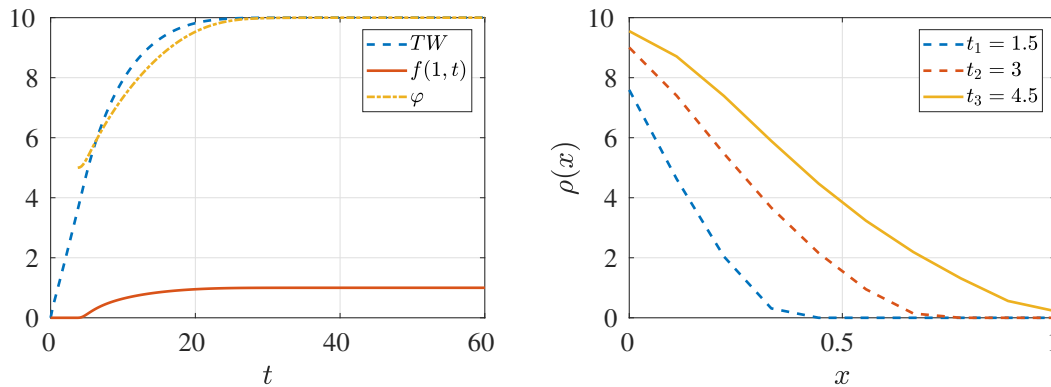


Figure 3.1: Ramp-up simulation, $u = 1$ lots/h with $n_x = 11$.

analytically from the inverse of the velocity $\varphi = \frac{m+\rho}{\mu}$. Therefore, when ρ is initially zero (no lots in the system at $t = 0$), the first flow time φ_1 is 5 h. In other words, the first lot is not waiting in any queue in the system because there are no lots when the system starts working. Therefore, the first lot is processed directly without the need to wait. For ten machines, the total processing time is 5 h, indicating that the first lot spends 5 h in the system. That is explained why the throughput $f(1,t)$ starts producing lots from time around 5 h. When the outflow $f(1,t)$ reaches the steady-state, the corresponding ρ equals 10 and the flow time at steady-state φ_s also reaches 10. Furthermore, the density ρ at the right boundary ($x = 1$), the first lot leaves the system almost at $t = 5$ h (exactly at $t = 4.6$ h), as shown analytically above.

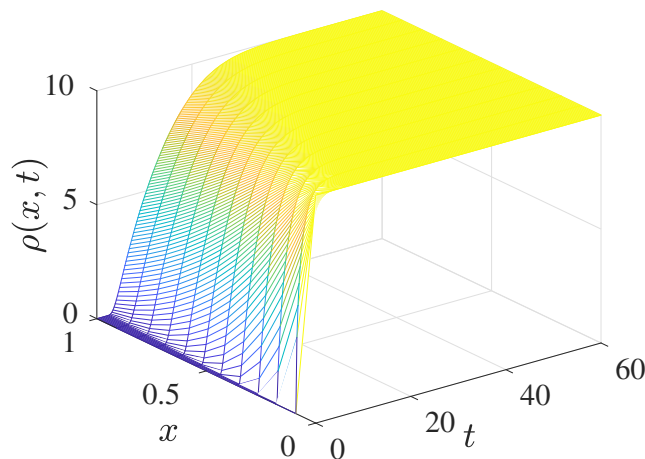


Figure 3.2: Density over space and time for ramp-up, $u = 1$ lots/h with $n_x = 11$.

For the density, a typical outcome of the ramp-up scenario is provided in Fig. 3.2, which depicts how the system behaves in the spatial and time domain. Also, the density can be viewed in the (x,t) -plane, giving the impression that the system reaches a steady-state.

The system attributes throughput $f(1,t)$, flow time φ , and total work in process TW are

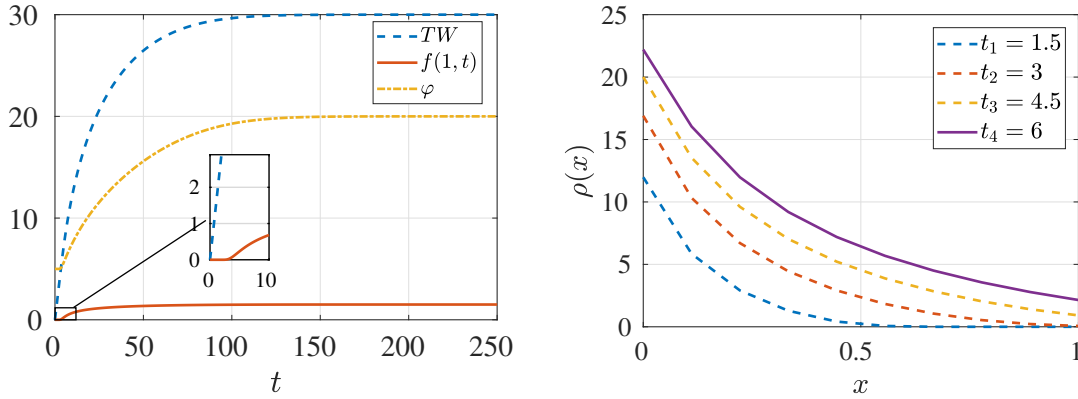


Figure 3.3: Ramp-up simulation for total WIP, flow time, throughput, and density where $u = 1.5$ lots/h with $n_x = 11$.

displayed on the left in Fig. 3.3, while the density is shown on the right. In the case of $u = 1.5$, after a 5-hour delay, the throughput begins to rise and reaches a steady-state of nearly 1.5 lots/h. When there are no lots in the system, the flow time φ takes 5 h and needs 20 h when the density ρ reaches the new steady-state. Since there are no lots in the system at $t = 0$, the total work in process TW starts from 0 to reach 30 lots per unit of place at the new steady-state. The snapshots of the density along the system have been taken at different time instances $t \in \{1.5, 3, 4.5, 6\}$. The density growth during the ramp-up scenario is depicted in the diagram.

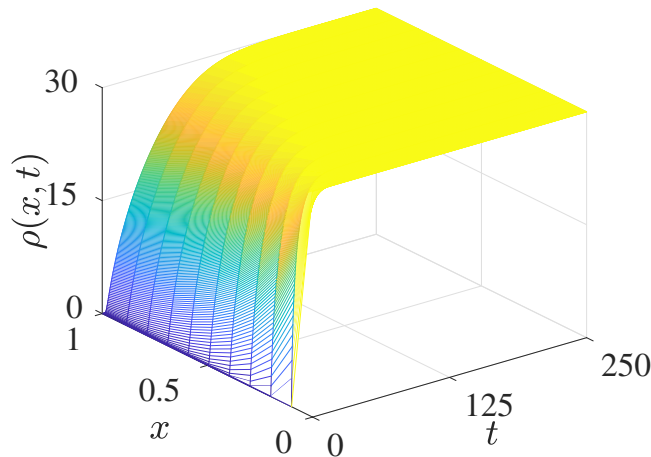


Figure 3.4: Density over space and time for ramp-up, $u = 1.5$ lots/h with $n_x = 11$.

Fig. 3.4 demonstrates how the density behaves in the (x, t) -domain and shows a typical outcome of the ramp-up scenario. In addition, providing the impression that the system reaches all x steady states in a large amount of time. In general, the higher arrival rate or utilization of the system applied, the longer time it takes for all variables to reach to the steady state as

obviously seen in the figures.

Ramp-down Scenario

In the ramp-down simulation, the flow starts from a high steady-state after that, the flow decreases until it reaches the low steady-state. The simulation shows that the arrival rate u starts from 1 lots/h and ends to 0.5 lots/h with n_x equal to 11 where the step size Δx is 0.1. The initial density is 10 lots per unit of place for all x . The time starts from 0 h and ends at 40 h.

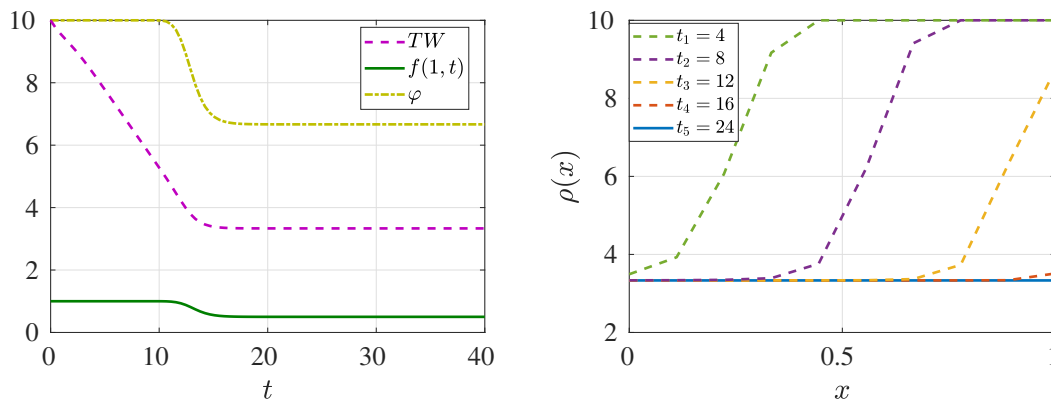


Figure 3.5: Ramp-down simulation, u from 1 lots/h to 0.5 lots/h, $n_x = 11$.

In Fig. 3.5 for the ramp-down scenario, the system variables throughput $f(1, t)$, flow time φ , and total work in process TW are shown on the left, whereas the density is shown on the right. In the beginning, the system has already lots, i.e., the density $\rho(x, 0) = 10$, so the inflow needs more time to show up at the outlet other than the ramp-up. In another way of describing, incoming lots must wait for the existing lots to finish and exit the system before proceeding. The required flow time φ is 10 h for the starting steady-state while the needed is 6.6667 h for the ending steady-state, as seen in the figure, and the transient became steep, indicating a short transition time. Similarly, the outflow $f(1, t)$ starts at 1 lots/h and quickly decreases to 0.5 lots/h after the delay time. The total work in process TW decreases gradually until reaching the steady-state at a value of 3.333. The density profile decreases from the inlet (left boundary) to the outlet (right boundary) of the system during the time evolution, as shown in the (right) figure. It starts as defined from the initial condition of the density $\rho(x, 0) = 10$ lots/unit of space and ends at 3,333 lots/unit of space. Figure 3.6 shows how the density behaves in spatial-temporal domain as a result of the ramp-down scenario. Furthermore, providing the sense that the system takes a short time to reach steady state in all x in contrast to the case of the ramp-up.

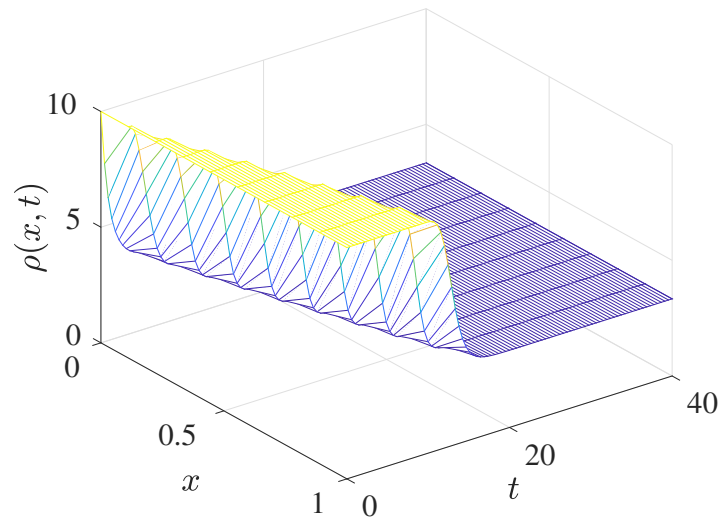


Figure 3.6: Density over space and time for ramp-down, from $u = 1$ lots/h to $u = 0.5$ lots/h with $n_x = 11$.

3.2 Validation of the PDE Model

Nonlinearity may cause a discrepancy in output measurements between models and real-world systems unless they are well modelled [62]. For discrete-event modeling, there are a variety of programs and simulation languages available, such as the χ simulation language, see, e.g., [105, 104], SimEvents in MATLAB, see, e.g., [37], Petri net, see, e.g., [27], or ARENA, a simulation program based on the computer simulation language SIMAN, see, e.g., [91]. The main benefit of ARENA is that it combines the simplicity of flowchart modules with the flexibility of simulation languages, stochastic distributions, and even Microsoft's event-driven programming language Visual Basic for specific tasks such as retrieving data from external tools or documents [2].

The validation is performed using (3.4) and (3.5) for the model. The goal of this section is to validate the PDE model using the DES simulation via ARENA. Specifically, the system behaviour in each of the parameters: flow time φ , outflow and total work in process are compared to their counterparts of the DES simulation. The system consists of 10 identical workstations in line. In both ramp-up and ramp-up-down scenarios, the system is initially empty which implies that the initial density equals zero in the PDE model and the queues contain no lots in the DES case.

3.2.1 Validation for Ramp-up Scenario

The mean processing rate μ is 2 lots/h and the mean arrival rate u is changing due to the system utilization Γ of 25%, 50% or 75%, which correspond to the mean arrival rates 0.5 lots/h, 1 lots/h

or 1.5 lots/h, respectively. The number of replications R is 10,000 in DES given that the inter-arrival times and processing times are exponentially distributed random variables. The PDE models are solved numerically using fully discrete methods. The step size in space Δx is 0.1. The mean flow time φ in the PDE follows a trajectory similar to the one of the DES in the

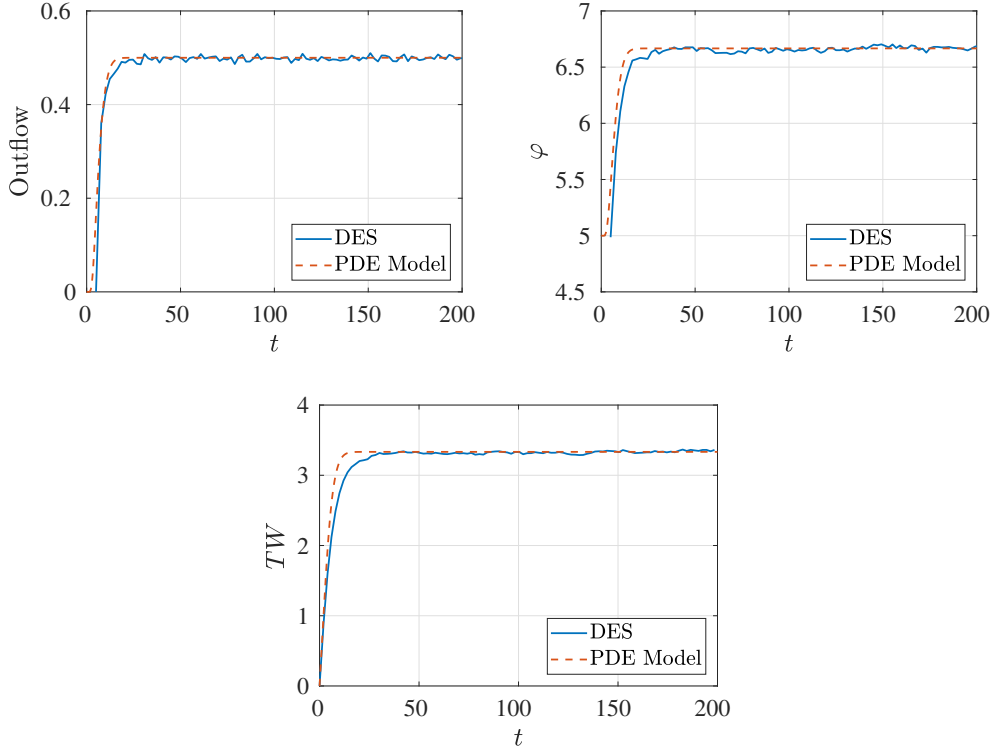


Figure 3.7: Outflow, flow time and total work in process with $M = 10$, $u = 0.5$ lots/h, $\mu = 2$ lots/h and $\Gamma = 25\%$.

case of $\Gamma = 25\%$, as shown in Fig. 3.7 although there is a variation. From the flow time figure, DES and PDE curves do not fully match in the transition period. In addition, when compared to the DES, the PDE model starts earlier. Both PDE and DES attain the target value in steady-state. The figure of the mean throughput also demonstrates that the PDE model and the DES generally follow a similar path with some differences. Compared to the DES model, the PDE model starts quicker and reaches steady-state faster. The TW graph indicates that the PDE and DES models are in satisfactory correlation at the start of the transition period. Afterwards, they start to deviate and display the most deviance around $t = 15$ h then both sides eventually converge to the proper steady-state value. In the case of $\Gamma = 50\%$, the mean throughput shows that the PDE model and the DES follow a comparable trajectory, with obvious exceptions. The PDE model significantly starts faster and reaches steady-state earlier than the DES model, as shown in Fig. 3.8. Although there is some variation, the PDE's mean flow time φ follows a similar behaviour as the DES. The PDE model and DES do not start at the same time. Moreover, the DES takes longer time to match the PDE model. However, both PDE and DES achieve the same value in the steady-state. At the beginning of the transition

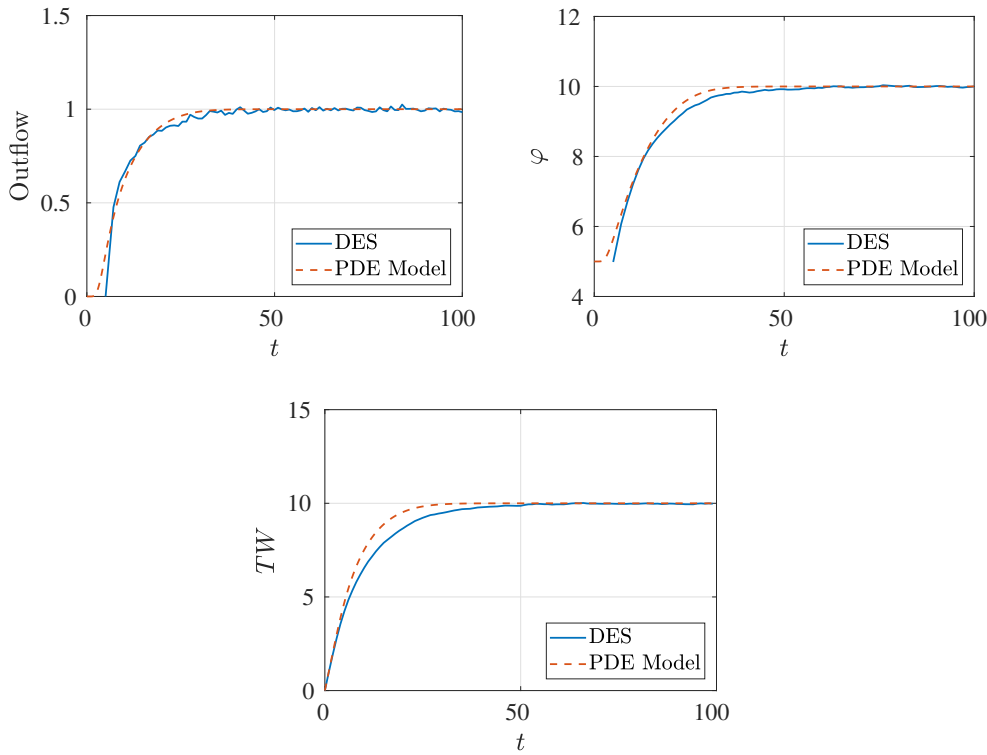


Figure 3.8: Outflow, flow time and total work in process with $M = 10$, $u = 1$ lots/h, $\mu = 2$ lots/h and $\Gamma = 50\%$.

period, the TW graph shows that the PDE and DES models are in good agreement. After that, they begin to deviate, with the most elevated deviation occurring around $t = 22$ h, until gradually converging to the proper steady-state value on both sides.

When $\Gamma = 75\%$, the mean outflow shows that the PDE model and the DES take a consistent trajectory with a few exceptions, such as the PDE model starts faster and reaches steady-state sooner than the DES model, as seen in Fig. 3.9. Despite notable deviations, the PDE's mean flow time φ follows a similar pattern to the DES. The range of both DES and PDE curves begins from the value 5, but they are generally not matched in the transition time where the PDE model converges to the steady-state faster than the DES. Again, both the PDE and DES curves reach the same value in steady-state. Regarding the TW , the figure shows that the PDE and DES models are in good accordance at the beginning of the transition period. Thereafter, they start to vary, with the highest deviation about $t = 80$ h, before slowly converging to each other.

From the above figures, it is noted that the transition time of the outflow increases as the system utilization Γ increases. Moreover, the outflow of the PDE model is the most convergent to the DES in the ramp-up scenario.

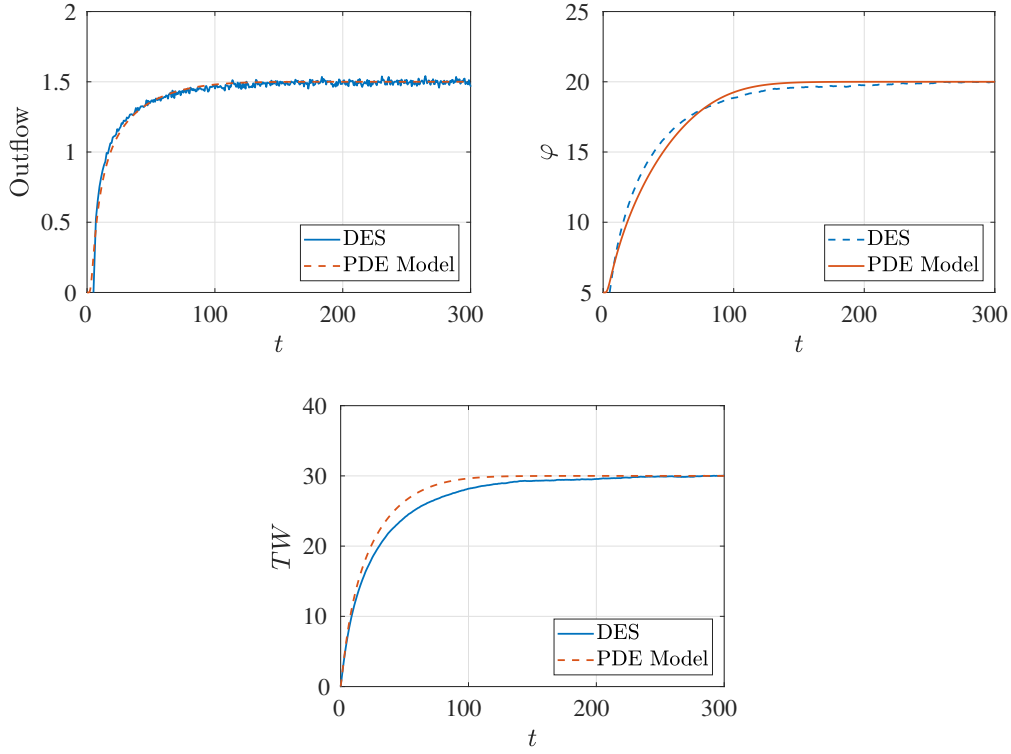


Figure 3.9: Outflow, flow time and total work in process with $M = 10$, $u = 1.5$ lots/h, $\mu = 2$ lots/h and $\Gamma = 75\%$.

3.2.2 Validation of Ramp-up-down Scenario

The combination of ramp-up and ramp-down results in a situation in which the inflow profile has two phases: The first phase is a causal function that reaches an upper steady-state. In the second phase, the arrival rate decreases in order to attain a lower steady-state. The system is initially empty. The ramp-up part is done by $\lambda = 1.5$ lots/h, and regarding the ramp-down part, two realizations are considered. These realizations are $\Gamma = 25\%$ and $\Gamma = 50\%$ which are corresponding to $u = 0.5$ lots/h and $u = 1$ lots/h. The release time for ramp-down is $t = 300$ h. The PDE model is also solved numerically with step size $\Delta x = 0.1$. The inflow or the arrival rate $u(t)$ in the first realization is defined as

$$u(t) = \begin{cases} 1.5, & \text{for } 0 \leq t < 300, \\ 0.5, & \text{for } t \geq 300, \end{cases} \quad (3.7)$$

and for the second realization, the inflow $u(t)$ reads

$$u(t) = \begin{cases} 1.5, & \text{for } 0 \leq t < 300, \\ 1.0, & \text{for } t \geq 300, \end{cases} \quad (3.8)$$

The maximum difference is detected at parameters of the mean flow time, the mean throughput, and the total work in process inside the transient phase of reducing the arrival rate in the case

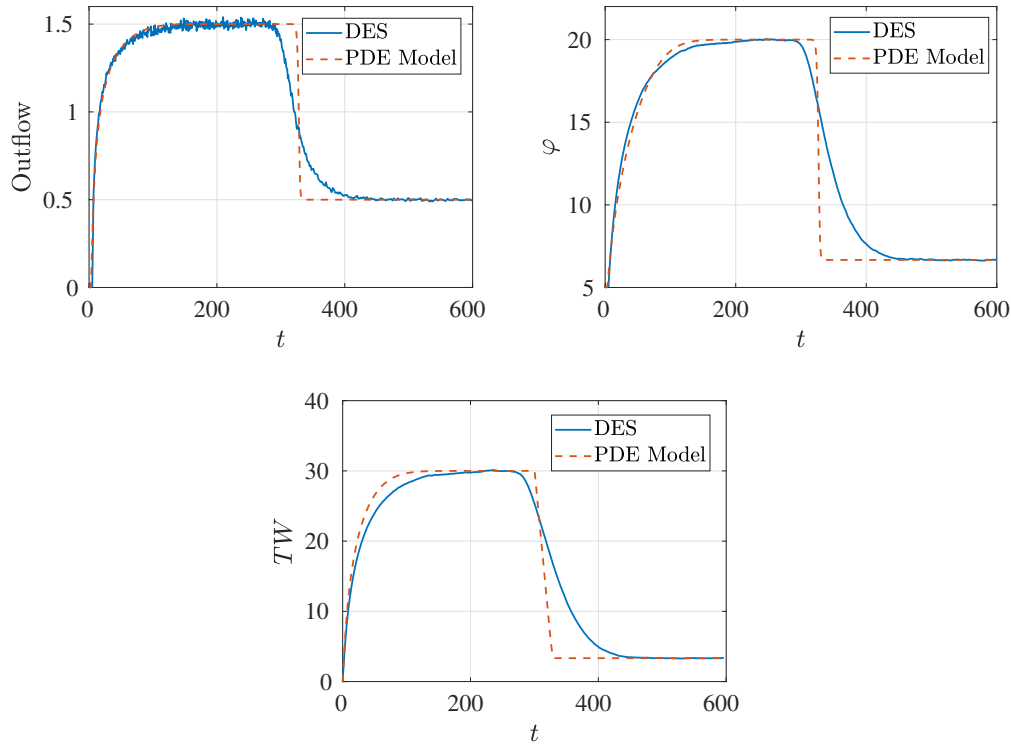


Figure 3.10: Outflow, flow time and total work in process with $M = 10$, from $u = 1.5$ lots/h to $u = 0.5$ lots/h, $\mu = 2$ lots/h and $\Gamma = 25\%$.

of the first realization, as shown in Fig. 3.10. When the inflow is tuned to $u(t) = 0.5$ lots/h, all plots in the DES show the beginning of a decrease before $t = 300$, and it takes them almost 145 h to reach the new steady state. The PDE model, on the other hand, diminishes at $t = 300$ h and achieves steady-state within 10 h. As a result, it is concluded that the behaviour of this transient portion varies immensely while the DES model shows a low gradient until the system is stable at the steady state. On the other hand, the PDE model reacts very quickly to the changes of the arrival rate.

Inside the transient phase of reducing the arrival rate in the case of the second realization, the highest difference is identified at parameters of the mean flow time, mean throughput, and total work in process, as shown in Fig. 3.11. Both figures of flow time and outflow in the DES show the beginning of a gradually fall at $t = 300$ h while the TW starts earlier when the inflow is adjusted to $u(t) = 1$ lots/h, and it takes them almost 40 h to reach the new steady state. The intersected lines of the φ and the outflow occurred at 15 h and 1.25 lots/h, respectively. These values are located in the middle of the minimum and maximum values. Similarly to the previous case, it is determined that the maximum difference exists within the transient of the ramp-down part.

To sum up this section, the M/M/1 PDE behaves similarly to the DES. However, it has been discovered that the applied PDE model inaccuracy is marginal if compared to the rapid response in the transient period according to [106]. For the upcoming section, the M/M/1 PDE model

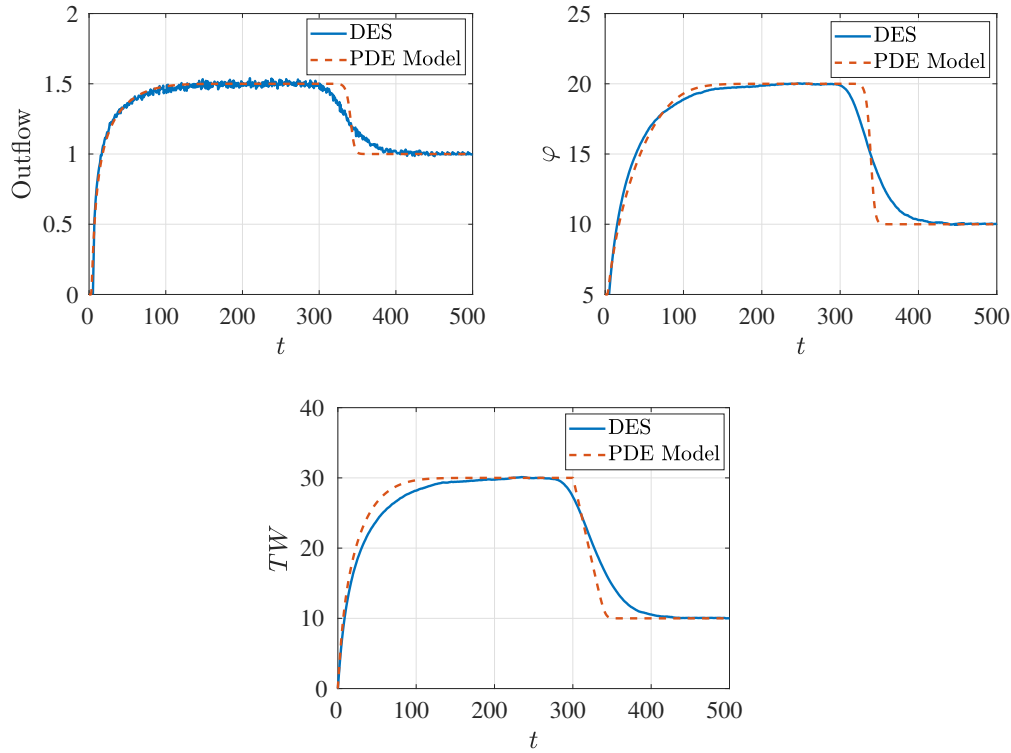


Figure 3.11: Outflow, flow time and total work in process with $M = 10$, from $u = 1.5$ lots/h to $u = 1$ lots/h, $\mu = 2$ lots/h and $\Gamma = 50\%$.

(2.24), (3.2), (3.3) are utilized to define a network of production systems.

3.3 Manufacturing System Networks

In this part, the mathematical model of the system is presented in the context of the production network. Conditions for each vertex of the network are provided to design either dispersing or merging networks. The network is represented by a directed graph $G(\mathcal{V}, \mathcal{E})$, where \mathcal{V} and \mathcal{E} are sets of vertices and arcs, respectively. Subsequently, buffer zones are represented by vertices $v \in \mathcal{V}$ and flow lines are given by arcs $e \in \mathcal{E}$. PDEs are used to model the arcs, while ODEs are used to model the vertices. The two are coupled together in various network topologies.

3.3.1 Dispersing Network Design:

The system for the dispersing network consists of three arcs. Herein, arc e_1 is the main flow line while the others are sub sequencing flow lines. These arcs are connected at vertex v (see Fig. 3.12). Suppose that each of these flow lines are represented arcs e_1 , e_2 and e_3 with different processing rates μ^{e_1} , μ^{e_2} and μ^{e_3} , respectively. The number of workstations is M^e in each flow line. The PDE model is assumed to have infinite buffer capacity which mean that the lots or

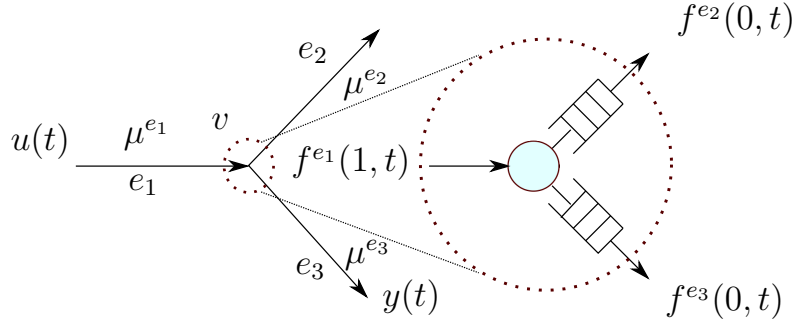


Figure 3.12: Configuration of dispersing network.

parts are preserved inside each flow line. They are stored in the buffer until their turn to come. The system dynamics for each flow line e can be described as

$$\frac{\partial}{\partial t} \rho^e(x, t) = -\frac{\partial}{\partial x} f^e(\rho^e(x, t)) \quad (3.9a)$$

$$f^e(\rho^e(x, t)) = \rho^e v^e = \frac{\mu^e \rho^e(x, t)}{M^e + \rho^e(x, t)}. \quad (3.9b)$$

Herein, ρ^e , f^e and v^e are the density, the flux and the velocity of each arc e , respectively. The buffer zone or the vertex v is the storage area between the end of one arc and the beginning of the next. The storage area at vertex v is necessary to compensating for the discrepancy in incoming flows from the predecessor arcs' outlets and outgoing flows to the successor arcs. Hence, $e^- \in \delta_{v^-}$, where δ_{v^-} is the set of arcs before the vertex v while $e^+ \in \delta_{v^+}$, where δ_{v^+} is the set of arcs after the vertex v . The buffer starts storing lots if the incoming flow is greater than the outgoing flow.

Remark 3.1. From the PDE (3.4), the density of lots $\rho(x, t)$ is non-negative. The density becomes negative when the inflow rate $u(t)$ is greater than the processing rate μ or undefined in case they are equal to each other in the boundary condition BC at (3.5). Therefore, it is necessary to keep the inflow lower than the processing rate. The buffer zone is used to match this property well in this case.

The rate of the change of the buffer load is the difference between the total incoming and outgoing flows and it can be mathematically represented in general form by the ODE

$$\frac{dq_v(t)}{dt} = \sum_{e^- \in \delta_{v^-}} f^{e^-}(1, t) - \sum_{e^+ \in \delta_{v^+}} f^{e^+}(0, t). \quad (3.10)$$

Where $q_v(t)$ is the storage area or the buffer load. In the case of the dispersing network as shown in Fig. 3.12, only one arc and two sub arcs such as $e^- = \{e_1\}$ and $e^+ = \{e_2, e_3\}$ hence, (3.10) becomes

$$\frac{dq_v(t)}{dt} = f^{e_1}(1, t) - \sum_{e^+ \in \delta_{v^+}} f^{e^+}(0, t). \quad (3.11)$$

Besides, the buffer load in (3.11) can be split into sub-buffers and written as

$$\frac{dq_v^{e_2}(t)}{dt} = A_v^{e_2}(t)f^{e_1}(1, t) - f^{e_2}(0, t), \quad (3.12a)$$

$$\frac{dq_v^{e_3}(t)}{dt} = A_v^{e_3}(t)f^{e_1}(1, t) - f^{e_3}(0, t), \quad (3.12b)$$

Here, $A_v^{e^+}(t) \in [0, 1]$ are the fractions. The conservation property holds when the summation of these flows must be equal to the outflow coming from e_1 . This can be achieved by giving the fractions $A_v^{e^+}(t)$ a certain value for each sub arc, so that $\sum A_v^e(t) = 1$ are complementary to each other. For example, if the fraction $A_v^{e_2}(t)$ is 0.1 at arc e_2 , the fraction $A_v^{e_3}$ at arc e_3 is the complement fraction, which is 0.9 from $A_v^{e_3}(t) = 1 - A_v^{e_2}(t)$. The outgoing flows $f^{e^+}(0, t)$ is computed from

$$f^{e^+}(0, t) = \min \left\{ \mu^{e^+}, \frac{q_v^{e^+}}{\kappa} \right\}, \quad 0 < \kappa \ll 1. \quad (3.13)$$

Remark 3.2. *The proposed equation (3.13) is the modified method from [55], $q_v^{e^+}(t)$ is written in this form due to (3.12). If the buffer is imposed as in (3.11) it can be denoted as $q_v(t)$. The scaling factor κ is used to enhance the smoothness of the outgoing flow from the (vertex) buffer zone. The outgoing flow from the vertex is the inflow of the successive flow line as well as the incoming flow to the vertex is the outflow of the preceding flow line.*

Example 3.1. *Consider for the dispersing network, the system parameters with three arcs: the number of machines in each arc is chosen as $M^e = 10$ with the processing rates μ^e being 2, 3 and 4 in e_1 , e_2 and e_3 respectively. The smoothing factor is chosen to be $\kappa = 0.2$ and $A_v^{e_2}(t) = 0.7$, $A_v^{e_3}(t) = 0.3$. The initial conditions for the density $\rho^e(x, 0)$ and the buffer load $q_v^{e^+}$ are zero which means there are no lots in the system at the initial time t_0 . The evolution of the flux inside the network is depicted in Fig. 3.13. As illustrated in Fig 3.14, the inlet (the blue line of the inflow profile) is applied at $x = 0$, and the flux grows in an arc e_1 (top-left). Both outflows of arcs e_2 and e_3 are the system outlets (the red lines). The lots are conserved throughout the system, according to the results. This is verified by integrating both the input and outflow of each arc in the time period with respect to time. The total number of lots at the arc's inlet, e_1 , is 50. These are divided into 35 and 15 lots, respectively, passing arcs e_2 and e_3 .*

3.3.2 Merging Network Design:

In the merging network, all incoming flows come from e_1 and e_2 are combined to enter the main arc e_3 as indicated in Fig. 3.15. The processing rates are μ^{e_1} , μ^{e_2} and μ^{e_3} for the corresponding e_1, e_2 and e_3 , respectively. In the case of the merging condition, the variable $A_v(t)$ is not the same as dispersing condition. The parameter $A_v(t)$ is defined as a fraction of the superimposed

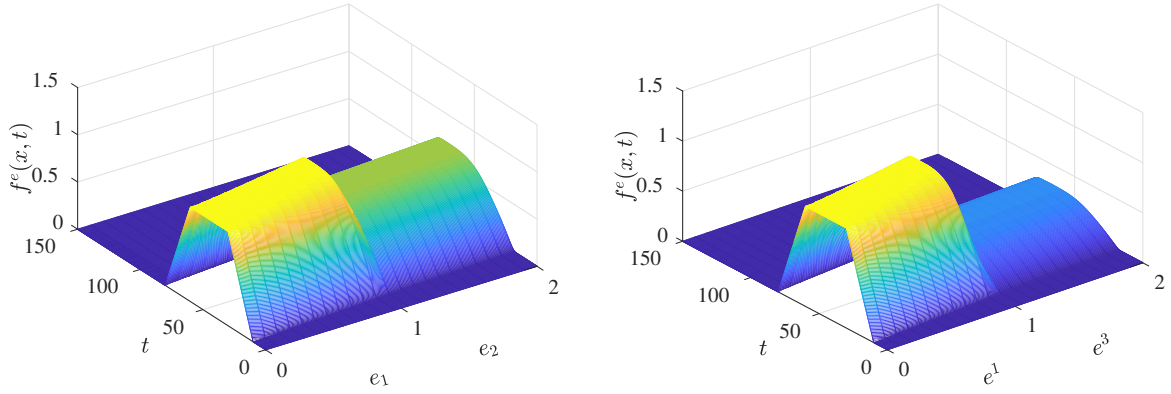


Figure 3.13: In the top, the flow goes through from area e_1 to area e_2 . In the bottom, the flow direction from area e_1 to area e_3 .

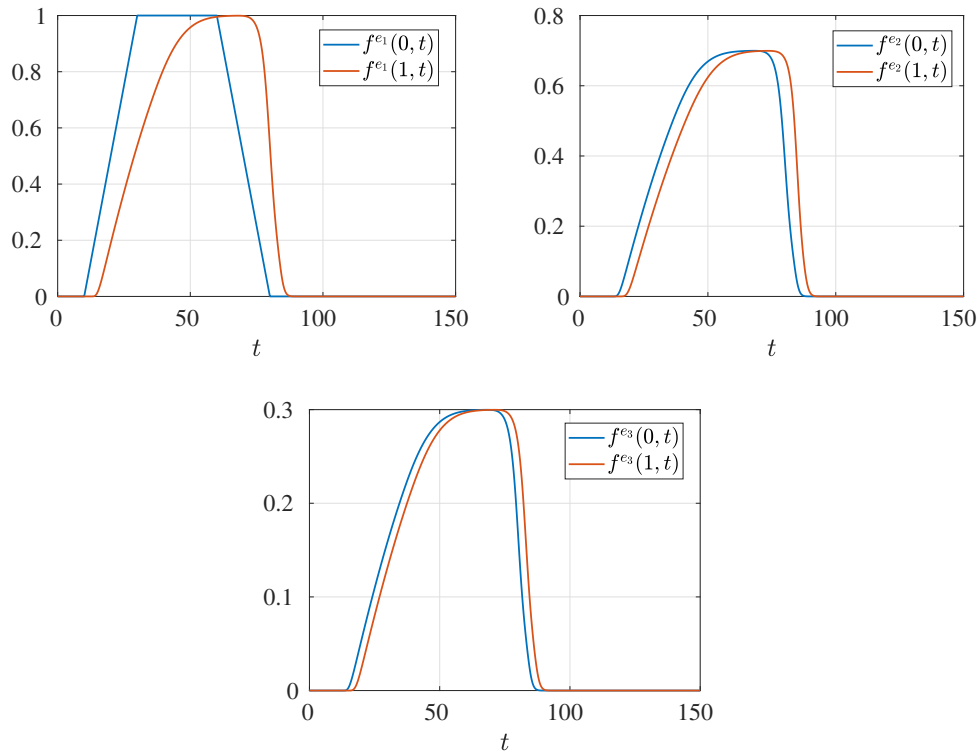


Figure 3.14: The flow state in each flow line e_1 , e_2 and e_3 .

inflows from e_1 and e_2 of the merged arc e_3 . The buffer load $q_v^{e_3}(t)$ obtained from the ODE as declared in [55], for this example becomes

$$\frac{dq_v^{e_3}(t)}{dt} = A_v^{e_3}(t) \sum_{e^- \in \delta_{v^-}} f^{e^-}(1, t) - f^{e_3}(0, t), \quad (3.14a)$$

$$f^{e_3}(0, t) = \min \left\{ \mu^{e_3}, \frac{q_v^{e_3}}{\kappa} \right\}, \quad 0 < \kappa \ll 1, \quad (3.14b)$$

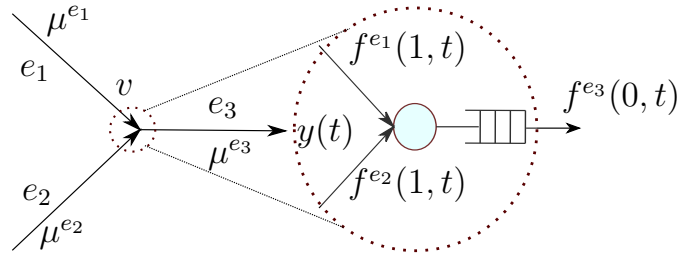


Figure 3.15: Configuration of merging network.

where $f^{e_1}(1, t)$ and $f^{e_2}(1, t)$ are the outflows from the areas e_1 and e_2 , respectively, and $f^{e_3}(0, t)$ is the inflow of the arc e_3 . When the buffer load is empty, the outgoing flow $f^{e_3}(0, t)$ is either a proportion of the sum of all incoming flows, as determined by $A_v^{e_3}(t)$, or the maximum processing capacity.

Example 3.2. Consider the system parameters for the merging network with three arcs: $M^e = 10$ for the number of machines in each arc, with μ^e processing rates of 4, 3, and 2 in e_1 , e_2 , and e_3 , respectively. The smoothing factor is chosen to be $\kappa = 0.2$ and $A_v^{e_3}(t) = 0.8$. There are no lots in the system at the initial time $t_0 = 0$ since the initial conditions for the density $\rho^e(x, 0)$ and the buffer load $q_v^{e^+}$ are zero.

The imposed boundary inflows (inlets) in e_1 and e_2 for the merging network are presented in Fig. 3.16. Because of the processing rate, μ_2^e , the outflow in arc e_2 cannot reach the maximum of the inflow level. The processing rate has a significant impact on system utilization $\Gamma^e = \frac{u^e}{\mu^e}$. The lower the utilization, the higher the processing rate. In the arc, the lots are still being processed. The difference between the inflow and outflow in this case is not zero. The identical situation occurs in arc e_3 . The total number of lots entering e_3 , for example, is 71, with 67 departing the arc at the outlet and 4 remaining processed. Except for inside the storage area (vertex), conservation of mass law holds everywhere in the system. When the utilization Γ^e becomes higher, the time to reach the steady-state is also longer. Therefore, when the inflow is less than and nearly the processing rate, the flow does not reach to the steady state (as shown in arc e_3 of Fig. 3.17) otherwise, it is compensate through the profile by becoming more wider.

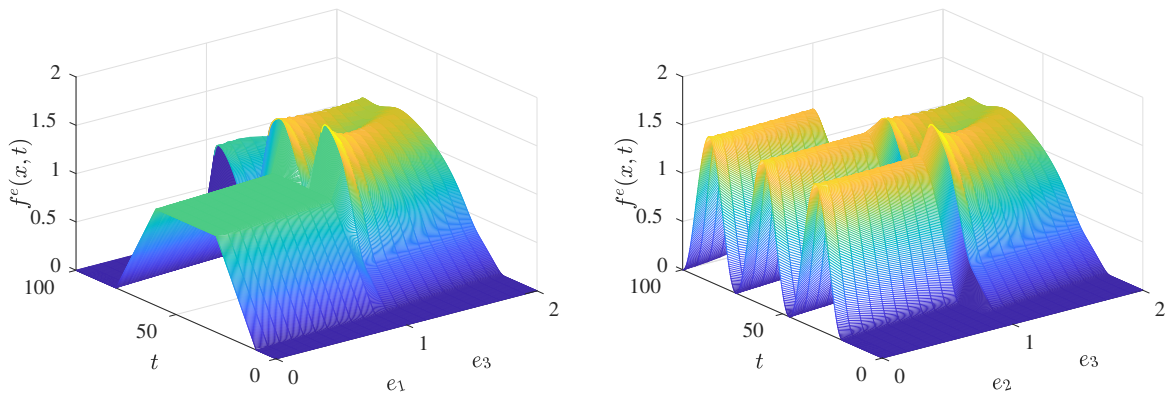


Figure 3.16: In the top, the flow evolution path from area e_1 to area e_3 . In the bottom, the flow evolution path from area e_2 to area e_3 .

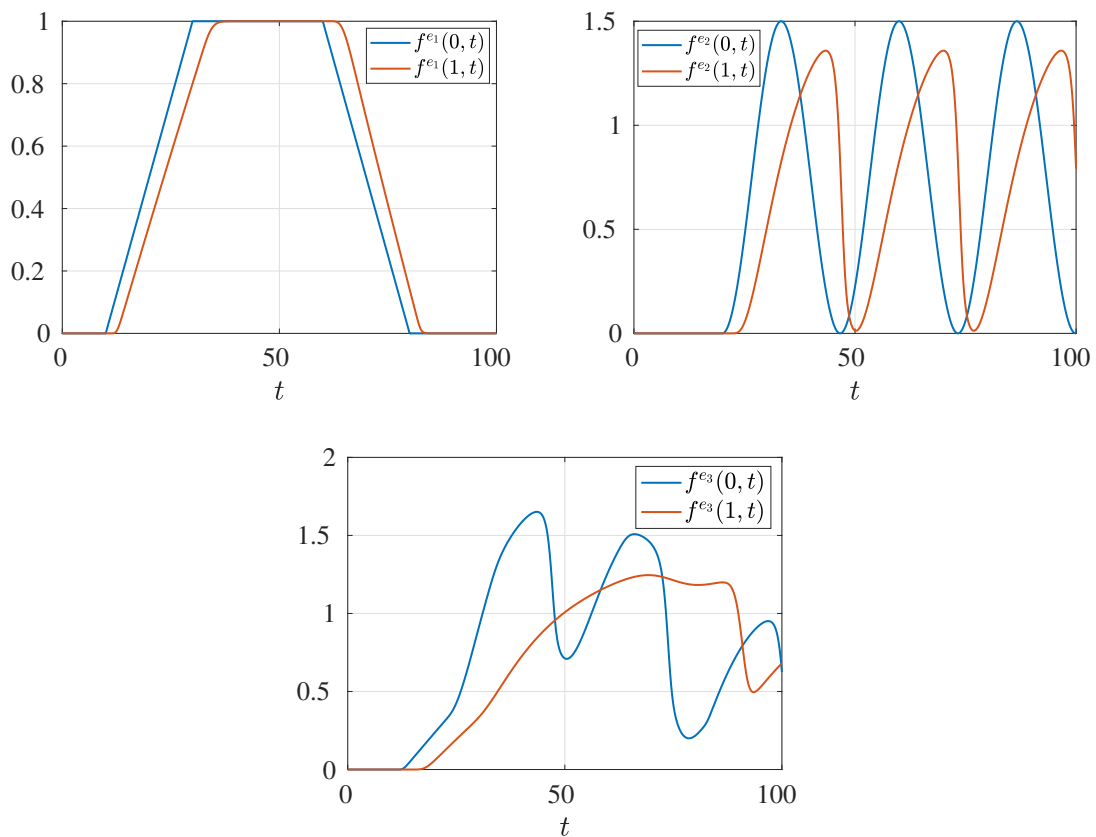


Figure 3.17: The flow state in each flow line e_1 , e_2 and e_3 .

Remark 3.3. In the dispersing example, if these outgoing lots are combined, they would equal the incoming lots at the vertex v . For example, the total number of lots at the inlet of the arc e_1 equals 50 lots. Due to $A_v^{e_2}(t) = 0.7$ and $A_v^{e_3}(t) = 0.3$, these are split into 35 and 15 lots for

arcs e_2 and e_3 , respectively. Therefore, the conservation of mass holds. The case is different in the merging network example due to the fraction $A_v(t)$, which is a percentage of all sum of incoming flows. Here, the total lots exiting from the arc e_1 are 50 lots and the total lots leaving the arc e_2 are 59 lots. If these lots combined together, the total lots are 109 lots but only 80% of them enter the the main flow in arc e_3 because of $A_v(t) = 0.8$. In other words, the parameter $A_v(t)$ prevents part of the system's lots from being utilized at the outgoing flow from the vertex v (the inflow to the arc e_3). As a result, the conservation of mass is restricted. Therefore, the equations (3.14) can be reformulated or modified to be

$$\frac{dq_v^{e_3}(t)}{dt} = \sum_{e^- \in \delta_v^-} f^{e^-}(1, t) - f^{e_3}(0, t), \quad (3.15)$$

$$f^{e_3}(0, t) = \min \left\{ \mu^{e_3} A_v^{e_3}(t), \frac{q_v^{e_3}}{\kappa} \right\}, \quad 0 < \kappa \ll 1. \quad (3.16)$$

Now, the inflow $f^e(0, t)$ is directly influenced by $A_v(t)$, which controls the utilization process of the flow line. Hence, the all lots are conserved inside the whole network.

3.4 Summary

The proposed PDE model flow line for M/M/1 processes is investigated. The model is mathematically specified and the dynamic behaviour is analyzed through ramp-up and ramp-down scenarios. It is also worth comparing the setup utilized for this study in the manufacturing flow line, which is made up of the PDE model, with setting up a DES in ARENA. The goal is to appropriately describe transient and steady-state behaviours of a simple manufacturing system which are considered acceptable results for PDE model validation. The extension of the general models for other distributed processes can be found in Appendix C. In the context of the network of the manufacturing systems, two different topologies are addressed. To construct either dispersing or merging networks, conditions for each vertex of the network are defined. A set of PDEs coupled to a set of ODEs is used to represent it mathematically. Arbitrary inflows are used to show the influence of the flow evolution among the entire network.

Chapter 4

Direct and Indirect Approaches for Optimal Control

4.1 General Overview

The modelling of manufacturing systems was investigated in the previous chapter. Such modelling is prerequisite for the control design. It is worth pointing out that DPS modelled by PDEs have complex dynamic behaviour, which makes the control design more challenging. Therefore, high performance for product quality and manufacturing efficiency, and advanced control systems are required [77, 73]. Control of PDE systems can generally be classified in terms of early and late lumping [75]. In the early lumping the governing PDEs are reduced to a finite-dimensional description using appropriate approximation and model reduction techniques. This contains techniques like finite difference or finite element [72], balanced truncation and correct orthogonal decomposition [94], and variants like inertial manifold approaches [50]. Well-developed control design methods arising from linear and nonlinear finite-dimensional control theory can be employed in this way. On the other hand, the early lumping technique may lead to high and complex control structures without fully exploiting the physical mechanism of the system. Furthermore, the disregarded dynamics may lead to a deterioration of the control performance [8]. Moreover, the validity of the finite-dimensional approximation, and hence the determined controller, is frequently limited to a subset of the state space for nonlinear distributed-parameter systems. As a result, the control action violates the model validity domain and leads to a loss of robustness and unstable behavior of the system [53].

The late lumping strategy incorporates the distributed nature into the control design and system analysis. It thus allows for a strict extension of finite-dimensional systems and control theory to systems defined by PDEs, as shown in [100]. The semigroup approach enables a theoretically powerful generalization of well-known control procedures for finite-dimensional systems in the context of linear systems. Frequency domain techniques is introduced in [76]. Linear and nonlinear semigroup theories are utilized in addition to spectral analysis [70]. Structural assignment of eigenvalues utilizing certain spectral properties of the system operator are

described in [109]. Also, many different methods are employed for numerous applications, see, e.g., [66, 11, 58, 75].

In the context of the optimal control, it is used widely in various applications modelled by PDEs, see, e.g., [68, 32, 90, 69, 63]. In this chapter, the goal is to design open-loop optimal boundary control for manufacturing systems to handle demand tracking and backlog problems. The optimal control approaches are examined based on conservation laws coupled with ODEs in different interconnection topologies that correspond to dispersing and merging networks to handle this challenge.

4.2 Background

In this section, some definitions of linear function spaces are covered, such as the properties of Banach and Hilbert spaces that help to analyse and design the optimal control.

Definition 4.1 (Normed space, Banach space [57]). *A normed space X is a vector space with a norm defined on it, a Banach space is a complete normed space. Here a norm on a (real or complex) vector space X is a real-valued function on X , whose value at an $x \in X$ is denoted by $\|x\|$ and which has the properties*

$$\begin{aligned}\|x\| &\geq 0 \\ \|x\| = 0 &\iff x = 0 \\ \|\alpha x\| &= |\alpha| \|x\| \\ \|x + y\| &\leq \|x\| + \|y\|\end{aligned}$$

here x and y are arbitrary vectors in X and α is a (real or complex) scalar. A norm on X defines a metric d on X which is given by

$$d(x, y) = \|x - y\| \quad \forall x, y \in X$$

and is called the metric induced by the norm. The normed space just defined is denoted by $(X, \|\cdot\|)$ or simply by X .

Definition 4.2 (Inner product space, Hilbert space [57]). *An inner product space (or pre-Hilbert space) is a vector space X with an inner product defined on X . A Hilbert space is a complete inner product space (complete in the metric defined by the inner product). Here, an inner product on X is a mapping of $X \times X$ into the scalar field K of X ; that is, with every pair of vectors x and y there is associated a scalar which is written $\langle \cdot, \cdot \rangle$ and is called the inner product of x and y , such that for all vectors x, y, z and scalars $\alpha \in K$ we have*

$$\begin{aligned}\langle x + y, z \rangle &= \langle x, z \rangle + \langle y, z \rangle \\ \langle x, x \rangle &\geq 0 \\ \langle x, x \rangle = 0 &\iff x = 0 \\ \langle \alpha x, y \rangle &= \alpha \langle x, y \rangle, \quad \alpha \in \mathbb{R} \\ \langle x, y \rangle &= \overline{\langle y, x \rangle},\end{aligned}$$

where the bar in $\overline{\langle y, x \rangle}$ refers to the complex conjugation. An inner product on X defines a norm on X given by

$$\|x\| = \sqrt{\langle x, x \rangle}$$

and a metric on X given by

$$d(x, y) = \|x - y\| = \sqrt{\langle x - y, x - y \rangle}.$$

Hence inner product spaces are normed spaces, and Hilbert spaces are Banach spaces.

Definition 4.3 (Gateaux Derivative [35]). Let f be a function on an open subset U of a Banach space X into the Banach space Y . We say f is Gateaux differentiable at $x \in U$ if there exists a bounded and linear operator $\delta : X \rightarrow Y$ such that

$$\lim_{t \rightarrow 0} \frac{f(x + th) - f(x)}{t} = \delta f$$

for every $h \in X$. The operator δ is called the Gateaux derivative of f at x .

4.3 Demand Tracking Problem

The demand tracking problem represents the mismatch between the rate of the desired demand and the outflow at the outlet of the system over a fixed time interval. The elimination of such effect is required by control the flow on the network along a prescribed desired outflow trajectory. The optimal control for the demand tracking is applied by considering the objective functional

$$\min_{\boldsymbol{\vartheta}} J_1(\boldsymbol{\vartheta}) = \frac{1}{2} \int_0^{t_f} (f^*(t) - y(t))^2 dt, \quad (4.1)$$

where the decision variables supplied by u , $A_v^{e_v^+}$ are then summarized by $\boldsymbol{\vartheta}$, $f^*(t)$ is the desired trajectory. The outflow $y(t) = f^{e_3}(1, t)$ is considered in the arc e_3 for the dispersing network as shown in Fig 3.12 or for the merging network as depicted in Fig 3.15. The optimization is handled for the control interval between $t = 0$ and t_f , where t_f refers to the final time.

Remark 4.4. For the sake of simplicity, the control variable $u(t)$ is picked at the inlet of the arc e_1 and the outflow $y(t)$ that has to be controlled is chosen at the arc e_3 regardless of the network type dispersing or merging. For example, in the dispersing case, if the controlled outputs exist at the arc e_2 and e_3 , respectively, that leads to suboptimal solution.

The network models from the previous chapter are recalled that are required to be managed,

and the system dynamics of the dispersing network are described as

$$\begin{aligned}
\frac{\partial}{\partial t} \rho^e(x, t) &= -\frac{\partial}{\partial x} f^e(x, t), \quad (x, t) \in (0, 1] \times (0, \mathbb{R}_0^+], \\
f^e(x, t) &= \rho^e v^e = \frac{\mu^e \rho^e(x, t)}{M^e + \rho^e(x, t)}, \\
\frac{dq_v^{e^+}(t)}{dt} &= A_v^{e^+}(t) f^{e^-}(1, t) - f^{e^+}(0, t), \\
\rho^e(x, 0) &= 0, \quad \forall x \in [0, 1], \\
\mathbb{R}_0^+ &= \{t \in \mathbb{R} : t > 0\}, \\
f^{e^+}(0, t) &= \min \left\{ \mu^{e^+}, \frac{q_v^{e^+}(t)}{\kappa} \right\}, \\
f^{e_1}(0, t) &= u(t), \quad \forall t \in [0, \mathbb{R}_0^+], \\
q_v^e(0) &= 0, \quad \sum_{e^+ \in \{e_2, e_3\}} A_v^{e^+}(t) = 1, \\
0 &\leq A_v^{e^+}(t) \leq 1, \quad 0 \leq u(t) < \mu^{e_1}, \\
e^- &\in \{e_1\}, \quad \forall e^+ \in \{e_2, e_3\}, \quad \forall e \in \mathcal{E}.
\end{aligned} \tag{4.2}$$

The main inflow $u(t)$ at the inlet of arc e_1 is the boundary condition and \mathcal{E} is the set of the all arcs. For the merging topology, the system dynamics are given as

$$\begin{aligned}
\frac{\partial}{\partial t} \rho^e(x, t) &= -\frac{\partial}{\partial x} f^e(x, t), \quad (x, t) \in (0, 1] \times (0, \mathbb{R}_0^+], \\
f^e(x, t) &= \rho^e v^e = \frac{\mu^e \rho^e(x, t)}{M^e + \rho^e(x, t)}, \\
\frac{dq_v^{e^+}(t)}{dt} &= A_v(t) \sum_{e^- \in \{e_1, e_2\}} f^{e^-}(1, t) - f^{e^+}(0, t), \\
\rho^e(x, 0) &= 0, \quad \forall x \in [0, 1], \\
f^{e_1}(0, t) &= u(t), \quad f^{e_2}(0, t) = \tilde{u}(t), \\
f^{e^+}(0, t) &= \min \left\{ \mu^{e^+}, \frac{q_v^{e^+}(t)}{\kappa} \right\}, \quad \forall t \in [0, \mathbb{R}_0^+], \\
q_v^{e^+}(0) &= 0, \quad \mathbb{R}_0^+ = \{t \in \mathbb{R} : t > 0\}, \\
0 &\leq u(t) < \mu^{e_1}, \quad 0 \leq \tilde{u}(t) < \mu^{e_2}, \quad 0 \leq A_v(t) \leq 1, \\
\forall e^- &\in \{e_1, e_2\}, \quad e^+ \in \{e_3\}, \quad \forall e \in \mathcal{E}.
\end{aligned} \tag{4.3}$$

Herein \tilde{u} is an arbitrary uncontrolled inflow at arc e_2 and \mathcal{E} denotes the set of the all arcs. The OCP for the demand tracking is considered according to the dispersing or the merging networks. Therefore, the dispersing optimization problem is structured as

$$\min_{\boldsymbol{\vartheta}} J_1(\boldsymbol{\vartheta}), \quad \text{subject to (4.2)}. \tag{4.4}$$

The merging optimization problem is structured as

$$\min_{\boldsymbol{\vartheta}} J_1(\boldsymbol{\vartheta}), \quad \text{subject to (4.3).} \quad (4.5)$$

different mechanisms are investigated to solve the above-mentioned problems by indirect and direct methods.

4.3.1 Indirect Method

The approach is classified under late lumping. It is focused on the optimize-then-discretize technique. Hence, the optimization is performed for the infinite-dimensional system. The Lagrangian L is constructed according to the system network.

Dispersing Network

The general Lagrangian \mathcal{L} considering the inequality constraints of problem (4.4) is defined as follows

$$\begin{aligned} \mathcal{L} = & \frac{1}{2} \int_0^{t_f} (f^*(t) - y(t))^2 dt \\ & + \sum_{e \in \mathcal{E}} \int_0^{t_f} \int_0^1 \lambda^e \left(\frac{\partial}{\partial t} \rho^e + \frac{\partial}{\partial x} f^e(x, t) \right) dx dt \\ & + \sum_{e^+ \in \{e_2, e_3\}} \int_0^{t_f} \phi_v^{e^+} \left(\dot{q}_v^{e^+} - A_v^{e_3} f^{e^-}(1, t) + f^{e^+}(0, t) \right) dt \\ & \left. \begin{aligned} & + \eta_1(u(t) - \mu^{e_1}) + \eta_2(u(t) - 0) \\ & + \eta_3(A_v^{e_3}(t) - 1) + \eta_4(A_v^{e_3}(t) - 0). \end{aligned} \right\} (\star) \end{aligned} \quad (4.6)$$

The additional term (\star) refers to the Lagrange multipliers with the inequality constraints. In the rest of the thesis, for the sake of simplicity, this part is not considered analytically to construct the adjoint equations to get the gradient information. After that, the numerical optimizer is used to fulfil the inequality constraints.

The Lagrangian L of problem (4.4) is defined according to [99] gets

$$\begin{aligned} L_1 = & \frac{1}{2} \int_0^{t_f} (f^*(t) - y(t))^2 dt \\ & + \sum_{e \in \mathcal{E}} \int_0^{t_f} \int_0^1 \lambda^e \left(\frac{\partial}{\partial t} \rho^e + \frac{\partial}{\partial x} f^e(x, t) \right) dx dt \\ & + \sum_{e^+ \in \{e_2, e_3\}} \int_0^{t_f} \phi_v^{e^+} \left(\dot{q}_v^{e^+} - A_v^{e_3} f^{e^-}(1, t) + f^{e^+}(0, t) \right) dt. \end{aligned} \quad (4.7)$$

The functions $\lambda^e(x, t)$ and $\phi_v^{e^+}(t)$ are the adjoint states for the equality constraints induced by the PDEs on the arcs and the ODEs at the vertices, respectively. After using the integration by parts the Lagrangian form of the network is obtained as follow

$$\begin{aligned}
L_1 = & \frac{1}{2} \int_0^{t_f} (f^*(t) - y(t))^2 dt \\
& + \sum_{e \in \mathcal{E}} \int_0^1 \lambda^e(x, t_f) \rho^e(x, t_f) dx \\
& - \sum_{e \in \mathcal{E}} \int_0^{t_f} \int_0^1 \frac{\partial \lambda^e}{\partial t} \rho^e dx dt + \sum_{e \in \mathcal{E}} \int_0^{t_f} \lambda^e(1, t) f^e(1, t) dt \\
& - \sum_{e \in \mathcal{E}} \int_0^{t_f} \lambda^e(0, t) f^e(0, t) dt - \sum_{e \in \mathcal{E}} \int_0^{t_f} \int_0^1 \frac{\partial \lambda^e}{\partial x} f^e(x, t) dx dt \\
& + \left[\sum_{e^+ \in \{e_2, e_3\}} \phi_v^{e^+} q_v^{e^+} \right]_{t=0}^{t=t_f} - \sum_{e^+ \in \{e_2, e_3\}} \int_0^{t_f} \dot{\phi}_v^{e^+} q_v^{e^+} dt \\
& + \sum_{e^+ \in \{e_2, e_3\}} \int_0^{t_f} \phi_v^{e^+} \left(f^{e^+}(0, t) - A_v^{e^+} f^{e^-}(1, t) \right) dt.
\end{aligned}$$

Using the relationships given by the system

$$\begin{aligned}
u(t) &= f^{e_1}(0, t), \\
y(t) &= f^{e_3}(1, t),
\end{aligned}$$

the first-order optimality condition for the dispersing network is established by evaluating the Gateaux derivative of L

$$\begin{aligned}
\delta L_1 = & - \int_0^{t_f} (f^*(t) - y(t)) \delta y(t) dt + \sum_{e \in \mathcal{E}} \int_0^1 \lambda^e(x, t_f) \delta \rho^e(x, t_f) dx \\
& - \sum_{e \in \mathcal{E}} \int_0^{t_f} \int_0^1 \frac{\partial \lambda^e(x, t)}{\partial t} \delta \rho^e(x, t) dx dt + \int_0^{t_f} \lambda^{e_3}(1, t) \delta y(t) dt \\
& + \int_0^{t_f} \lambda^{e_2}(1, t) \delta f^{e_2}(1, t) dt - \int_0^{t_f} \lambda^{e_2}(0, t) \delta f^{e_2}(0, t) dt \\
& + \int_0^{t_f} \lambda^{e_1}(1, t) \delta f^{e_1}(1, t) dt - \int_0^{t_f} \lambda^{e_1}(0, t) \delta u dt \\
& - \int_0^{t_f} \lambda^{e_3}(0, t) \delta f^{e_3}(0, t) dt - \sum_{e \in \mathcal{E}} \int_0^{t_f} \int_0^1 \left(\frac{\mu^e M^e}{(M^e + \rho^e(x, t))^2} \right) \frac{\partial \lambda^e(x, t)}{\partial x} \delta \rho^e(x, t) dx dt \\
& - \int_0^{t_f} \phi^{e_3}(t) f^{e^-}(1, t) \delta A_v^{e_3} dt - \int_0^{t_f} \phi^{e_3}(t) A_v^{e_3}(t) \delta f^{e_1}(1, t) dt \\
& - \int_0^{t_f} \phi^{e_2}(t) f^{e^-}(1, t) \delta A_v^{e_2} dt - \int_0^{t_f} \phi^{e_2}(t) A_v^{e_2}(t) \delta f^{e_1}(1, t) dt
\end{aligned}$$

$$\begin{aligned}
& + \int_0^{t_f} \phi^{e_2}(t) \delta f^{e_2}(0, t) dt + \int_0^{t_f} \phi^{e_3}(t) \delta f^{e_3}(0, t) dt \\
& + \left[\sum_{e^+ \in \{e_2, e_3\}} \phi_v^{e^+} q_v^{e^+} \right]_{t=0}^{t=t_f} - \sum_{e^+ \in \{e_2, e_3\}} \int_0^{t_f} \dot{\phi}_v^{e^+} q_v^{e^+} dt \\
& = 0.
\end{aligned}$$

By substituting $\delta(1 - A_v^{e_3}) = \delta A_v^{e_2}$ from the complementary equation, after that, the final step is regrouping to obtain the adjoint equations in the form

$$\begin{aligned}
\frac{\partial}{\partial t} \lambda^e(x, t) &= - \left(\frac{\mu^e M^e}{(M^e + \rho^e(x, t))^2} \right) \frac{\partial}{\partial x} \lambda^e(x, t), \\
\lambda^e(x, t_f) &= 0, \\
\lambda^{e_3}(1, t) &= f^*(t) - y(t), \\
\phi_v^{e_2}(t) &= \lambda^{e_2}(0, t), \\
\phi_v^{e_3}(t) &= \lambda^{e_3}(0, t), \\
\delta_u J(t) &= -\lambda^{e_1}(0, t), \\
\lambda^{e_1}(1, t) &= \lambda^{e_2}(0, t) A_v^{e_2}(t) + \lambda^{e_3}(0, t) A_v^{e_3}(t), \\
\delta_{A_v^{e_3}} J(t) &= (\lambda^{e_2}(0, t) - \lambda^{e_3}(0, t)) f^{e_1}(1, t).
\end{aligned} \tag{4.8}$$

Herein, $\delta_{A_v^{e_3}} J(t)$ refers to the variational derivative with respect to the fraction $A_v^{e_3}$. The variational derivative with respect to the inflow u is denoted by $\delta_u J(t)$, whereas the terminal and boundary conditions are denoted by $\lambda^e(x, t_f)$ and $\lambda^{e_3}(1, t)$, respectively.

Remark 4.5. *The outflow at the arc e_2 is arbitrary because the only interesting outflow from the optimization problem that has to be tracked is the outflow of the arc e_3 . Therefore, the adjoint state $\lambda^{e_2}(x, t)$ is considered to be zero to reduce the computational burden and the compact form of the adjoint equation (4.8) is expressed as*

$$\begin{aligned}
\frac{\partial}{\partial t} \lambda^e(x, t) &= - \left(\frac{\mu^e M^e}{(M^e + \rho^e(x, t))^2} \right) \frac{\partial}{\partial x} \lambda^e(x, t), \\
\lambda^e(x, t_f) &= 0, \\
\lambda^{e_3}(1, t) &= f^*(t) - y(t), \\
\phi_v^{e_3}(t) &= \lambda^{e_3}(0, t), \\
\delta_u J(t) &= -\lambda^{e_1}(0, t), \\
\lambda^{e_1}(1, t) &= \lambda^{e_3}(0, t) A_v^{e_3}(t), \\
\delta_{A_v^{e_3}} J(t) &= -\lambda^{e_3}(0, t) f^{e_1}(1, t).
\end{aligned} \tag{4.9}$$

Merging Network

The Lagrangian L of problem (4.5) is obtained as

$$\begin{aligned}
L_2 = & \frac{1}{2} \int_0^{t_f} (f^*(t) - y(t))^2 dt \\
& + \sum_{e \in \mathcal{E}} \int_0^{t_f} \int_0^1 \lambda^e \left(\frac{\partial}{\partial t} \rho^e + \frac{\partial}{\partial x} f^e(x, t) \right) dx dt \\
& + \int_0^{t_f} \phi_v^{e^+} \left(\dot{q}_v^{e^+} - A_v \sum_{e^- \in \{e_1, e_2\}} f^{e^-}(1, t) + f^{e^+}(0, t) \right) dt.
\end{aligned} \tag{4.10}$$

After applying integration by parts one obtains

$$\begin{aligned}
L_2 = & \frac{1}{2} \int_0^{t_f} (f^*(t) - y(t))^2 dt \\
& + \sum_{e \in \mathcal{E}} \int_0^1 \lambda^e(x, t_f) \rho^e(x, t_f) dx \\
& - \sum_{e \in \mathcal{E}} \int_0^{t_f} \int_0^1 \frac{\partial \lambda^e}{\partial t} \rho^e dx dt + \sum_{e \in \mathcal{E}} \int_0^{t_f} \lambda^e(1, t) f^e(1, t) dt \\
& - \sum_{e \in \mathcal{E}} \int_0^{t_f} \lambda^e(0, t) f^e(0, t) dt - \sum_{e \in \mathcal{E}} \int_0^{t_f} \int_0^1 \frac{\partial \lambda^e}{\partial x} f^e(x, t) dx dt \\
& + \left[\phi_v^{e^+} q_v^{e^+} \right]_{t=0}^{t=t_f} - \int_0^{t_f} \dot{\phi}_v^{e^+} q_v^{e^+} dt \\
& + \int_0^{t_f} \phi_v^{e^+} \left(f^{e^+}(0, t) - A_v(t) \sum_{e^- \in \{e_1, e_2\}} f^{e^-}(1, t) \right) dt.
\end{aligned}$$

By using the relationships provided by the system

$$\begin{aligned}
u(t) &= f^{e_1}(0, t), \\
y(t) &= f^{e_3}(1, t),
\end{aligned}$$

the Gateaux derivative of L reads

$$\begin{aligned}
\delta L_2 = & - \int_0^{t_f} (f^*(t) - y(t)) \delta y(t) dt + \sum_{e \in \mathcal{E}} \int_0^1 \lambda^e(x, t_f) \delta \rho^e(x, t_f) dx \\
& - \sum_{e \in \mathcal{E}} \int_0^{t_f} \int_0^1 \frac{\partial \lambda^e(x, t)}{\partial t} \delta \rho^e(x, t) dx dt + \int_0^{t_f} \lambda^{e_3}(1, t) \delta y(t) dt \\
& + \int_0^{t_f} \lambda^{e_1}(1, t) \delta f^{e_1}(1, t) dt - \int_0^{t_f} \lambda^{e_1}(0, t) \delta u dt \\
& + \int_0^{t_f} \lambda^{e_2}(1, t) \delta f^{e_2}(1, t) dt - \int_0^{t_f} \lambda^{e_2}(0, t) \delta f^{e_2}(0, t) dt \\
& - \int_0^{t_f} \lambda^{e_3}(0, t) \delta f^{e_3}(0, t) dt - \sum_{e \in \mathcal{E}} \int_0^{t_f} \int_0^1 \left(\frac{\mu^e M^e}{(M^e + \rho^e(x, t))^2} \right) \frac{\partial \lambda^e(x, t)}{\partial x} \delta \rho^e(x, t) dx dt
\end{aligned}$$

$$\begin{aligned}
& - \int_0^{t_f} \phi^{e_3}(t) \left(f^{e_1}(1, t) + f^{e_2}(1, t) \right) \delta A_v(t) dt - \int_0^{t_f} \phi^{e_3}(t) A_v(t) \delta f^{e_1}(1, t) dt \\
& + \int_0^{t_f} \phi^{e_3}(t) \delta f^{e_3}(0, t) dt - \int_0^{t_f} \phi^{e_3}(t) A_v(t) \delta f^{e_2}(1, t) dt \\
& = 0.
\end{aligned}$$

The final step is regrouping to obtain the adjoint equations in the form

$$\begin{aligned}
\frac{\partial}{\partial t} \lambda^e(x, t) &= - \left(\frac{\mu^e M^e}{(M^e + \rho^e(x, t))^2} \right) \frac{\partial}{\partial x} \lambda^e(x, t), \\
\lambda^e(x, t_f) &= 0, \\
\lambda^{e_3}(1, t) &= f^*(t) - y(t), \\
\phi_v^{e_3}(t) &= \lambda^{e_3}(0, t), \\
\delta_u J(t) &= -\lambda^{e_1}(0, t), \\
\lambda^{e_1}(1, t) &= A_v(t) \lambda^{e_3}(0, t), \\
\delta_{A_v} J(t) &= -\lambda^{e_3}(0, t) (f^{e_1}(1, t) + f^{e_2}(1, t)).
\end{aligned} \tag{4.11}$$

Herein, $\delta_{A_v} J(t)$ refers to the variational derivative with respect to the fraction A_v .

4.3.1.1 Discretization Approach for the Numerical Solution

For the discretization, an upwind scheme is used for spatial discretization, and the explicit Euler method is applied for time discretization. Let $\Delta x = 1/M^e$ and Δt denote the spatial and time step where Δt and Δx are connected by the Courant-Friedrichs-Lewy condition $CFL = \frac{V_m^e \Delta t}{\Delta x} \leq 1$ for numerical stability purposes, where $V_m^e = \frac{\mu^e}{M^e + \rho_{\min}^e}$ is the maximum speed of the arc e . In addition introduce $\rho_{i,j}^e = \rho^e(i\Delta x, j\Delta t)$, $f_{i,j}^e = f^e(i\Delta x, j\Delta t)$, $q_{v,j}^{e+} = q_v^{e+}(j\Delta t)$, $y_j = y(j\Delta t)$, $u_j = u(j\Delta t)$, $A_{v,j} = A_v(j\Delta t)$ for $i = 1, 2, \dots, M^e$, $j = 0, 1, \dots, N$. The system dynamics (4.2) for the dispersing network are discretized as

$$\begin{aligned}
\rho_{i,j+1}^e &= \rho_{i,j}^e - \frac{\Delta t}{\Delta x} (f_{i,j}^e - f_{i-1,j}^e), \\
q_{v,j+1}^{e_2} &= q_{v,j}^{e_2} + \Delta t \left(A_{v,j}^{e_2} f_{M^e,j}^{e_1} - f_{0,j}^{e_2} \right), \\
q_{v,j+1}^{e_3} &= q_{v,j}^{e_3} + \Delta t \left((1 - A_{v,j}^{e_2}) f_{M^e,j}^{e_1} - f_{0,j}^{e_3} \right), \\
f_{0,j}^{e+} &= \min \left\{ \mu^{e+}, \frac{q_{v,j}^{e+}}{\kappa} \right\}, \\
\rho_{i,0}^e &= 0, \quad q_{v,0}^{e+} = 0, \quad f_{0,j}^{e_1} = u_j \\
e^+ &\in \{e_2, e_3\}, \quad 0 \leq u_j < \mu^{e_1}, \quad 0 \leq A_{v,j}^{e+} \leq 1,
\end{aligned} \tag{4.12}$$

In the case of the merging network, the PDEs/ODE in (4.3) are discretized in the form

$$\begin{aligned}
\rho_{i,j+1}^e &= \rho_{i,j}^e - \frac{\Delta t}{\Delta x} (f_{i,j}^e - f_{i-1,j}^e), \\
q_{v,j+1}^{e+} &= q_{v,j}^{e+} + \Delta t \left(A_{v,j} \sum_{e^- \in \{e_1, e_2\}} f_{M^e, j}^{e-} - f_{0,j}^{e+} \right), \\
f_{0,j}^{e+} &= \min \left\{ \mu^{e+}, \frac{q_{v,j}^{e+}}{\kappa} \right\}, \\
\rho_{i,0}^e &= 0, \quad q_{v,0}^{e+} = 0, \quad f_{0,j}^{e_1} = u_j \\
e^+ &\in \{e_3\}, \quad 0 \leq u_j < \mu^{e_1}, \quad 0 \leq A_{v,j} \leq 1.
\end{aligned} \tag{4.13}$$

The adjoint equations are discretized for $i = M^e - 1, \dots, 2, 1$, $j = N + 1, \dots, 2, 1$, according to the discretized form of (4.9) in the dispersing network becomes

$$\begin{aligned}
\lambda_{i,j-1}^e &= \lambda_{i,j}^e - \frac{\Delta t}{\Delta x} \left(\frac{\mu^e M^e}{(M^e + \rho_{i,j}^e)^2} \right) (\lambda_{i+1,j}^e - \lambda_{i,j}^e), \\
\lambda_{i,N}^e &= 0, \\
\lambda_{M^e, j}^{e_3} &= f_j^* - y_j, \\
\phi_{v,j}^{e_3} &= \lambda_{0,j}^{e_3}, \\
\delta_u J_j &= -\lambda_{0,j}^{e_1}, \\
\lambda_{M^e, j}^{e_1} &= \lambda_{0,j}^{e_3} A_{v,j}^{e_3}, \\
\delta_{A_v^{e_3}} J_j &= -\lambda_{0,j}^{e_3} f_{M^e, j}^{e_1}.
\end{aligned} \tag{4.14}$$

While for the merging network (4.11) implies

$$\begin{aligned}
\lambda_{i,j-1}^e &= \lambda_{i,j}^e - \frac{\Delta t}{\Delta x} \left(\frac{\mu^e M^e}{(M^e + \rho_{i,j}^e)^2} \right) (\lambda_{i+1,j}^e - \lambda_{i,j}^e), \\
\lambda_{i,N}^e &= 0, \\
\lambda_{M^e, j}^{e_3} &= f_j^* - y_j, \\
\phi_{v,j}^{e_3} &= \lambda_{0,j}^{e_3}, \\
\delta_u J_j &= -\lambda_{0,j}^{e_1}, \\
\lambda_{M^e, j}^{e_1} &= A_{v,j} \lambda_{0,j}^{e_3}, \\
\delta_{A_v} J_j &= -\lambda_{0,j}^{e_3} (f_{M^e, j}^{e_1} + f_{M^e, j}^{e_2}).
\end{aligned} \tag{4.15}$$

The discretized state equations are solved forward in time while the discretized adjoint equations are solved backward in time. The gradients are then computed from (4.14) or (4.15), respectively, and are combined with the SQP solver in the MATLAB function `fmincon` to find local minimizers $\boldsymbol{\vartheta}$. For the inequality constraints $0 \leq u_j < \mu^{e_1}$ and $0 \leq A_{v,j}^{e_3} \leq 1$ for the dispersing network or $0 \leq u_j < \mu^{e_1}$ and $0 \leq A_{v,j} \leq 1$ for the merging network, the corresponding optimal values can be obtained by Pontryagin's maximum principle [29]. However, in addition to the substantial analytical effort required to obtain the gradient information by imposing these constraints is tedious work. Accordingly, these inequality constraints are handled numerically by the function `fmincon`.

4.3.2 Direct Method

Alternatively, the method is based on discretize-then-optimize mechanism and is classified under the early lumping approach for PDE control design. In the direct approach, the optimization problem (4.4) for the dispersing network or (4.5) for the merging network are fully discretized to obtain

$$\min_{\boldsymbol{\vartheta}} J_{1d}(\boldsymbol{\vartheta}) = \frac{1}{2} \sum_{j=0}^N (f_j^* - y_j)^2 \Delta t, \quad (4.16)$$

subject to (4.12) or (4.13) in the case of the dispersing network or the case of the merging network, respectively. After the discretization is performed by the upwind finite difference scheme for the PDEs and explicit Euler for the ODEs, the problem is generally formulated as a static optimization problem by

$$\begin{aligned} & \min_{\boldsymbol{\vartheta}} J_{1d}(\boldsymbol{\vartheta}) \\ & \text{subject to} \\ & g_j(\boldsymbol{\vartheta}) = 0, \quad j = 1, 2, \dots, r, \\ & h_l(\boldsymbol{\vartheta}) \leq 0, \quad l = 1, 2, \dots, p, \end{aligned} \quad (4.17)$$

where $g_j(\boldsymbol{\vartheta})$ are the equality constraints and $h_l(\boldsymbol{\vartheta})$ denote for the inequality constraints. The Karush-Kuhn-Tucker (KKT) conditions must be satisfied in order to solve the optimal control problem in (4.17). The optimizers are obtained by satisfying KKT first-order necessary optimality conditions [14], which is defined as follows

$$\begin{aligned} \nabla J_{1d}(\boldsymbol{\vartheta}^*) + \sum_{j=1}^r \lambda_j \nabla g_j(\boldsymbol{\vartheta}^*) + \sum_{l=1}^p \Lambda_l \nabla h_l(\boldsymbol{\vartheta}^*) &= 0 \\ g_j(\boldsymbol{\vartheta}^*) &= 0, \quad j = 1, 2, \dots, r, \\ h_l(\boldsymbol{\vartheta}^*) &\leq 0, \quad l = 1, 2, \dots, p, \\ \Lambda_l &\geq 0, \quad l = 1, 2, \dots, p, \\ \Lambda_l h_l(\boldsymbol{\vartheta}^*) &= 0, \quad l = 1, 2, \dots, p. \end{aligned} \quad (4.18)$$

Herein, the optimizers are defined by $\boldsymbol{\vartheta}^*$ besides λ_j , and Λ_l are the Lagrange multipliers for equality and inequality constraints, respectively. The optimization problem is solved using sequential quadratic programming (SQP) in `fmincon` provided by MATLAB. The control variables $\boldsymbol{\vartheta}$ are needed as an initial guess to solve the problem. In each iteration, the gradient is updated by finding a new step length and search direction.

4.4 Backlog Problem

The backlog problem represents the mismatch between the total number of lots at the outlet and the desired accumulation of lots over a fixed time interval. The backlog is categorized into two types: (i) positive backlog (under-production), (ii) negative backlog (over-production). The backlog $B(t)$ is mathematically expressed as

$$B(t) = \int_0^t (f^*(\tau) - y(\tau))d\tau, \quad \forall t \in [0, t_f], \quad (4.19)$$

where f^* is the desired reference and y is the outflow at a certain time τ of the outlet. Note that the optimal control applies both stage cost and terminal cost by considering the objective functional

$$\min_{\boldsymbol{\vartheta}} J_2(\boldsymbol{\vartheta}) = \frac{1}{2} \int_0^{t_f} (B(t))^2 dt + \frac{1}{2} (B(t_f))^2, \quad (4.20)$$

where the decision variables supplied by u, A_v are then aggregated by $\boldsymbol{\vartheta}$. To this end, the OCP for the backlog is considered according to the dispersing or the merging networks. Therefore, the dispersing optimization problem is structured as

$$\min_{\boldsymbol{\vartheta}} J_2(\boldsymbol{\vartheta}), \quad \text{subject to (4.2)}. \quad (4.21)$$

The merging optimization problem is structured as

$$\min_{\boldsymbol{\vartheta}} J_2(\boldsymbol{\vartheta}), \quad \text{subject to (4.3)}. \quad (4.22)$$

4.4.1 Indirect Method

In this approach, the optimization is performed for the infinite-dimensional system. The Lagrangian L is determined based on the type of the network, either dispersing or merging.

Dispersing Network

The Lagrangian L of problem (4.21) is obtained as

$$\begin{aligned} L_3 = & \frac{1}{2} \int_0^{t_f} (B(t))^2 dt + \frac{1}{2} (B(t_f))^2 \\ & + \sum_{e \in \mathcal{E}} \int_0^{t_f} \int_0^1 \lambda^e \left(\frac{\partial}{\partial t} \rho^e + \frac{\partial}{\partial x} f^e(x, t) \right) dx dt \\ & + \sum_{e^+ \in \{e_2, e_3\}} \int_0^{t_f} \phi_v^{e^+} \left(\dot{q}_v^{e^+} - A_v^{e^+} f^{e^-}(1, t) + f^{e^+}(0, t) \right) dt. \end{aligned} \quad (4.23)$$

The functions $\lambda^e(x, t)$ and $\phi_v^{e^+}(t)$ are the adjoint states for the equality constraints induced by the PDEs on the arcs and the ODEs at the vertices, respectively. By using the integration by parts one can get

$$\begin{aligned}
L_3 = & \frac{1}{2} \int_0^{t_f} (B(t))^2 dt + \frac{1}{2} (B(t_f))^2 \\
& + \sum_{e \in \mathcal{E}} \int_0^1 \lambda^e(x, t_f) \rho^e(x, t_f) dx \\
& - \sum_{e \in \mathcal{E}} \int_0^{t_f} \int_0^1 \frac{\partial \lambda^e}{\partial t} \rho^e dx dt + \sum_{e \in \mathcal{E}} \int_0^{t_f} \lambda^e(1, t) f^e(1, t) dt \\
& - \sum_{e \in \mathcal{E}} \int_0^{t_f} \lambda^e(0, t) f^e(0, t) dt - \sum_{e \in \mathcal{E}} \int_0^{t_f} \int_0^1 \frac{\partial \lambda^e}{\partial x} f^e(x, t) dx dt \\
& + \left[\sum_{e^+ \in \{e_2, e_3\}} \phi_v^{e^+} q_v^{e^+} \right]_{t=0}^{t=t_f} - \sum_{e^+ \in \{e_2, e_3\}} \int_0^{t_f} \dot{\phi}_v^{e^+} q_v^{e^+} dt \\
& + \sum_{e^+ \in \{e_2, e_3\}} \int_0^{t_f} \phi_v^{e^+} \left(f^{e^+}(0, t) - A_v^{e^+} f^{e^-}(1, t) \right) dt.
\end{aligned}$$

Employing the relations provided by the system

$$\begin{aligned}
u(t) &= f^{e_1}(0, t), \\
y(t) &= f^{e_3}(1, t).
\end{aligned}$$

The Gateaux derivative of L is used to determine the first-order optimality condition

$$\begin{aligned}
\delta L_3 = & - \int_0^{t_f} B(t) \int_0^t \delta y(\tau) d\tau dt + B(t_f) \delta B(t_f) + \sum_{e \in \mathcal{E}} \int_0^1 \lambda^e(x, t_f) \delta \rho^e(x, t_f) dx \\
& - \sum_{e \in \mathcal{E}} \int_0^{t_f} \int_0^1 \frac{\partial \lambda^e(x, t)}{\partial t} \delta \rho^e(x, t) dx dt + \int_0^{t_f} \lambda^{e_3}(1, t) \delta y(t) dt \\
& + \int_0^{t_f} \lambda^{e_2}(1, t) \delta f^{e_2}(1, t) dt - \int_0^{t_f} \lambda^{e_2}(0, t) \delta f^{e_2}(0, t) dt \\
& + \int_0^{t_f} \lambda^{e_1}(1, t) \delta f^{e_1}(1, t) dt - \int_0^{t_f} \lambda^{e_1}(0, t) \delta u dt \\
& - \int_0^{t_f} \lambda^{e_3}(0, t) \delta f^{e_3}(0, t) dt - \sum_{e \in \mathcal{E}} \int_0^{t_f} \int_0^1 \left(\frac{\mu^e M^e}{(M^e + \rho^e(x, t))^2} \right) \frac{\partial \lambda^e(x, t)}{\partial x} \delta \rho^e(x, t) dx dt \\
& - \int_0^{t_f} \phi^{e_3}(t) f^{e^-}(1, t) \delta A_v^{e_3} dt - \int_0^{t_f} \phi^{e_3}(t) A_v^{e_3}(t) \delta f^{e^-}(1, t) dt \\
& - \int_0^{t_f} \phi^{e_2}(t) f^{e^-}(1, t) \delta A_v^{e_2} dt - \int_0^{t_f} \phi^{e_2}(t) A_v^{e_2}(t) \delta f^{e^-}(1, t) dt
\end{aligned}$$

$$\begin{aligned}
& + \int_0^{t_f} \phi^{e_2}(t) \delta f^{e_2}(0, t) dt + \int_0^{t_f} \phi^{e_3}(t) \delta f^{e_3}(0, t) dt \\
& + \left[\sum_{e^+ \in \{e_2, e_3\}} \phi_v^{e^+} q_v^{e^+} \right]_{t=0}^{t=t_f} - \sum_{e^+ \in \{e_2, e_3\}} \int_0^{t_f} \dot{\phi}_v^{e^+} q_v^{e^+} dt \\
& = 0.
\end{aligned}$$

By substituting

$$\begin{aligned}
\delta y(t) &= \delta_d(t - \gamma), \quad \gamma \in (0, t_f), \\
\delta y(\tau) &= \delta_d(\tau - \gamma), \\
\delta(1 - A_v^{e_3}) &= \delta A_v^{e_2},
\end{aligned}$$

into the variational derivative, where δ_d is similar to a delta function. The variational derivative becomes

$$\begin{aligned}
\delta L_3 = & - \int_0^{t_f} B(r) \int_0^r \delta_d(\tau - \gamma) d\tau dr - B(t_f) \int_0^{t_f} \delta_d(t - \gamma) dt + \sum_{e \in \mathcal{E}} \int_0^1 \lambda^e(x, t_f) \delta \rho^e(x, t_f) dx \\
& - \sum_{e \in \mathcal{E}} \int_0^{t_f} \int_0^1 \frac{\partial \lambda^e(x, t)}{\partial t} \delta \rho^e(x, t) dx dt + \int_0^{t_f} \lambda^{e_3}(1, t) \delta_d(t - \gamma) dt \\
& + \int_0^{t_f} \lambda^{e_2}(1, t) \delta f^{e_2}(1, t) dt - \int_0^{t_f} \lambda^{e_2}(0, t) \delta f^{e_2}(0, t) dt \\
& + \int_0^{t_f} \lambda^{e_1}(1, t) \delta f^{e^-}(1, t) dt - \int_0^{t_f} \lambda^{e_1}(0, t) \delta u dt \\
& - \int_0^{t_f} \lambda^{e_3}(0, t) \delta f^{e_3}(0, t) dt - \sum_{e \in \mathcal{E}} \int_0^{t_f} \int_0^1 \left(\frac{\mu^e M^e}{(M^e + \rho^e(x, t))^2} \right) \frac{\partial \lambda^e(x, t)}{\partial x} \delta \rho^e(x, t) dx dt \\
& - \int_0^{t_f} \phi^{e_3}(t) f^{e^-}(1, t) \delta A_v^{e_3} dt - \int_0^{t_f} \phi^{e_3}(t) A_v^{e_3}(t) \delta f^{e^-}(1, t) dt \\
& + \int_0^{t_f} \phi^{e_2}(t) f^{e^-}(1, t) \delta A_v^{e_3} dt - \int_0^{t_f} \phi^{e_2}(t) A_v^{e_2}(t) \delta f^{e^-}(1, t) dt \\
& + \int_0^{t_f} \phi^{e_2}(t) \delta f^{e_2}(0, t) dt + \int_0^{t_f} \phi^{e_3}(t) \delta f^{e_3}(0, t) dt \\
& + \left[\sum_{e^+ \in \{e_2, e_3\}} \phi_v^{e^+} q_v^{e^+} \right]_{t=0}^{t=t_f} - \sum_{e^+ \in \{e_2, e_3\}} \int_0^{t_f} \dot{\phi}_v^{e^+} q_v^{e^+} dt \\
& = 0.
\end{aligned}$$

From the shifting property of the delta function, one reads

$$\begin{aligned}
\lambda^{e_3}(1, \gamma) &= \int_0^{t_f} \lambda^{e_3}(1, t) \delta_d(t - \gamma) dt, \\
\int_\gamma^{t_f} B(r) dr &= \int_0^{t_f} B(r) \int_0^r \delta_d(\tau - \gamma) d\tau dr.
\end{aligned}$$

Where $\gamma \in (0, t_f)$ is any value in the domain t and it can be replaced by t and the final step is regrouping and gets the adjoint equations as follows

$$\begin{aligned}
\frac{\partial}{\partial t} \lambda^e(x, t) &= - \left(\frac{\mu^e M^e}{(M^e + \rho^e(x, t))^2} \right) \frac{\partial}{\partial x} \lambda^e(x, t), \\
\lambda^e(x, t_f) &= 0, \quad \forall e \in \mathcal{E}, \\
\lambda^{e_3}(1, t) &= \int_t^{t_f} B(r) dr + B(t_f), \\
\phi_v^{e_3}(t) &= \lambda^{e_3}(0, t), \\
\delta_u J(t) &= -\lambda^{e_1}(0, t), \\
\lambda^{e_1}(1, t) &= \lambda^{e_3}(0, t) A_v^{e_3}(t), \\
\delta_{A_v^{e_3}} J(t) &= -\lambda^{e_3}(0, t) f^{e_1}(1, t).
\end{aligned} \tag{4.24}$$

Herein $\delta_u J(t)$ and $\delta_{A_v^{e_3}} J(t)$ refer to the variational derivative with respect to inflow u and $A_v^{e_3}$, respectively. Besides, $\lambda^e(x, t_f)$ and $\lambda^{e_3}(1, t)$ are the terminal conditions and the boundary condition, respectively.

Merging Network

The form of L of problem (4.22) is obtained as

$$\begin{aligned}
L_4 &= \frac{1}{2} \int_0^{t_f} (B(t))^2 dt + \frac{1}{2} (B(t_f))^2 \\
&+ \sum_{e \in \mathcal{E}} \int_0^{t_f} \int_0^1 \lambda^e \left(\frac{\partial}{\partial t} \rho^e + \frac{\partial}{\partial x} f^e(x, t) \right) dx dt \\
&+ \int_0^{t_f} \phi_v^{e^+} \left(\dot{q}_v^{e^+} - A_v(t) \sum_{e^- \in \{e_1, e_2\}} f^{e^-}(1, t) + f^{e^+}(0, t) \right) dt.
\end{aligned} \tag{4.25}$$

By using the integration by parts one obtains

$$\begin{aligned}
L_4 &= \frac{1}{2} \int_0^{t_f} (B(t))^2 dt + \frac{1}{2} (B(t_f))^2 \\
&+ \sum_{e \in \mathcal{E}} \int_0^1 \lambda^e(x, t_f) \rho^e(x, t_f) dx \\
&- \sum_{e \in \mathcal{E}} \int_0^{t_f} \int_0^1 \frac{\partial \lambda^e}{\partial t} \rho^e dx dt + \sum_{e \in \mathcal{E}} \int_0^{t_f} \lambda^e(1, t) f^e(1, t) dt \\
&- \sum_{e \in \mathcal{E}} \int_0^{t_f} \lambda^e(0, t) f^e(0, t) dt - \sum_{e \in \mathcal{E}} \int_0^{t_f} \int_0^1 \frac{\partial \lambda^e}{\partial x} f^e(x, t) dx dt \\
&+ \left[\phi_v^{e^+} q_v^{e^+} \right]_{t=0}^{t=t_f} - \int_0^{t_f} \dot{\phi}_v^{e^+} q_v^{e^+} dt
\end{aligned}$$

$$+ \int_0^{t_f} \phi_v^{e^+} \left(f^{e^+}(0, t) - A_v(t) \sum_{e^- \in \{e_1, e_2\}} f^{e^-}(1, t) \right) dt.$$

By using the relationships provided by the system

$$\begin{aligned} u(t) &= f^{e_1}(0, t), \\ y(t) &= f^{e_3}(1, t). \end{aligned}$$

The Gateaux derivative of L reads

$$\begin{aligned} \delta L_4 &= - \int_0^{t_f} B(t) \int_0^t \delta y(\tau) d\tau dt + B(t_f) \delta B(t_f) + \sum_{e \in \mathcal{E}} \int_0^1 \lambda^e(x, t_f) \delta \rho^e(x, t_f) dx \\ &\quad - \sum_{e \in \mathcal{E}} \int_0^{t_f} \int_0^1 \frac{\partial \lambda^e(x, t)}{\partial t} \delta \rho^e(x, t) dx dt + \int_0^{t_f} \lambda^{e_3}(1, t) \delta y(t) dt \\ &\quad + \int_0^{t_f} \lambda^{e_1}(1, t) \delta f^{e_1}(1, t) dt - \int_0^{t_f} \lambda^{e_1}(0, t) \delta u dt \\ &\quad + \int_0^{t_f} \lambda^{e_2}(1, t) \delta f^{e_2}(1, t) dt - \int_0^{t_f} \lambda^{e_2}(0, t) \delta f^{e_2}(0, t) dt \\ &\quad - \int_0^{t_f} \lambda^{e_3}(0, t) \delta f^{e_3}(0, t) dt - \sum_{e \in \mathcal{E}} \int_0^{t_f} \int_0^1 \left(\frac{\mu^e M^e}{(M^e + \rho^e(x, t))^2} \right) \frac{\partial \lambda^e(x, t)}{\partial x} \delta \rho^e(x, t) dx dt \\ &\quad - \int_0^{t_f} \phi^{e_3}(t) \left(f^{e_1}(1, t) + f^{e_2}(1, t) \right) \delta A_v(t) dt - \int_0^{t_f} \phi^{e_3}(t) A_v(t) \delta f^{e_1}(1, t) dt \\ &\quad + \int_0^{t_f} \phi^{e_3}(t) \delta f^{e_3}(0, t) dt - \int_0^{t_f} \phi^{e_3}(t) A_v(t) \delta f^{e_2}(1, t) dt \\ &= 0. \end{aligned}$$

By substituting

$$\begin{aligned} \delta y(t) &= \delta_d(t - \gamma), \quad \gamma \in (0, t_f), \\ \delta y(\tau) &= \delta_d(\tau - \gamma), \end{aligned}$$

into the variational derivative. The variational derivative reads

$$\begin{aligned} \delta L_4 &= - \int_0^{t_f} B(r) \int_0^r \delta_d(\tau - \gamma) d\tau dr - B(t_f) \int_0^{t_f} \delta_d(t - \gamma) dt + \sum_{e \in \mathcal{E}} \int_0^1 \lambda^e(x, t_f) \delta \rho^e(x, t_f) dx \\ &\quad - \sum_{e \in \mathcal{E}} \int_0^{t_f} \int_0^1 \frac{\partial \lambda^e(x, t)}{\partial t} \delta \rho^e(x, t) dx dt + \int_0^{t_f} \lambda^{e_3}(1, t) \delta_d(t - \gamma) dt \\ &\quad + \int_0^{t_f} \lambda^{e_1}(1, t) \delta f^{e^-}(1, t) dt - \int_0^{t_f} \lambda^{e_1}(0, t) \delta u dt \end{aligned}$$

$$\begin{aligned}
& - \int_0^{t_f} \lambda^{e_3}(0, t) \delta f^{e_3}(0, t) dt - \sum_{e \in \mathcal{E}} \int_0^{t_f} \int_0^1 \left(\frac{\mu^e M^e}{(M^e + \rho^e(x, t))^2} \right) \frac{\partial \lambda^e(x, t)}{\partial x} \delta \rho^e(x, t) dx dt \\
& - \int_0^{t_f} \phi^{e_3}(t) \left(f^{e_1}(1, t) + f^{e_2}(1, t) \right) \delta A_v(t) dt - \int_0^{t_f} \phi^{e_3}(t) A_v(t) \delta f^{e_1}(1, t) dt \\
& + \int_0^{t_f} \phi^{e_3}(t) \delta f^{e_3}(0, t) dt \\
& = 0.
\end{aligned}$$

By using the shifting property of the delta function, one can get

$$\begin{aligned}
\lambda^{e_3}(1, \gamma) &= \int_0^{t_f} \lambda^{e_3}(1, t) \delta_d(t - \gamma) dt, \\
\int_\gamma^{t_f} B(r) dr &= \int_0^{t_f} B(r) \int_0^r \delta_d(\tau - \gamma) d\tau dr.
\end{aligned}$$

The adjoint equations is obtained after regrouping to become

$$\begin{aligned}
\frac{\partial}{\partial t} \lambda^e(x, t) &= - \left(\frac{\mu^e M^e}{(M^e + \rho^e(x, t))^2} \right) \frac{\partial}{\partial x} \lambda^e(x, t), \\
\lambda^e(x, t_f) &= 0, \quad \forall e \in \mathcal{E}, \\
\lambda^{e_3}(1, t) &= \int_t^{t_f} B(r) dr + B(t_f), \\
\phi_v^{e_3}(t) &= \lambda^{e_3}(0, t), \\
\delta_u J(t) &= -\lambda^{e_1}(0, t), \\
\lambda^{e_1}(1, t) &= A_v(t) \lambda^{e_3}(0, t), \\
\delta_{A_v} J(t) &= -\lambda^{e_3}(0, t) (f^{e_1}(1, t) + f^{e_2}(1, t)),
\end{aligned} \tag{4.26}$$

where, $\delta_{A_v} J(t)$ refers to the variational derivative with respect to the fraction A_v . The system dynamics (4.2) or (4.3) are discretized and solved forward in time as in (4.12) or (4.13), respectively. The adjoint equations are discretized and solved backward in time. The discretized form of (4.24) in the dispersing network becomes

$$\begin{aligned}
\lambda_{i,j-1}^e &= \lambda_{i,j}^e - \frac{\Delta t}{\Delta x} \left(\frac{\mu^e M^e}{(M^e + \rho_{i,j}^e)^2} \right) (\lambda_{i+1,j}^e - \lambda_{i,j}^e), \\
\lambda_{i,N}^e &= 0, \\
\lambda_{M^e,j}^{e_3} &= \sum_{r=j}^N B_r \Delta r + B_N, \\
\phi_{v,j}^{e_3} &= \lambda_{0,j}^{e_3}, \\
\delta_u J_j &= -\lambda_{0,j}^{e_1}, \\
\lambda_{M^e,j}^{e_1} &= \lambda_{0,j}^{e_3} A_{v,j}^{e_3}, \\
\delta_{A_v} J_j &= -\lambda_{0,j}^{e_3} f_{M^e,j}^{e_1}.
\end{aligned} \tag{4.27}$$

While for the merging network (4.26) implies

$$\begin{aligned}
\lambda_{i,j-1}^e &= \lambda_{i,j}^e - \frac{\Delta t}{\Delta x} \left(\frac{\mu^e M^e}{(M^e + \rho_{i,j}^e)^2} \right) (\lambda_{i+1,j}^e - \lambda_{i,j}^e), \\
\lambda_{i,N}^e &= 0, \\
\lambda_{M^e,j}^{e3} &= \sum_{r=j}^N B_r \Delta r + B_N, \\
\phi_{v,j}^{e3} &= \lambda_{0,j}^{e3}, \\
\delta_u J_j &= -\lambda_{0,j}^{e1}, \\
\lambda_{M^e,j}^{e1} &= A_{v,j} \lambda_{0,j}^{e3}, \\
\delta_{A_v} J_j &= -\lambda_{0,j}^{e3} (f_{M^e,j}^{e1} + f_{M^e,j}^{e2}).
\end{aligned} \tag{4.28}$$

The `fmincon` generates the corresponding optimal values numerically based on the obtained gradient information and the inequality constraints.

4.4.2 Direct Method

The finite-dimensional static optimization problem is considered after the discretization of (4.20) is chosen as

$$\min_{\boldsymbol{\vartheta}} J_{2d}(\boldsymbol{\vartheta}) = \frac{1}{2} \sum_{j=0}^N \left(\sum_{k=0}^j (f_k^* - y_k) \Delta \tau \right)^2 \Delta t + \frac{1}{2} \left(\sum_{k=0}^N (f_k^* - y_k) \Delta \tau \right)^2, \tag{4.29}$$

where $J_{2d}(\boldsymbol{\vartheta})$ is the approximated cost functional. The discretization is performed by the upwind finite difference scheme for the PDEs and explicit Euler for the ODEs. The terms Δt and $\Delta \tau$ denote the time steps herein $\Delta t = n \Delta \tau$ in which n is the number of the equidistant subintervals while $y_k = y(k \Delta \tau); j = 0, 1, 2, \dots, N$ and $k = 0, 1, 2, \dots, j$. Therefore, the dispersing optimization problem is structured as

$$\min_{\boldsymbol{\vartheta}} J_{2d}(\boldsymbol{\vartheta}) \quad \text{subject to (4.12)}. \tag{4.30}$$

The merging optimization problem is structured as

$$\min_{\boldsymbol{\vartheta}} J_{2d}(\boldsymbol{\vartheta}) \quad \text{subject to (4.13)}. \tag{4.31}$$

The constrained static optimization problems (4.30) and (4.31) are addressed using SQP implemented in the MATLAB Optimization Toolbox function `fmincon`. The gradients are updated iteratively by the solver finding the proper step length and search direction using the Newton-type method.

4.5 Simulation Results

This part shows the system configuration and discusses the simulation results for the two represented problems: (i) demand tracking and (ii) backlog.

4.5.1 Demand Tracking Problem

The control strategies for the demand tracking problem are assessed, which are associated with dispersing and merging networks. The system parameters for the dispersing network contains three arcs where the number of machines in each arc is chosen as $M^e = 10$ with the processing rates μ^e being 2 lots/h, 3 lots/h and 4 lots/h in e_1 , e_2 and e_3 respectively. In case of the merging network $\mu^{e_1} = 4$ lots/h, $\mu^{e_2} = 3$ lots/h and $\mu^{e_3} = 2$ lots/h are used. The numerical parameters are defined as $\Delta x = 0.1$ which is referred to the spatial step size in each arc e and CFL is 0.5. The temporal step size $\Delta t = 0.2$ h and the smoothing factor is chosen as $\kappa = 0.2$.

4.5.1.1 Dispersing Network

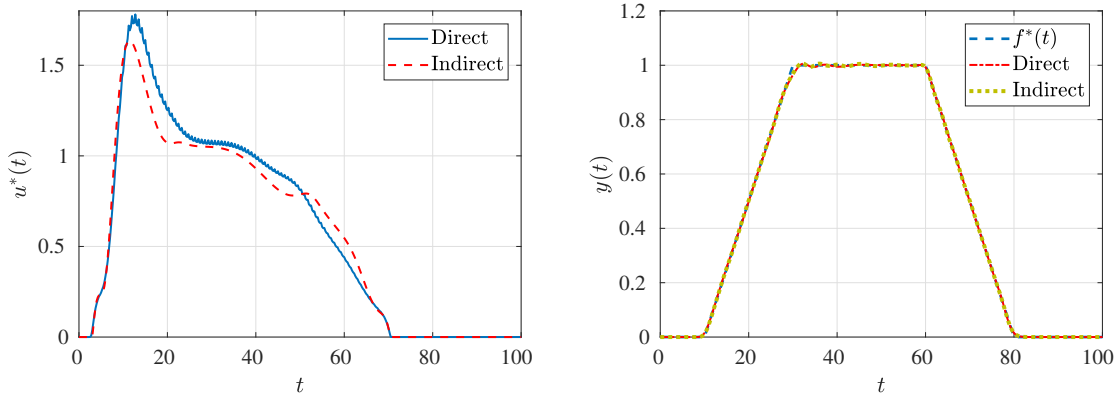


Figure 4.1: Input $u^*(t)$ (left) and comparison of the desired demand trajectory $f^*(t)$ and $y(t) = f^{e_3}(1, t)$ (right) in case of direct and indirect method.

The optimal boundary control is utilized by the direct and the indirect approaches. In the case of the dispersing network, the final value of the objective functional (4.1) is 1.03×10^{-3} by the direct method. The approach is achieved reasonably to track the demand. When compared to the direct method, the indirect method takes a significantly shorter time to compute. Herein, the relative computational load is reduced by 84.6%. As is shown in Fig. 4.1 the input from the indirect method is smoother than the input from the direct method. Changing the `fmincon` option, such as optimality tolerance or finite difference step size, can solve the problem of the high-frequency oscillation in the input utilizing the direct approach. However, the goal is to compare different control strategies with the same configuration. The output in arc e_3 perfectly matches the desired flow trajectory. The final value of the objective functional (4.1) is 7.29×10^{-4} .

4.5.1.2 Merging Network

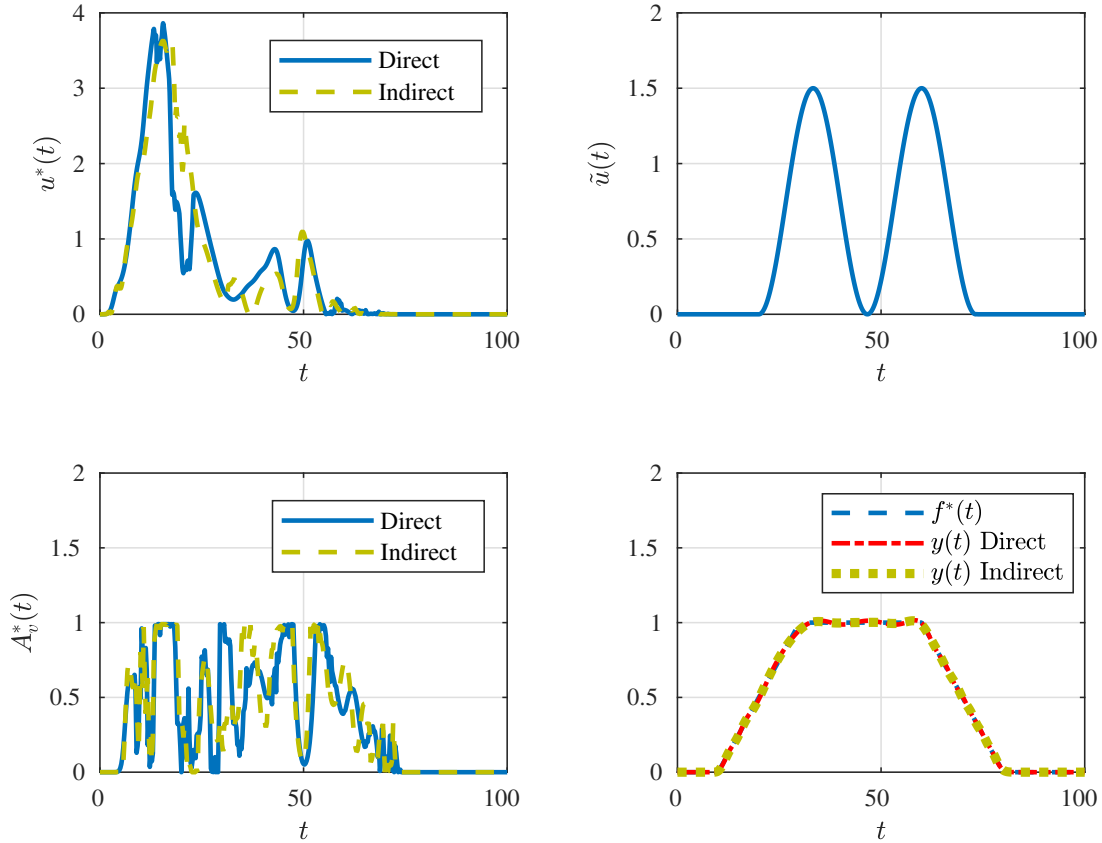


Figure 4.2: Direct and indirect approaches used for demand tracking in the merging network.

By applying the direct approach in the merging network, the outflux is reasonably tracking the desired demand, see Fig. 4.2. However, it slightly oscillates in steady state region from the time ranging from 30 to 60 h. The final value of the objective functional equals 4.19×10^{-3} for the direct method and 3.19×10^{-3} for the indirect method. When comparing the direct and indirect methods, the indirect method saves 93.2% of the computational load. The outflux $y(t)$ matches the desired demand, especially in the the ramp-up and the ramp-down.

4.5.2 Backlog Problem

Subsequently, the control designs are evaluated for the dispersing and the merging networks of production system topologies. For the dispersing and merging scenarios, the problems are solved by the indirect and the direct methods. In the case of dispersing network, the system parameters for both methods are assigned as $\mu^{e1} = 8$ lots/h, $\mu^{e2} = 4$ lots/h, $\mu^{e3} = 6$ lots/h, the number of machines in each arc $M^{e1} = M^{e2} = M^{e3} = 10$, $\kappa = 0.1$, and the final time $t_f = 20$

h. The numerical parameters are defined as $\Delta t = 0.1$ h, $CFL = 0.5$, and $\Delta x = 0.1$. In case of the merging network, the processing rates are set $\mu^{e1} = 8$ lots/h, $\mu^{e2} = 3$ lots/h and $\mu^{e3} = 5$ lots/h and the other parameters are kept the same as the previous case.

4.5.2.1 Dispersing Network

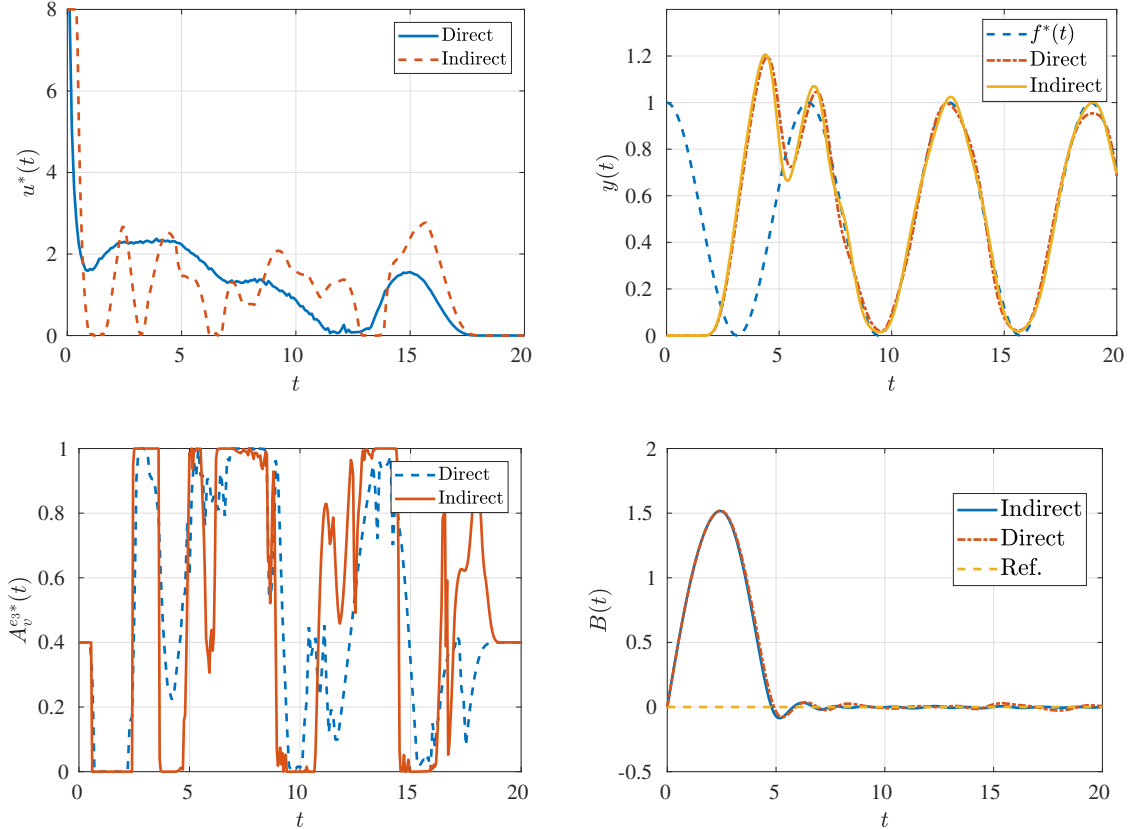


Figure 4.3: Inflows in the dispersing network for the backlog problem (top-left), outflows (top-right), $A_v^{e3*}(t)$ (bottom-left) and $B(t)$ (bottom-right).

The final value of the objective functional (4.20) of the both methods are approximately the same. It has been noticed that the computational time of the direct method is large compared to the indirect one. Herein, the relative computational load is reduced by 93% compared to the direct one. Fig. 4.3 illustrates the control variables $u^*(t)$ and $A_v^{e3*}(t)$, the outflow $y(t)$ and the backlog $B(t)$. As shown from the figure, the outflow from the indirect method almost matches the reference after compensating the intractable lots. However, in the direct case, $y(t)$ is not accurate enough to fully track the peaks of the reference trajectory. The reference in the backlog figure indicates that the system has no backlog, and the outflow completely follows the desired demand. Therefore, the indirect approach shows that the backlog remains at zero after the compensation of the required lots, while it fluctuates around the zero value in the case of the direct approach.

4.5.2.2 Merging Network

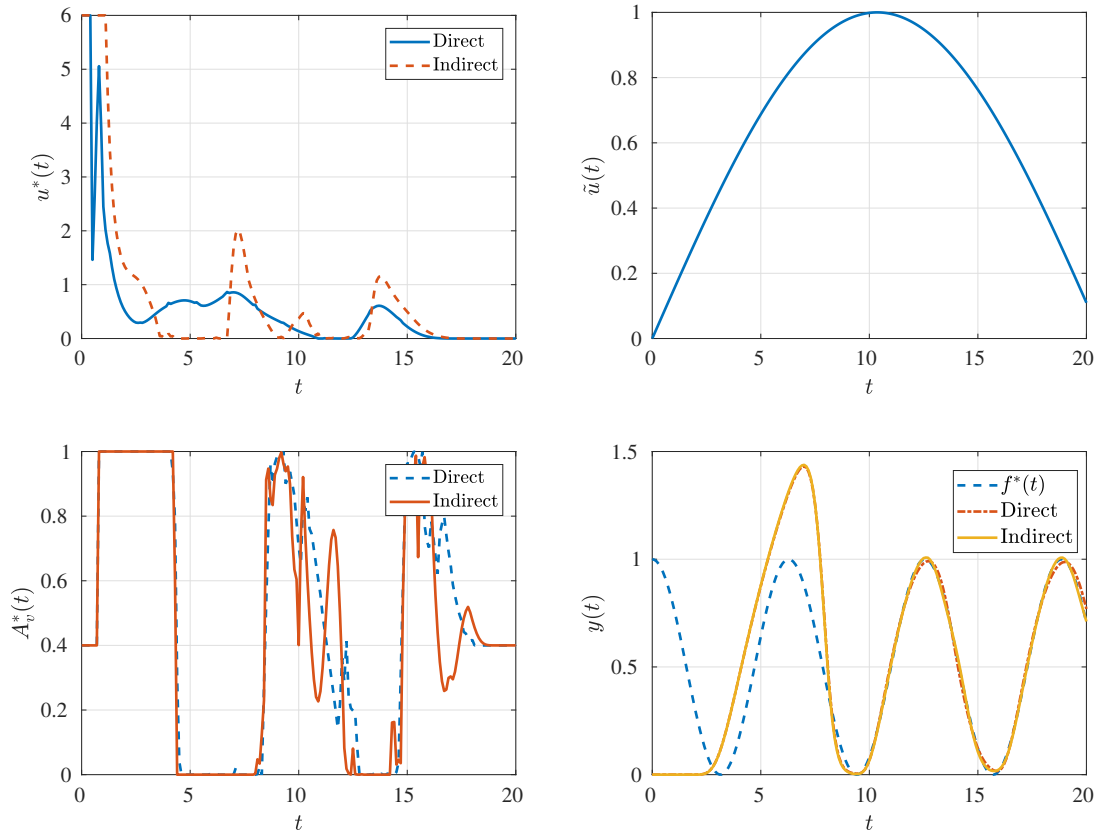


Figure 4.4: Inflows at arc e_1 in merging network for the backlog problem (top-left), the inflow at arc e_2 (top-right), the fraction $A_v^*(t)$ (bottom-left) and the outflows (bottom-right).

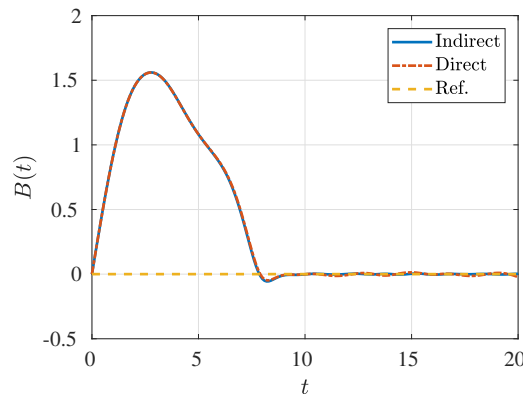


Figure 4.5: Backlog $B(t)$ of the merging network.

In the merging network, the computational time is reduced by 95.5% when applying the indirect method compared to the direct one. The final values of the objective functional of both approaches are almost similar. Fig. 4.4 shows the control variables $u^*(t)$ at arc e_1 and $A_v^*(t)$, the

arbitrary uncontrolled input \tilde{u} at arc e_2 the outflow $y(t)$, and the backlog $B(t)$ is shown in Fig. 4.5. The outflow of the indirect method converges to the reference after the compensation, as observed in the figure. In the direct case $y(t)$ is not as accurate as in the indirect method does not follow the reference trajectory, specifically the peaks. The backlog after the compensation of the demanded lots converges to zero in the case of the indirect method, while it oscillates around the zero value in the direct approach.

4.6 Summary

In this chapter, two different control challenges, demand tracking and backlog are considered in the context of the production system network. The backlog problem is an accumulated error that describes the mismatch between the desired lot accumulation and the total number of lots at the system outlet over a finite time interval that leads to either under- or over-production. Two different yet challenging networks consisting of arcs and storage areas are modelled by coupling their corresponding PDEs and ODEs. The networks cover dispersing and merging structures. The problems are optimized utilizing open-loop optimal control according to the direct (discretize-then-optimize) and the indirect (optimize-then-discretize) approaches. The proposed approaches enable the solution of the OCPs. Generally, all the approaches reach a local minima with common behaviour converging to the steady-state. The analysis of the results demonstrates unique features for each method. The indirect technique is characterized by high accuracy and low computational load; nevertheless, it is a sensitive method due to the information required to compute the gradient. The direct approach is featured by the ease of use and adaptability to any problem. This method applied an approximate finite difference to obtain the Lagrangian gradient. However, this approach takes substantially longer to achieve a solution when compared to the indirect method. On the other hand, the comparison in view of analytical effort is somewhat unfair. As for the indirect method, gradient information is needed to be provided. On the contrary, no gradient and Hessian information are provided for the direct approach.

Chapter 5

Model Predictive Control of a Manufacturing Network

Automation and control are key elements in production engineering and manufacturing to solve problems such as cost reduction, energy savings, optimizing machines utilization, and time savings, which leads to maximizing profitability.

Constrained optimization problems are formulated to reduce the output rate of the system to track a desired demand rate trajectory as closely as possible or to minimize the difference between total desired lots and total lots of the system output. These problems are known as demand tracking or backlog problems, respectively. These problems are subject to system constraints, such as the capacity of the production systems, which limits the ability of the system to achieve the desired targets. In this chapter, an adjoint-based model predictive control (AMPC) is developed in a production system complex network to address these problems in terms of conservation laws connected with ordinary differential equations. The network is composed of a hybrid of dispersing and merging networks. The adjoint method is used to obtain the gradient of the cost functional as a powerful tool for the constrained optimization problems by evaluating the necessary optimality conditions, which is combined with the model predictive control. The traditional or the standard approach of MPC depends mainly on the direct method. The numerical results demonstrate the solvability and the value of using the adjoint-based model predictive control for reducing the computational load compared to the standard approach. In addition, it shows robustness concerning the effect of disturbance.

5.1 Problem Statement

In the previous chapter, rather simple networks are considered focussing on dispersion and merging. In this chapter, a complex model is addressed. This one includes the combination of two dispersing and two merging networks. The network in Fig. 5.1 contains seven arcs and four vertices with the same characteristics of the previous networks.

System Model

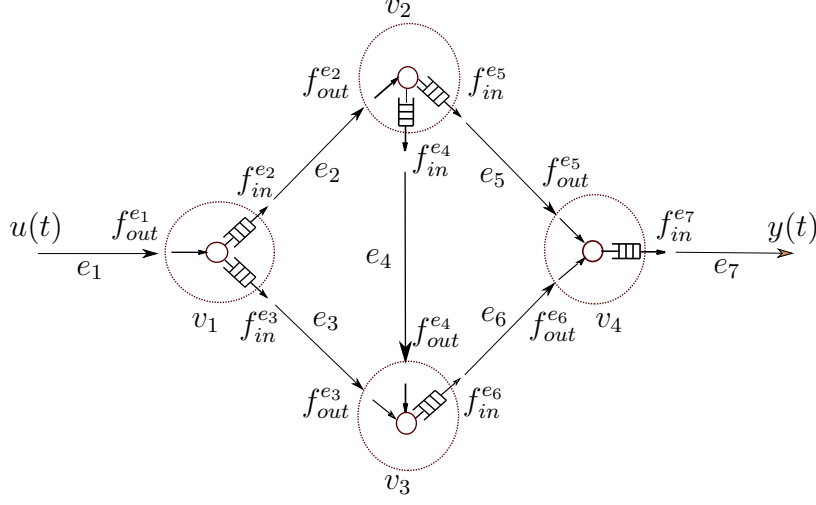


Figure 5.1: The structure of the complex network.

The system is represented by the directed graph $G(\mathcal{V}, \mathcal{E})$, where $\mathcal{V} = \{v_1, v_2, v_3, v_4\}$ is the set of vertices and $\mathcal{E} = \{e_1, e_2, \dots, e_7\}$ is the set of arcs. The components are connected as shown in Fig. 5.1. Each arc e is made up of a single flow line with a homogeneous number of workstations. A machine and a buffer are included in every workstation. The production flow is based on the M/M/1 model, in which both process time and inter-arrival time are distributed exponentially. Each arc $e \in \mathcal{E}$ is modeled by a single PDE. The vertex $v \in \mathcal{V}$ is placed between two consecutive arcs and modeled as a single ODE, which refers to a storage area. The system network consists a group of dispersing vertices, here v_1, v_2 , and merging vertices, here v_3, v_4 . The normalized coordinate $x \in [0, 1]$ denotes the position of the workstation inside each arc. The inlet of the arc e is located at $x = 0$ while $x = 1$ is the location of the outlet. The system dynamics for each flow line e can be described as

$$\begin{aligned}
 \frac{\partial}{\partial t} \rho^e(x, t) &= -\frac{\partial}{\partial x} f^e(x, t), \quad (x, t) \in (0, 1] \times (0, t_f], \\
 f^e(x, t) &= \rho^e v^e = \frac{\mu^e \rho^e(x, t)}{M^e + \rho^e(x, t)}, \\
 \rho^e(x, 0) &= 0, \quad \forall x \in [0, 1], \\
 f^{e_1}(0, t) &= u(t) + d(t), \quad \forall t \in [0, t_f], \\
 0 &\leq u(t) < \mu^{e_1}, \quad \forall t \in [0, t_f].
 \end{aligned} \tag{5.1}$$

Herein, $f(x, t)$ is the flux and $\rho(x, t) \in \mathbb{R}_0^+$ is the density of the lots. The individual features of each arc e are determined by the mean processing rate μ^e and the number of machines M^e . The main inflow $u(t)$ exists at the inlet of the arc e_1 and $d(t)$ is the additive disturbance to the inflow of the system.

The structure of the storage area at v differs depending on the network topology. For the dispersing structures of the network at v_1 and v_2 as shown in Fig. 5.1, the PDE model (5.1) is

associated with

$$\begin{aligned}
\frac{dq_{v_1}^{e_{v_1}^+}(t)}{dt} &= A_{v_1}^{e_{v_1}^+}(t) f^{e_{v_1}^-}(1, t) - f^{e_{v_1}^+}(0, t), \\
\frac{dq_{v_2}^{e_{v_2}^+}(t)}{dt} &= A_{v_2}^{e_{v_2}^+}(t) f^{e_{v_2}^-}(1, t) - f^{e_{v_2}^+}(0, t), \\
f^{e_{v_1}^+}(0, t) &= \min \left\{ \mu^{e_{v_1}^+}, \frac{q_{v_1}^{e_{v_1}^+}(t)}{\kappa} \right\}, \\
f^{e_{v_2}^+}(0, t) &= \min \left\{ \mu^{e_{v_2}^+}, \frac{q_{v_2}^{e_{v_2}^+}(t)}{\kappa} \right\}, \\
q_{v_1}^{e_{v_1}^+}(0) &= 0, \quad 0 \leq A_{v_1}^{e_{v_1}^+}(t) \leq 1, \quad \sum A_{v_1}^{e_{v_1}^+}(t) = 1, \\
q_{v_2}^{e_{v_2}^+}(0) &= 0, \quad 0 \leq A_{v_2}^{e_{v_2}^+}(t) \leq 1, \quad \sum A_{v_2}^{e_{v_2}^+}(t) = 1, \\
e_{v_1}^- &\in \{e_1\}, \quad e_{v_1}^+ \in \{e_2, e_3\}, \\
e_{v_2}^- &\in \{e_2\}, \quad e_{v_2}^+ \in \{e_4, e_5\}.
\end{aligned} \tag{5.2}$$

The storage load of v_\bullet is represented by $q_{v_\bullet}^{e_{v_\bullet}^+}(t)$. The arcs $e_{v_\bullet}^-$ and $e_{v_\bullet}^+$, respectively, correspond to the arcs before and after the vertex v_\bullet . The parameter κ is a smoothing parameter. The outflow from arc $e_{v_\bullet}^-$ splits into two flows. The sum of these flows at $e_{v_\bullet}^+$, which is covered by the distribution rate $A_{v_\bullet}^{e_{v_\bullet}^+}(t) \in [0, 1]$ must be equal to the outflow coming from $e_{v_\bullet}^-$. It is assumed that there are no lots in the system at time $t = 0$. In addition, the incoming flow is limited to a value between zero and the arc's processing rate. For the merging topologies at v_3 and v_4 the PDE model (5.1) is also associated with

$$\begin{aligned}
\frac{dq_{v_3}^{e_{v_3}^+}(t)}{dt} &= A_{v_3}(t) \sum_{e_{v_3}^-} f^{e_{v_3}^-}(1, t) - f^{e_{v_3}^+}(0, t), \\
\frac{dq_{v_4}^{e_{v_4}^+}(t)}{dt} &= A_{v_4}(t) \sum_{e_{v_4}^-} f^{e_{v_4}^-}(1, t) - f^{e_{v_4}^+}(0, t), \\
f^{e_{v_3}^+}(0, t) &= \min \left\{ \mu^{e_{v_3}^+}, \frac{q_{v_3}^{e_{v_3}^+}(t)}{\kappa} \right\}, \\
f^{e_{v_4}^+}(0, t) &= \min \left\{ \mu^{e_{v_4}^+}, \frac{q_{v_4}^{e_{v_4}^+}(t)}{\kappa} \right\}, \\
q_{v_3}^{e_{v_3}^+}(0) &= 0, \quad 0 \leq A_{v_3}(t) \leq 1, \\
q_{v_4}^{e_{v_4}^+}(0) &= 0, \quad 0 \leq A_{v_4}(t) \leq 1, \\
e_{v_3}^- &\in \{e_3, e_4\}, \quad e_{v_3}^+ \in \{e_6\}, \\
e_{v_4}^- &\in \{e_5, e_6\}, \quad e_{v_4}^+ \in \{e_7\}.
\end{aligned} \tag{5.3}$$

All incoming flows $e_{v_\bullet}^-$ are merged before entering the main arc $e_{v_\bullet}^+$. A fraction of the total incoming flows at vertex v_\bullet is represented by the value $A_{v_\bullet}(t) \in [0, 1]$.

5.2 Model Predictive Control

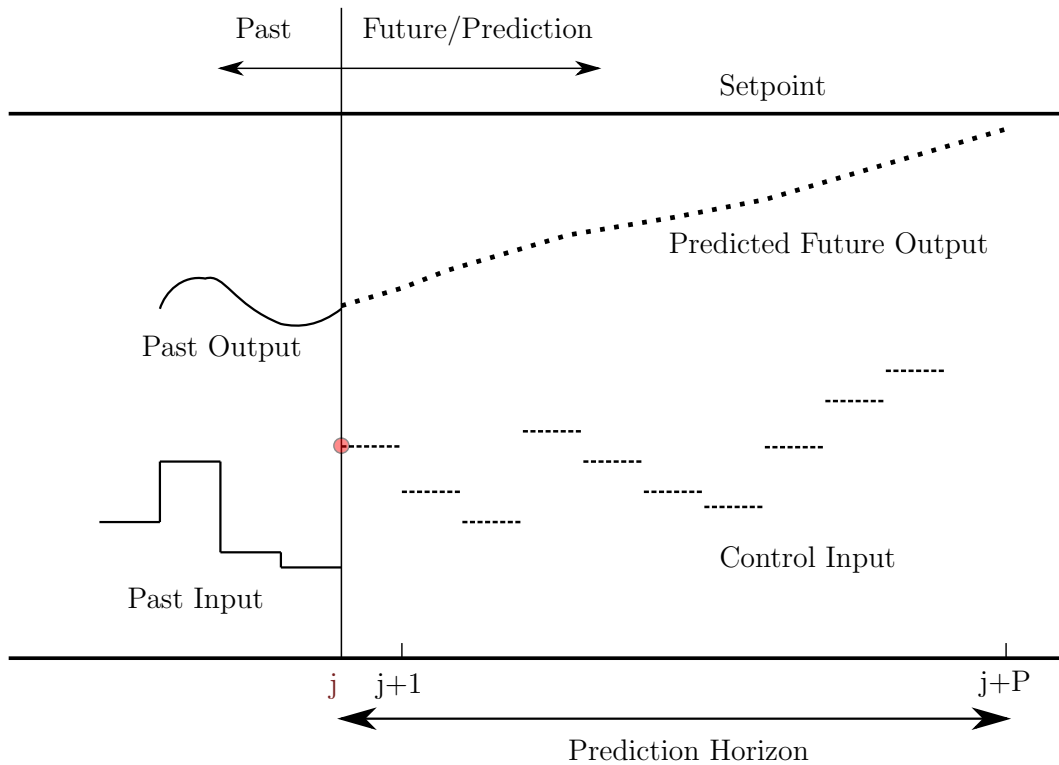


Figure 5.2: MPC and the receding horizon mechanism.

In real-world systems, there is a deviation between the actual and predicted model behaviours. The ability to predict the future response of the system is MPC's key characteristic that sets it apart from other controllers. The MPC can address such issues providing stabilization and robustness. Without loss of generality, it can be developed by different algorithms according to the industrial application of interest, e.g. slow, fast or real-time processes. The MPC emerged as an efficient technique for dealing with multivariable constrained control problems. The main goal of MPC in this work is to investigate the effect of disturbances in the demand tracking and the backlog problems. MPC is considered a particular type of optimal feedback control. It relies on a receding horizon implementation to mimic an infinite horizon. An MPC algorithm attempts to optimize future system behavior for each control interval by computing a sequence of future manipulated variable adjustments, as shown in Fig. 5.2. The performance depends on two tunable parameters which are defined as prediction horizon P and control horizon C . The prediction horizon is the number of the expected time steps over a finite time window. The window can be shifted by the control horizon parameter whose value refers to the number of moves of the manipulated variables to be optimized during the prediction horizon. The value of the control horizon parameter has to be lower than or equal to the prediction horizon parameter. The implementation mechanism of the MPC algorithm is summarized in the following scheme

Algorithm 1: Model Predictive Control

Set prediction horizon P and control horizon C ;

Initialize $\boldsymbol{\vartheta}$;

Start $t_0 = 0$;

Count = 0;

for $j = 1, 2, \dots$ **do**

 ICs = ICs(t_j);

 if Count == 0 **then**

 Solve the OCP along P horizon

$$\min_{\boldsymbol{\vartheta}} J(\boldsymbol{\vartheta}) = \frac{1}{2} \int_{t_j}^{t_j+P} \xi(f^*(t), y(t)) dt + \frac{1}{2} \chi(f^*(t_j + P), y(t_j + P)); \quad (5.4)$$

subject to the complex network (5.1), (5.2) and (5.3);

 Output: ($\boldsymbol{\vartheta}_1, \boldsymbol{\vartheta}_2, \boldsymbol{\vartheta}_3, \dots, \boldsymbol{\vartheta}_P$);

 Count = C ;

 end

 Set $\boldsymbol{\vartheta}_j = \boldsymbol{\vartheta}_k$; $k = C - \text{Count} + 1$;

Count = Count - 1;

end

The general scheme (5.4) is solved by feedback control to avoid the effect of the additive disturbance. The cost functional consists of the stage cost $\xi(\cdot)$ and the terminal cost $\chi(\cdot)$. The terminal cost of the problem helps for the system stability, especially in the occurrence of the perturbations. The objective functional in (5.4) and the system dynamics (5.1), (5.2), and (5.3) are discretized first in the traditional MPC, as well as the direct method. Then the optimization in **Algorithm 1** is solved by the SQP method from the function `fmincon` provided in the MATLAB to obtain the manipulated variables $\boldsymbol{\vartheta}^*$.

5.3 Problems Formulation

The OCPs are the demand tracking and the backlog problems. The difference to the OCPs considered before that arise due to MPC are the integration limits. In the case of the open-loop optimal control, the integration limits are in the entire time domain. In the case of the MPC, the lower and upper limits are set by the control and prediction horizons, respectively. The decision variables supplied by u , $A_{v\bullet}$ and $A_{v\bullet}^{e\ddagger}$ are then summarized by $\boldsymbol{\vartheta}$ and the optimal control for the demand tracking problem is used by considering the objective functional.

$$\min_{\boldsymbol{\vartheta}} J_1(\boldsymbol{\vartheta}) = \frac{1}{2} \int_{t_j}^{t_j+P} (f^*(t) - y(t))^2 dt, \quad (5.5)$$

subject to (5.1), (5.2) and (5.3). Here, $f^*(t)$ is the desired trajectory and $y(t) = f^{e_7}(1, t)$ is the outflow from the arc e_7 . The optimization is handled for every control interval between t_i and $t_i + P$ where P refers to the prediction horizon. In the backlog case, the optimal control applies both stage cost and terminal cost by considering the objective functional

$$\min_{\vartheta} J_2(\vartheta) = \frac{1}{2} \int_{t_j}^{t_j+P} (B(t))^2 dt + \frac{1}{2} (B(t_i + P))^2, \quad (5.6)$$

subject to the system constraints (5.1), (5.2) and (5.3). To this end, the optimization problems (5.5) and (5.6) can be solved by the proposed MPC based on adjoint approach as will be described in the following section.

5.4 Adjoint-based MPC

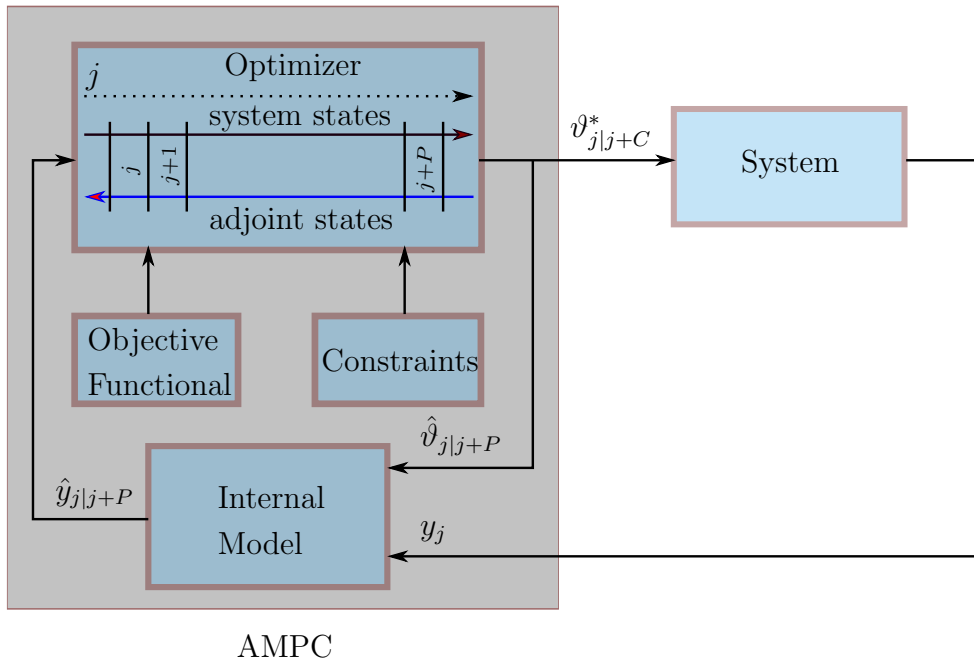


Figure 5.3: Scheme of the AMPC framework.

Adjoint-based Model Predictive Control has shown to be a feasible and successful approach for offline and online optimization of control sequences for dynamic systems governed by differentiable nonlinear equations over the years [96]. The traditional MPC relies on the direct approach, which can provide for the systems' stability and robustness. However, it is characterized by high computational complexity. The proposed technique contains a generalized adjoint-based dynamic optimization where it is reduced the computational burden, as proven in the previous chapter. The way to suppress the computational load based on the gradient

information provided from adjoint-state equations, which is combined to the model predictive control as illustrated in Fig. 5.3. The procedures to solve successive OCPs in AMPC are required for both two demand tracking and backlog problems. The AMPC starts with optimization and then moves on to discretization.

5.4.1 Optimization Phase

The PDE-ODE constrained optimization problem is reformulated as unconstrained optimization by using the Lagrange multipliers. The optimization is performed for the infinite-dimensional system. The following result summarizes the necessary optimality condition in terms of the adjoint PDE-ODE system.

Demand Tracking Problem

Proposition 1. *The adjoint equations from the complex network in Fig. 5.1 of the demand tracking problem (5.5) subject to (5.1), (5.2), and (5.3) after neglecting the inequality constraints are*

$$\begin{aligned}
\frac{\partial \lambda^e}{\partial t} &= -\frac{\mu^e M^e}{(M^e + \rho^e(x, t))^2} \frac{\partial \lambda^e}{\partial x}, \quad (x, t) \in (0, 1] \times (t_j, t_j + P], \\
\lambda^e(x, t_j + P) &= 0, \\
\lambda^{e7}(1, t) &= f^*(t) - y(t), \\
\phi_{v_1}^{e2}(t) &= \lambda^{e2}(0, t), \quad \phi_{v_1}^{e3}(t) = \lambda^{e3}(0, t) \\
\phi_{v_2}^{e4}(t) &= \lambda^{e4}(0, t), \quad \phi_{v_2}^{e5}(t) = \lambda^{e5}(0, t) \\
\phi_{v_3}^{e6}(t) &= \lambda^{e6}(0, t), \quad \phi_{v_4}^{e7}(t) = \lambda^{e7}(0, t) \\
\lambda^{e1}(1, t) &= \lambda^{e2}(0, t)A_{v_1}^{e2}(t) + \lambda^{e3}(0, t)A_{v_1}^{e3}(t), \\
\lambda^{e2}(1, t) &= \lambda^{e4}(0, t)A_{v_2}^{e4}(t) + \lambda^{e5}(0, t)A_{v_2}^{e5}(t), \\
\lambda^{e3}(1, t) &= \lambda^{e4}(1, t) = A_{v_3}(t)\lambda^{e6}(0, t), \\
\lambda^{e5}(1, t) &= \lambda^{e6}(1, t) = A_{v_4}(t)\lambda^{e7}(0, t), \\
\delta_u J_1(t) &= -\lambda^{e1}(0, t), \\
\delta_{A_{v_1}^{e3}} J_1(t) &= (\lambda^{e2}(0, t) - \lambda^{e3}(0, t))f^{e1}(1, t), \\
\delta_{A_{v_2}^{e5}} J_1(t) &= (\lambda^{e4}(0, t) - \lambda^{e5}(0, t))f^{e2}(1, t), \\
\delta_{A_{v_3}} J_1(t) &= -\lambda^{e6}(0, t)(f^{e3}(1, t) + f^{e4}(1, t)), \\
\delta_{A_{v_4}} J_1(t) &= -\lambda^{e7}(0, t)(f^{e5}(1, t) + f^{e6}(1, t)).
\end{aligned} \tag{5.7}$$

Herein the functions $\lambda(x, t)$ and $\phi(t)$ are the adjoint states for the equality constraints induced by the PDEs on the arcs and the ODEs at the vertices, respectively.

Remark 5.6. *Since the specified fractions are defined by the system as $\sum A_{v_1}^{e+}(t) = 1$, and $\sum A_{v_2}^{e+}(t) = 1$ in the dispersing vertices v_1 and v_2 , respectively. the variables $A_{v_1}^{e3}$ and $A_{v_2}^{e5}$ are the controllable ones, where the others can be obtained from these complementary equations.*

Proof. The Lagrangian L is constructed to evaluate the necessary first order optimality conditions to obtain

$$\begin{aligned}
L_1 = & \frac{1}{2} \int_{t_j}^{t_j+P} (f^*(t) - f^{e\tau}(1, t))^2 dt \\
& + \sum_{e \in \{e_1, e_2, \dots, e_7\}} \int_{t_j}^{t_j+P} \int_0^1 \lambda^e \left(\frac{\partial}{\partial t} \rho^e + \frac{\partial}{\partial x} f^e(x, t) \right) dx dt \\
& + \sum_{e_{v_1}^+ \in \{e_2, e_3\}} \int_{t_j}^{t_j+P} \phi_{v_1}^{e_{v_1}^+} \left(\dot{q}_{v_1}^{e_{v_1}^+} - A_{v_1}^{e_{v_1}^+} f^{e_{v_1}^-}(1, t) + f^{e_{v_1}^+}(0, t) \right) dt \\
& + \sum_{e_{v_2}^+ \in \{e_4, e_5\}} \int_{t_j}^{t_j+P} \phi_{v_2}^{e_{v_2}^+} \left(\dot{q}_{v_2}^{e_{v_2}^+} - A_{v_2}^{e_{v_2}^+} f^{e_{v_2}^-}(1, t) + f^{e_{v_2}^+}(0, t) \right) dt \\
& + \int_{t_j}^{t_j+P} \phi_{v_3}^{e_{v_3}^+} \left(\dot{q}_{v_3}^{e_{v_3}^+} - A_{v_3}(t) \sum_{e_{v_3}^- \in \{e_3, e_4\}} f^{e_{v_3}^-}(1, t) + f^{e_{v_3}^+}(0, t) \right) dt \\
& + \int_{t_j}^{t_j+P} \phi_{v_4}^{e_{v_4}^+} \left(\dot{q}_{v_4}^{e_{v_4}^+} - A_{v_4}(t) \sum_{e_{v_4}^- \in \{e_5, e_6\}} f^{e_{v_4}^-}(1, t) + f^{e_{v_4}^+}(0, t) \right) dt.
\end{aligned} \tag{5.8}$$

By using the integration by parts in (5.8) becomes

$$\begin{aligned}
L_1 = & \frac{1}{2} \int_{t_j}^{t_j+P} (f^*(t) - f^{e\tau}(1, t))^2 dt \\
& + \sum_e \int_0^1 \lambda^e(x, t_j + P) \rho^e(x, t_j + P) dx - \sum_e \int_0^1 \lambda^e(x, t_j) \rho^e(x, t_j) dx \\
& - \sum_e \int_{t_j}^{t_j+P} \int_0^1 \frac{\partial \lambda^e}{\partial t} \rho^e dx dt + \sum_e \int_{t_j}^{t_j+P} \lambda^e(1, t) f^e(1, t) dt \\
& - \sum_e \int_{t_j}^{t_j+P} \lambda^e(0, t) f^e(0, t) dt - \sum_e \int_{t_j}^{t_j+P} \int_0^1 \frac{\partial \lambda^e}{\partial x} f^e(x, t) dx dt \\
& + \left[\sum_{e_{v_1}^+ \in \{e_2, e_3\}} \phi_{v_1}^{e_{v_1}^+} \dot{q}_{v_1}^{e_{v_1}^+} \right]_{t=t_j}^{t=t_j+P} - \sum_{e_{v_1}^+ \in \{e_2, e_3\}} \int_{t_j}^{t_j+P} \dot{\phi}_{v_1}^{e_{v_1}^+} \dot{q}_{v_1}^{e_{v_1}^+} dt \\
& + \sum_{e_{v_1}^+ \in \{e_2, e_3\}} \int_{t_j}^{t_j+P} \phi_{v_1}^{e_{v_1}^+} \left(f^{e_{v_1}^+}(0, t) - A_{v_1}^{e_{v_1}^+} f^{e_{v_1}^-}(1, t) \right) dt \\
& + \left[\sum_{e_{v_2}^+ \in \{e_4, e_5\}} \phi_{v_2}^{e_{v_2}^+} \dot{q}_{v_2}^{e_{v_2}^+} \right]_{t=t_j}^{t=t_j+P} - \sum_{e_{v_2}^+ \in \{e_4, e_5\}} \int_{t_j}^{t_j+P} \dot{\phi}_{v_2}^{e_{v_2}^+} \dot{q}_{v_2}^{e_{v_2}^+} dt \\
& + \sum_{e_{v_2}^+ \in \{e_4, e_5\}} \int_{t_j}^{t_j+P} \phi_{v_2}^{e_{v_2}^+} \left(f^{e_{v_2}^+}(0, t) - A_{v_2}^{e_{v_2}^+} f^{e_{v_2}^-}(1, t) \right) dt
\end{aligned}$$

$$\begin{aligned}
& + \left[\phi_{v_3}^{e_{v_3}^+} q_{v_3}^{e_{v_3}^+} \right]_{t=t_j}^{t=t_j+P} - \int_{t_j}^{t_j+P} \dot{\phi}_{v_3}^{e_{v_3}^+} q_{v_3}^{e_{v_3}^+} dt \\
& + \int_{t_j}^{t_j+P} \phi_{v_3}^{e_{v_3}^+} \left(f^{e_{v_3}^+}(0, t) - A_{v_3}(t) \sum_{e_{v_3}^- \in \{e_3, e_4\}} f^{e_{v_3}^-}(1, t) \right) dt \\
& + \left[\phi_{v_4}^{e_{v_4}^+} q_{v_4}^{e_{v_4}^+} \right]_{t=t_j}^{t=t_j+P} - \int_{t_j}^{t_j+P} \dot{\phi}_{v_4}^{e_{v_4}^+} q_{v_4}^{e_{v_4}^+} dt \\
& + \int_{t_j}^{t_j+P} \phi_{v_4}^{e_{v_4}^+} \left(f^{e_{v_4}^+}(0, t) - A_{v_4}(t) \sum_{e_{v_4}^- \in \{e_5, e_6\}} f^{e_{v_4}^-}(1, t) \right) dt.
\end{aligned}$$

Utilizing the relations are given by the system such as the main inflow, main outflow, outflow before the vertex v , and inflow after the vertex v

$$\begin{aligned}
u(t) &= \frac{\mu^{e_1} \rho^{e_1}(0, t)}{M^{e_1} + \rho^{e_1}(0, t)}, \\
y(t) &= \frac{\mu^{e_7} \rho^{e_7}(1, t)}{M^{e_7} + \rho^{e_7}(1, t)}, \\
f^{e_v^-}(1, t) &= \frac{\mu^{e_v^-} \rho^{e_v^-}(1, t)}{M^{e_v^-} + \rho^{e_v^-}(1, t)}, \\
f^{e_v^+}(0, t) &= \frac{\mu^{e_v^+} \rho^{e_v^+}(0, t)}{M^{e_v^+} + \rho^{e_v^+}(0, t)}.
\end{aligned}$$

After substituting $\delta(1 - A_{v_1}^{e_3}) = \delta A_{v_1}^{e_2}$ and $\delta(1 - A_{v_2}^{e_5}) = \delta A_{v_2}^{e_4}$, and taking the variance due to $u(t)$, $y(t)$, $A_{v_\bullet}^{e_\bullet^+}(t)$, $A_{v_\bullet}(t)$, ρ^e , $f^{e_v^-}(1, t)$, and $f^{e_v^+}(0, t)$ at any vertex v , the Gateaux derivative of L_1 is obtained from the first order optimality condition by

$$\begin{aligned}
\delta L_1 = & \int_{t_j}^{t_j+P} (f^*(t) - y(t))\delta y(t)dt + \sum_e \int_0^1 \lambda^e(x, t_j + P)\delta\rho^e(x, t_j + P)dx \\
& - \sum_e \int_{t_j}^{t_j+P} \int_0^1 \frac{\partial\lambda^e(x, t)}{\partial t} \delta\rho^e(x, t)dxdt + \int_{t_j}^{t_j+P} \lambda^{e_7}(1, t)\delta y(t)dt \\
& + \sum_{i \in \{2,3,\dots,6\}} \int_{t_j}^{t_j+P} \lambda^{e_i}(1, t)\delta f^{e_i}(1, t)dt - \sum_{i \in \{2,3,\dots,6\}} \int_{t_j}^{t_j+P} \lambda^{e_i}(0, t)\delta f^{e_i}(0, t)dt \\
& + \int_{t_j}^{t_j+P} \lambda^{e_1}(1, t)\delta f^{e_1}(1, t)dt - \int_{t_j}^{t_j+P} \lambda^{e_1}(0, t)\delta u(t)dt \\
& - \int_{t_j}^{t_j+P} \lambda^{e_7}(0, t)\delta f^{e_7}(0, t)dt - \sum_e \int_{t_j}^{t_j+P} \int_0^1 \left(\frac{\mu^e M^e}{(M^e + \rho^e(x, t))^2} \right) \frac{\partial\lambda^e(x, t)}{\partial x} \delta\rho^e(x, t)dxdt \\
& + \int_{t_j}^{t_j+P} \left(\phi^{e_{v_1}^{e_2}}(t) - \phi^{e_{v_1}^{e_3}}(t) \right) f^{e_{v_1}^-}(1, t)\delta A_{v_1}^{e_3}dt - \sum_{e_{v_1}^+} \int_{t_j}^{t_j+P} \phi_{v_1}^{e_{v_1}^+}(t) A_{v_1}^{e_{v_1}^+}(t)\delta f^{e_{v_1}^-}(1, t)dt \\
& + \sum_{e_{v_1}^+} \int_{t_j}^{t_j+P} \phi_{v_1}^{e_{v_1}^+}(t)\delta f^{e_{v_1}^+}(0, t)dt + \sum_{e_{v_2}^+} \int_{t_j}^{t_j+P} \phi_{v_2}^{e_{v_2}^+}(t)\delta f^{e_{v_2}^+}(0, t)dt \\
& + \int_{t_j}^{t_j+P} \left(\phi^{e_{v_2}^{e_4}}(t) - \phi^{e_{v_2}^{e_5}}(t) \right) f^{e_{v_2}^-}(1, t)\delta A_{v_2}^{e_5}dt - \sum_{e_{v_2}^+} \int_{t_j}^{t_j+P} \phi_{v_2}^{e_{v_2}^+}(t) A_{v_2}^{e_{v_2}^+}(t)\delta f^{e_{v_2}^-}(1, t)dt \\
& - \int_{t_j}^{t_j+P} \phi_{v_3}^{e_{v_3}^+}(t) \left(f^{e_3}(1, t) + f^{e_4}(1, t) \right) \delta A_{v_3}(t)dt - \int_{t_j}^{t_j+P} \phi_{v_3}^{e_{v_3}^+}(t) A_{v_3}(t)\delta f^{e_3}(1, t)dt \\
& - \int_{t_j}^{t_j+P} \phi_{v_3}^{e_{v_3}^+}(t) A_{v_3}(t)\delta f^{e_4}(1, t)dt + \int_{t_j}^{t_j+P} \phi_{v_3}^{e_{v_3}^+}(t)\delta f^{e_6}(0, t)dt \\
& - \int_{t_j}^{t_j+P} \phi_{v_4}^{e_{v_4}^+}(t) \left(f^{e_5}(1, t) + f^{e_6}(1, t) \right) \delta A_{v_4}(t)dt - \int_{t_j}^{t_j+P} \phi_{v_4}^{e_{v_4}^+}(t) A_{v_4}(t)\delta f^{e_5}(1, t)dt \\
& - \int_{t_j}^{t_j+P} \phi_{v_4}^{e_{v_4}^+}(t) A_{v_4}(t)\delta f^{e_6}(1, t)dt + \int_{t_j}^{t_j+P} \phi_{v_4}^{e_{v_4}^+}(t)\delta f^{e_7}(0, t)dt \\
= & 0.
\end{aligned} \tag{5.9}$$

After reforming and regrouping (5.9), the adjoint equation set (5.7) is derived. \square

Backlog Problem

The optimization is performed for the infinite-dimensional system.

Proposition 2. *The adjoint equations from the complex network in Fig. 5.1 of the Backlog problem (5.6) subject to (5.1), (5.2), and (5.3) after neglecting the inequality constraints are*

defined as

$$\begin{aligned}
\frac{\partial \lambda^e}{\partial t} &= -\frac{\mu^e M^e}{(M^e + \rho^e(x, t))^2} \frac{\partial \lambda^e}{\partial x}, \quad (x, t) \in (0, 1] \times (t_j, t_j + P], \\
\lambda^e(x, t_j + P) &= 0, \\
\lambda^{e_7}(1, t) &= \int_t^{t_j+P} B(r) dr + B(t_j + P), \quad \forall t \in [t_j, t_j + P] \\
\phi_{v_1}^{e_2}(t) &= \lambda^{e_2}(0, t), \quad \phi_{v_1}^{e_3}(t) = \lambda^{e_3}(0, t) \\
\phi_{v_2}^{e_4}(t) &= \lambda^{e_4}(0, t), \quad \phi_{v_2}^{e_5}(t) = \lambda^{e_5}(0, t) \\
\phi_{v_3}^{e_6}(t) &= \lambda^{e_6}(0, t), \quad \phi_{v_4}^{e_7}(t) = \lambda^{e_7}(0, t) \\
\lambda^{e_1}(1, t) &= \lambda^{e_2}(0, t)A_{v_1}^{e_2}(t) + \lambda^{e_3}(0, t)A_{v_1}^{e_3}(t), \\
\lambda^{e_2}(1, t) &= \lambda^{e_4}(0, t)A_{v_2}^{e_4}(t) + \lambda^{e_5}(0, t)A_{v_2}^{e_5}(t), \\
\lambda^{e_3}(1, t) &= \lambda^{e_4}(1, t) = A_{v_3}(t)\lambda^{e_6}(0, t), \\
\lambda^{e_5}(1, t) &= \lambda^{e_6}(1, t) = A_{v_4}(t)\lambda^{e_7}(0, t), \\
\delta_u J_2(t) &= -\lambda^{e_1}(0, t), \\
\delta_{A_{v_1}^{e_3}} J_2(t) &= (\lambda^{e_2}(0, t) - \lambda^{e_3}(0, t))f^{e_1}(1, t), \\
\delta_{A_{v_2}^{e_5}} J_2(t) &= (\lambda^{e_4}(0, t) - \lambda^{e_5}(0, t))f^{e_2}(1, t), \\
\delta_{A_{v_3}} J_2(t) &= -\lambda^{e_6}(0, t)(f^{e_3}(1, t) + f^{e_4}(1, t)), \\
\delta_{A_{v_4}} J_2(t) &= -\lambda^{e_7}(0, t)(f^{e_5}(1, t) + f^{e_6}(1, t)).
\end{aligned} \tag{5.10}$$

where the functions $\{\lambda^e(x, t)\}$ and $\{\phi_{v_i}^{e_j}(t)\}$ are the adjoint states for the equality constraints induced by the PDEs on the arcs and the ODEs at the vertices, respectively.

Proof. : The formulation of the Lagrangian L_2 is constructed by

$$\begin{aligned}
L_2 &= \frac{1}{2} \int_{t_j}^{t_j+P} (B(t))^2 dt + \frac{1}{2} (B(t_j + P))^2 \\
&+ \sum_{e \in \{e_1, e_2, \dots, e_7\}} \int_{t_j}^{t_j+P} \int_0^1 \lambda^e \left(\frac{\partial}{\partial t} \rho^e + \frac{\partial}{\partial x} f^e(x, t) \right) dx dt \\
&+ \sum_{e_1^+ \in \{e_2, e_3\}} \int_{t_j}^{t_j+P} \phi_{v_1}^{e_1^+} \left(\dot{q}_{v_1}^{e_1^+} - A_{v_1}^{e_1^+} f^{e_{v_1}^-}(1, t) + f^{e_{v_1}^+}(0, t) \right) dt \\
&+ \sum_{e_2^+ \in \{e_4, e_5\}} \int_{t_j}^{t_j+P} \phi_{v_2}^{e_2^+} \left(\dot{q}_{v_2}^{e_2^+} - A_{v_2}^{e_2^+} f^{e_{v_2}^-}(1, t) + f^{e_{v_2}^+}(0, t) \right) dt \\
&+ \int_{t_j}^{t_j+P} \phi_{v_3}^{e_3^+} \left(\dot{q}_{v_3}^{e_3^+} - A_{v_3}(t) \sum_{e_{v_3}^- \in \{e_3, e_4\}} f^{e_{v_3}^-}(1, t) + f^{e_{v_3}^+}(0, t) \right) dt \\
&+ \int_{t_j}^{t_j+P} \phi_{v_4}^{e_4^+} \left(\dot{q}_{v_4}^{e_4^+} - A_{v_4}(t) \sum_{e_{v_4}^- \in \{e_5, e_6\}} f^{e_{v_4}^-}(1, t) + f^{e_{v_4}^+}(0, t) \right) dt.
\end{aligned} \tag{5.11}$$

After taking the integration by parts, one gets

$$\begin{aligned}
L_2 = & \frac{1}{2} \int_{t_j}^{t_j+P} (B(t))^2 dt + \frac{1}{2} (B(t_j + P))^2 \\
& + \sum_e \int_0^1 \lambda^e(x, t_j + P) \rho^e(x, t_j + P) dx - \sum_e \int_0^1 \lambda^e(x, t_j) \rho^e(x, t_j) dx \\
& - \sum_e \int_{t_j}^{t_j+P} \int_0^1 \frac{\partial \lambda^e}{\partial t} \rho^e dx dt + \sum_e \int_{t_j}^{t_j+P} \lambda^e(1, t) f^e(1, t) dt \\
& - \sum_e \int_{t_j}^{t_j+P} \lambda^e(0, t) f^e(0, t) dt - \sum_e \int_{t_j}^{t_j+P} \int_0^1 \frac{\partial \lambda^e}{\partial x} f^e(x, t) dx dt \\
& + \left[\sum_{e_{v_1}^+ \in \{e_2, e_3\}} \phi_{v_1}^{e_{v_1}^+} q_{v_1}^{e_{v_1}^+} \right]_{t=t_j}^{t=t_j+P} - \sum_{e_{v_1}^+ \in \{e_2, e_3\}} \int_{t_j}^{t_j+P} \dot{\phi}_{v_1}^{e_{v_1}^+} q_{v_1}^{e_{v_1}^+} dt \\
& + \sum_{e_{v_1}^+ \in \{e_2, e_3\}} \int_{t_j}^{t_j+P} \phi_{v_1}^{e_{v_1}^+} \left(f^{e_{v_1}^+}(0, t) - A_{v_1}^{e_{v_1}^+} f^{e_{v_1}^-}(1, t) \right) dt \\
& + \left[\sum_{e_{v_2}^+ \in \{e_4, e_5\}} \phi_{v_2}^{e_{v_2}^+} q_{v_2}^{e_{v_2}^+} \right]_{t=t_j}^{t=t_j+P} - \sum_{e_{v_2}^+ \in \{e_4, e_5\}} \int_{t_j}^{t_j+P} \dot{\phi}_{v_2}^{e_{v_2}^+} q_{v_2}^{e_{v_2}^+} dt \\
& + \sum_{e_{v_2}^+ \in \{e_4, e_5\}} \int_{t_j}^{t_j+P} \phi_{v_2}^{e_{v_2}^+} \left(f^{e_{v_2}^+}(0, t) - A_{v_2}^{e_{v_2}^+} f^{e_{v_2}^-}(1, t) \right) dt \\
& + \left[\phi_{v_3}^{e_{v_3}^+} q_{v_3}^{e_{v_3}^+} \right]_{t=t_j}^{t=t_j+P} - \int_{t_j}^{t_j+P} \dot{\phi}_{v_3}^{e_{v_3}^+} q_{v_3}^{e_{v_3}^+} dt \\
& + \int_{t_j}^{t_j+P} \phi_{v_3}^{e_{v_3}^+} \left(f^{e_{v_3}^+}(0, t) - A_{v_3}(t) \sum_{e_{v_3}^- \in \{e_3, e_4\}} f^{e_{v_3}^-}(1, t) \right) dt \\
& + \left[\phi_{v_4}^{e_{v_4}^+} q_{v_4}^{e_{v_4}^+} \right]_{t=t_j}^{t=t_j+P} - \int_{t_j}^{t_j+P} \dot{\phi}_{v_4}^{e_{v_4}^+} q_{v_4}^{e_{v_4}^+} dt \\
& + \int_{t_j}^{t_j+P} \phi_{v_4}^{e_{v_4}^+} \left(f^{e_{v_4}^+}(0, t) - A_{v_4}(t) \sum_{e_{v_4}^- \in \{e_5, e_6\}} f^{e_{v_4}^-}(1, t) \right) dt.
\end{aligned} \tag{5.12}$$

Likewise the demand tracking case, $u(t)$, $y(t)$, $f^{e_{v \bullet}^-}(1, t)$, and $f^{e_{v \bullet}^+}(0, t)$ are given from the system

and taking the variational of L_2 and equalizing with zero as follows

$$\begin{aligned}
\delta L_2 = & - \int_{t_j}^{t_j+P} B(r) \int_{t_j}^r \delta y(\tau) d\tau dt + B(t_j + P) \delta B(t_j + P) \\
& + \sum_e \int_0^1 \lambda^e(x, t_f) \delta \rho^e(x, t_j + P) dx \\
& - \sum_e \int_{t_j}^{t_j+P} \int_0^1 \frac{\partial \lambda^e(x, t)}{\partial t} \delta \rho^e(x, t) dx dt + \int_{t_j}^{t_j+P} \lambda^{e_7}(1, t) \delta y(t) dt \\
& + \sum_{i \in \{2,3,\dots,6\}} \int_{t_j}^{t_j+P} \lambda^{e_i}(1, t) \delta f^{e_i}(1, t) dt - \sum_{i \in \{2,3,\dots,6\}} \int_{t_j}^{t_j+P} \lambda^{e_i}(0, t) \delta f^{e_i}(0, t) dt \\
& + \int_{t_j}^{t_j+P} \lambda^{e_1}(1, t) \delta f^{e_1}(1, t) dt - \int_{t_j}^{t_j+P} \lambda^{e_1}(0, t) \delta u(t) dt \\
& - \int_{t_j}^{t_j+P} \lambda^{e_7}(0, t) \delta f^{e_7}(0, t) dt - \sum_e \int_{t_j}^{t_j+P} \int_0^1 \left(\frac{\mu^e M^e}{(M^e + \rho^e(x, t))^2} \right) \frac{\partial \lambda^e(x, t)}{\partial x} \delta \rho^e(x, t) dx dt \\
& + \sum_{e_{v_1}^+} \int_{t_j}^{t_j+P} \phi_{v_1}^{e_{v_1}^+} \dot{q}_{v_1}^{e_{v_1}^+} dt + \sum_{e_{v_2}^+} \int_{t_j}^{t_j+P} \phi_{v_2}^{e_{v_2}^+} \dot{q}_{v_2}^{e_{v_2}^+} dt \\
& - \sum_{e_{v_1}^+} \int_{t_j}^{t_j+P} \phi_{v_1}^{e_{v_1}^+}(t) f^{e_{v_1}^-}(1, t) \delta A_{v_1}^{e_{v_1}^+} dt - \sum_{e_{v_1}^+} \int_{t_j}^{t_j+P} \phi_{v_1}^{e_{v_1}^+}(t) A_{v_1}^{e_{v_1}^+}(t) \delta f^{e_{v_1}^-}(1, t) dt \\
& + \sum_{e_{v_1}^+} \int_{t_j}^{t_j+P} \phi_{v_1}^{e_{v_1}^+}(t) \delta f^{e_{v_1}^+}(0, t) dt + \sum_{e_{v_2}^+} \int_{t_j}^{t_j+P} \phi_{v_2}^{e_{v_2}^+}(t) \delta f^{e_{v_2}^+}(0, t) dt \\
& - \sum_{e_{v_2}^+} \int_{t_j}^{t_j+P} \phi_{v_2}^{e_{v_2}^+}(t) f^{e_{v_2}^-}(1, t) \delta A_{v_2}^{e_{v_2}^+} dt - \sum_{e_{v_2}^+} \int_{t_j}^{t_j+P} \phi_{v_2}^{e_{v_2}^+}(t) A_{v_2}^{e_{v_2}^+}(t) \delta f^{e_{v_2}^-}(1, t) dt \\
& + \int_{t_j}^{t_j+P} \phi_{v_3}^{e_{v_3}^+} \dot{q}_{v_3}^{e_{v_3}^+} dt + \int_{t_j}^{t_j+P} \phi_{v_4}^{e_{v_4}^+} \dot{q}_{v_4}^{e_{v_4}^+} dt \\
& - \int_{t_j}^{t_j+P} \phi_{v_3}^{e_{v_3}^+}(t) \left(f^{e_3}(1, t) + f^{e_4}(1, t) \right) \delta A_{v_3}(t) dt - \int_{t_j}^{t_j+P} \phi_{v_3}^{e_{v_3}^+}(t) A_{v_3}(t) \delta f^{e_3}(1, t) dt \\
& - \int_{t_j}^{t_j+P} \phi_{v_3}^{e_{v_3}^+}(t) A_{v_3}(t) \delta f^{e_4}(1, t) dt + \int_{t_j}^{t_j+P} \phi_{v_3}^{e_{v_3}^+}(t) \delta f^{e_6}(0, t) dt \\
& - \int_{t_j}^{t_j+P} \phi_{v_4}^{e_{v_4}^+}(t) \left(f^{e_5}(1, t) + f^{e_6}(1, t) \right) \delta A_{v_4}(t) dt - \int_{t_j}^{t_j+P} \phi_{v_4}^{e_{v_4}^+}(t) A_{v_4}(t) \delta f^{e_5}(1, t) dt \\
& - \int_{t_j}^{t_j+P} \phi_{v_4}^{e_{v_4}^+}(t) A_{v_4}(t) \delta f^{e_6}(1, t) dt + \int_{t_j}^{t_j+P} \phi_{v_4}^{e_{v_4}^+}(t) \delta f^{e_7}(0, t) dt \\
& = 0.
\end{aligned} \tag{5.13}$$

By substituting

$$\delta y(t) = \delta_d(t - \gamma), \quad \gamma \in (t_j, t_j + P),$$

$$\begin{aligned}\delta y(\tau) &= \delta_d(\tau - \gamma), \\ \delta(1 - A_{v_1}^{e_3}) &= \delta A_{v_1}^{e_2}, \\ \delta(1 - A_{v_2}^{e_5}) &= \delta A_{v_2}^{e_4},\end{aligned}$$

into (5.13), and the first order optimality condition is expressed by

$$\begin{aligned}\delta L_2 &= - \int_{t_j}^{t_j+P} B(r) \int_{t_j}^r \delta_d(\tau - \gamma) d\tau dr - B(t_f) \int_{t_j}^{t_j+P} \delta_d(t - \gamma) dt \\ &+ \sum_e \int_0^1 \lambda^e(x, t_j + P) \delta \rho^e(x, t_j + P) dx \\ &- \sum_e \int_{t_j}^{t_j+P} \int_0^1 \frac{\partial \lambda^e(x, t)}{\partial t} \delta \rho^e(x, t) dx dt + \int_{t_j}^{t_j+P} \lambda^{e_7}(1, t) \delta_{Dirac}(t - \gamma) dt \\ &+ \sum_{i \in \{2, 3, \dots, 6\}} \int_{t_j}^{t_j+P} \lambda^{e_i}(1, t) \delta f^{e_i}(1, t) dt - \sum_{i \in \{2, 3, \dots, 6\}} \int_{t_j}^{t_j+P} \lambda^{e_i}(0, t) \delta f^{e_i}(0, t) dt \\ &+ \int_{t_j}^{t_j+P} \lambda^{e_1}(1, t) \delta f^{e_1}(1, t) dt - \int_{t_j}^{t_j+P} \lambda^{e_1}(0, t) \delta u(t) dt \\ &- \int_{t_j}^{t_j+P} \lambda^{e_7}(0, t) \delta f^{e_7}(0, t) dt - \sum_e \int_{t_j}^{t_j+P} \int_0^1 \left(\frac{\mu^e M^e}{(M^e + \rho^e(x, t))^2} \right) \frac{\partial \lambda^e(x, t)}{\partial x} \delta \rho^e(x, t) dx dt \\ &+ \int_{t_j}^{t_j+P} \left(\phi_{v_1}^{e_{v_2}}(t) - \phi_{v_1}^{e_{v_3}}(t) \right) f^{e_{v_1}}(1, t) \delta A_{v_1}^{e_3} dt - \sum_{e_{v_1}^+} \int_{t_j}^{t_j+P} \phi_{v_1}^{e_{v_1}^+}(t) A_{v_1}^{e_{v_1}^+}(t) \delta f^{e_{v_1}}(1, t) dt \\ &+ \sum_{e_{v_1}^+} \int_{t_j}^{t_j+P} \phi_{v_1}^{e_{v_1}^+}(t) \delta f^{e_{v_1}^+}(0, t) dt + \sum_{e_{v_2}^+} \int_{t_j}^{t_j+P} \phi_{v_2}^{e_{v_2}^+}(t) \delta f^{e_{v_2}^+}(0, t) dt \\ &+ \int_{t_j}^{t_j+P} \left(\phi_{v_2}^{e_{v_4}}(t) - \phi_{v_2}^{e_{v_5}}(t) \right) f^{e_{v_2}}(1, t) \delta A_{v_2}^{e_5} dt - \sum_{e_{v_2}^+} \int_{t_j}^{t_j+P} \phi_{v_2}^{e_{v_2}^+}(t) A_{v_2}^{e_{v_2}^+}(t) \delta f^{e_{v_2}}(1, t) dt \\ &- \int_{t_j}^{t_j+P} \phi_{v_3}^{e_{v_3}^+}(t) \left(f^{e_3}(1, t) + f^{e_4}(1, t) \right) \delta A_{v_3}(t) dt - \int_{t_j}^{t_j+P} \phi_{v_3}^{e_{v_3}^+}(t) A_{v_3}(t) \delta f^{e_3}(1, t) dt \\ &- \int_{t_j}^{t_j+P} \phi_{v_3}^{e_{v_3}^+}(t) A_{v_3}(t) \delta f^{e_4}(1, t) dt + \int_{t_j}^{t_j+P} \phi_{v_3}^{e_{v_3}^+}(t) \delta f^{e_6}(0, t) dt \\ &- \int_{t_j}^{t_j+P} \phi_{v_4}^{e_{v_4}^+}(t) \left(f^{e_5}(1, t) + f^{e_6}(1, t) \right) \delta A_{v_4}(t) dt - \int_{t_j}^{t_j+P} \phi_{v_4}^{e_{v_4}^+}(t) A_{v_4}(t) \delta f^{e_5}(1, t) dt \\ &- \int_{t_j}^{t_j+P} \phi_{v_4}^{e_{v_4}^+}(t) A_{v_4}(t) \delta f^{e_6}(1, t) dt + \int_{t_j}^{t_j+P} \phi_{v_4}^{e_{v_4}^+}(t) \delta f^{e_7}(0, t) dt \\ &= 0.\end{aligned}$$

(5.14)

By applying the shifting property of the delta function, one obtains

$$\begin{aligned}\lambda^{e\tau}(1, \gamma) &= \int_{t_j}^{t_j+P} \lambda^{e\tau}(1, t) \delta_d(t - \gamma) dt, \\ \int_{\gamma}^{t_f} B(r) dr &= \int_{t_j}^{t_j+P} B(r) \int_{t_j}^r \delta_d(\tau - \gamma) d\tau dr.\end{aligned}\tag{5.15}$$

Where $\gamma \in (t_j, t_j + P)$ is any value in the domain t and it can be replaced by t . By reforming and regrouping (5.14), the adjoint equations (5.10) are derived. \square

5.4.2 Discretization Phase

Generally speaking, the discretization is performed after getting the closed-form of the adjoint state equations and the gradients from (5.7) and (5.10) of each OCP (demand tracking or backlog). The demand tracking problem (5.5) is discretized in a form

$$\min_{\boldsymbol{\vartheta}} J_1(\boldsymbol{\vartheta}) = \frac{1}{2} \sum_{j=\alpha}^{\alpha+P} \left(f_j^* - y_j \right)^2 \Delta t,\tag{5.16}$$

and the discretization of backlog problem (5.6) is chosen as

$$\min_{\boldsymbol{\vartheta}} J_2(\boldsymbol{\vartheta}) = \frac{1}{2} \sum_{j=\alpha}^{\alpha+P} \left(\sum_{r=\alpha}^j (f_r^* - y_r) \Delta \tau \right)^2 \Delta t + \frac{1}{2} \left(\sum_{r=\alpha}^{\alpha+P} (f_r^* - y_r) \Delta \tau \right)^2,\tag{5.17}$$

where Δt and $\Delta \tau$ denote the time steps where $\Delta t = n \Delta \tau$ and $y_r = y(r \Delta \tau)$; $j = \alpha, \alpha + 1, \alpha + 2, \dots, \alpha + P$ and $r = \alpha, \alpha + 1, \alpha + 2, \dots, j$, and $\forall \alpha, r, j \in \mathbb{Z}$. The PDE of the arc e is discretized using the FD upwind scheme [60, 106] according to

$$\begin{bmatrix} \rho_{1,j+1}^e \\ \rho_{2,j+1}^e \\ \vdots \\ \rho_{M,j+1}^e \end{bmatrix} = \begin{bmatrix} (1 - S(\rho_{1,j}^e)) & 0 & \cdots & 0 \\ S(\rho_{1,j}^e) & (1 - S(\rho_{2,j}^e)) & \cdots & 0 \\ \vdots & \vdots & \ddots & \vdots \\ 0 & \cdots & S(\rho_{M-1,j}^e) & (1 - S(\rho_{M,j}^e)) \end{bmatrix} \begin{bmatrix} \rho_{1,j}^e \\ \rho_{2,j}^e \\ \vdots \\ \rho_{M,j}^e \end{bmatrix} + \begin{bmatrix} \frac{\Delta t}{\Delta x} \\ 0 \\ \vdots \\ 0 \end{bmatrix} (u_j + d_j),\tag{5.18}$$

where $S(\rho_{i,j}^e) = \frac{\Delta t}{\Delta x} \frac{\mu^e}{(M^e + \rho_{i,j}^e)}$, $\rho_{i,j}^e = \rho^e(i \Delta x, j \Delta t)$, $f_{i,j}^e = f^e(\rho_{i,j}^e)$, $\Delta x = 1/M^e$, and $u_j = u(j \Delta t)$ for $i = 1, 2, \dots, M^e$. For numerical stability, Δt is adapted to fulfill the Courant-Friedrichs-Lewy condition $CFL = \frac{V_m^e \Delta t}{\Delta x} \leq 1$, where $V_m^e = \frac{\mu^e}{M^e + \rho_{\min}^e}$ is the maximum speed of the arc e .

Subsequently, the time discretization of the ODEs (5.2) in the dispersing case has the following structure

$$\begin{aligned}
q_{v_1,j+1}^{e_{v_1}^+} &= q_{v_1,j}^{e_{v_1}^+} + \Delta t \left(A_{v_1,j}^{e_{v_1}^+} f_{M^e,j}^{e_{v_1}^-} - f_{0,j}^{e_{v_1}^+} \right), \\
q_{v_2,j+1}^{e_{v_2}^+} &= q_{v_2,j}^{e_{v_2}^+} + \Delta t \left(A_{v_2,j}^{e_{v_2}^+} f_{M^e,j}^{e_{v_2}^-} - f_{0,j}^{e_{v_2}^+} \right), \\
f_{0,j}^{e_{v_1}^+} &= \min \left\{ \mu^{e_{v_1}^+}, \frac{q_{v_1,j}^{e_{v_1}^+}}{\kappa} \right\}, \\
f_{0,j}^{e_{v_2}^+} &= \min \left\{ \mu^{e_{v_2}^+}, \frac{q_{v_2,j}^{e_{v_2}^+}}{\kappa} \right\}, \\
q_{v_1,0}^{e_{v_1}^+} &= 0, \quad q_{v_2,0}^{e_{v_2}^+} = 0,
\end{aligned} \tag{5.19}$$

where $q_{v_\bullet,j}^{e_{v_\bullet}^+} = q_{v_\bullet}^{e_{v_\bullet}^+}(j\Delta t)$, and $A_{v_\bullet,j}^{e_{v_\bullet}^+} = A_{v_\bullet}^{e_{v_\bullet}^+}(j\Delta t)$. Furthermore, time discretization of the ODEs in (5.3) for the merging case reads

$$\begin{aligned}
q_{v_3,j+1}^{e_{v_3}^+} &= q_{v_3,j}^{e_{v_3}^+} + \Delta t \left(A_{v_3,j}^{e_{v_3}^+} \sum_{e_{v_3}^-} f_{M^e,j}^{e_{v_3}^-} - f_{0,j}^{e_{v_3}^+} \right), \\
q_{v_4,j+1}^{e_{v_4}^+} &= q_{v_4,j}^{e_{v_4}^+} + \Delta t \left(A_{v_4,j}^{e_{v_4}^+} \sum_{e_{v_4}^-} f_{M^e,j}^{e_{v_4}^-} - f_{0,j}^{e_{v_4}^+} \right), \\
f_{0,j}^{e_{v_3}^+} &= \min \left\{ \mu^{e_{v_3}^+}, \frac{q_{v_3,j}^{e_{v_3}^+}}{\kappa} \right\}, \\
f_{0,j}^{e_{v_4}^+} &= \min \left\{ \mu^{e_{v_4}^+}, \frac{q_{v_4,j}^{e_{v_4}^+}}{\kappa} \right\}, \\
q_{v_3,0}^{e_{v_3}^+} &= 0, \quad q_{v_4,0}^{e_{v_4}^+} = 0,
\end{aligned} \tag{5.20}$$

The resulting finite dimensional approximation of (5.1), (5.2) and (5.3) is given by (5.18), (5.19) and (5.20), respectively. The temporal-spatial discretization of the adjoint equations is the same as the discretization of the system dynamic, for $i = M^e - 1, \dots, 2, 1$, $j = \alpha + P + 1, \dots, \alpha + 1$

yield

$$\begin{aligned}
\lambda_{i,j-1}^e &= \lambda_{i,j}^e - \frac{\Delta t}{\Delta x} \left(\frac{\mu^e M^e}{(M^e + \rho_{i,j}^e)^2} \right) (\lambda_{i+1,j}^e - \lambda_{i,j}^e), \\
\lambda_{i,N}^e &= 0, \quad \text{for terminal conditions,} \\
\lambda_{M^e,j}^{e7} &= -(y_j - f_j^*), \quad \text{for BC of the demand tracking,} \\
\lambda_{M^e,j}^{e7} &= \sum_{j=\alpha+P}^{\alpha} B_j \Delta t + B_{\alpha+P}, \quad \text{for BC of the backlog,} \\
\phi_{v_1,j}^{e2} &= \lambda_{0,j}^{e2}, \quad \phi_{v_1,j}^{e3} = \lambda_{0,j}^{e3} \\
\phi_{v_2,j}^{e4} &= \lambda_{0,j}^{e4}, \quad \phi_{v_2,j}^{e5} = \lambda_{0,j}^{e5} \\
\phi_{v_3,j}^{e6} &= \lambda_{0,j}^{e6}, \quad \phi_{v_4,j}^{e7} = \lambda_{0,j}^{e7} \\
\lambda_{M^e,j}^{e1} &= \lambda_{0,j}^{e2} A_{v_1,j}^{e2} + \lambda_{0,j}^{e3} A_{v_1,j}^{e3}, \\
\lambda_{M^e,j}^{e2} &= \lambda_{0,j}^{e4} A_{v_2,j}^{e4} + \lambda_{0,j}^{e5} A_{v_2,j}^{e5}, \\
\lambda_{M^e,j}^{e3} &= \lambda_{M^e,j}^{e4} = A_{v_3,j} \lambda_{0,j}^{e6}, \\
\lambda_{M^e,j}^{e5} &= \lambda_{M^e,j}^{e6} = A_{v_4,j} \lambda_{0,j}^{e7}, \\
\delta_u J_j &= -\lambda_{0,j}^{e1}, \\
\delta_{A_{v_1}^{e3}} J_j &= (\lambda_{0,j}^{e2} - \lambda_{0,j}^{e3}) f_{M^e,j}^{e1}, \\
\delta_{A_{v_2}^{e5}} J_j &= (\lambda_{0,j}^{e4} - \lambda_{0,j}^{e5}) f_{M^e,j}^{e2}, \\
\delta_{A_{v_3}} J_j &= -\lambda_{0,j}^{e6} (f_{M^e,j}^{e3} + f_{M^e,j}^{e4}), \\
\delta_{A_{v_4}} J_j &= -\lambda_{0,j}^{e7} (f_{M^e,j}^{e5} + f_{M^e,j}^{e6}).
\end{aligned} \tag{5.21}$$

For obtaining the gradient information, the prediction horizon is utilized two times to solve the system states (5.18), (5.19), (5.20) and the adjoint equations (5.21) numerically forward and backward in time. Based on the gradient information and taking into account the constraints $0 \leq u_j < \mu^{e1}$ and $0 \leq A_{v_{\bullet}}^{e_{\bullet}} \leq 1$, the corresponding optimal values $\boldsymbol{\vartheta}^*$ can be obtained.

Remark 5.7. *The OCPs concerning the inequality constraints can be solved after getting the adjoint equations by Pontryagin's maximum principle. This leads to extra analytical effort and exhausted work specially for this kind of the complex optimization problem. Therefore, these inequality constraints are handled numerically by the function `fmincon` provided by MATLAB.*

5.5 Simulation Results

In this section, several experiments have been conducted: (i) the proper selection of prediction horizon, (ii) the OCPs for the complex networks shown in Fig. 5.1.

5.5.1 Selection of Prediction Horizon

The investigation is performed only on the demand tracking problem. The system parameters are chosen as $\kappa = 0.1$, $M^e = 10$, $\mu^{e1} = 8$ lots/h, $\mu^{e2} = 4$ lots/h, $\mu^{e3} = 5$ lots/h, $\mu^{e4} = 3.5$ lots/h, $\mu^{e5} = 4$ lots/h, $\mu^{e6} = 5$ lots/h, and $\mu^{e7} = 8$ lots/h. The final time $t_f = 40$ h. For the numerical settings are picked as, $\Delta x = 0.1$ and $CFL = 0.5$ in each arc e , $\Delta t = 0.25$, and $C = 1$. The prediction samples P are picked to be 20, 25, 27, 30, 70 and 150 for the corresponding the prediction horizons 5 h, 6.25 h, 6.75 h, 7.5 h, 17.5 h and 37.5 h, respectively. Herein the prediction horizon is the product of the number of the prediction samples P and the time step Δt .

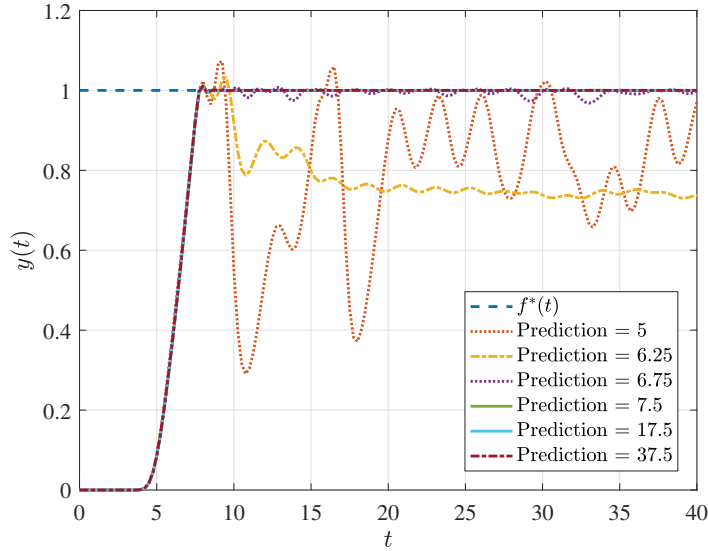


Figure 5.4: AMPC performance for different prediction horizons.

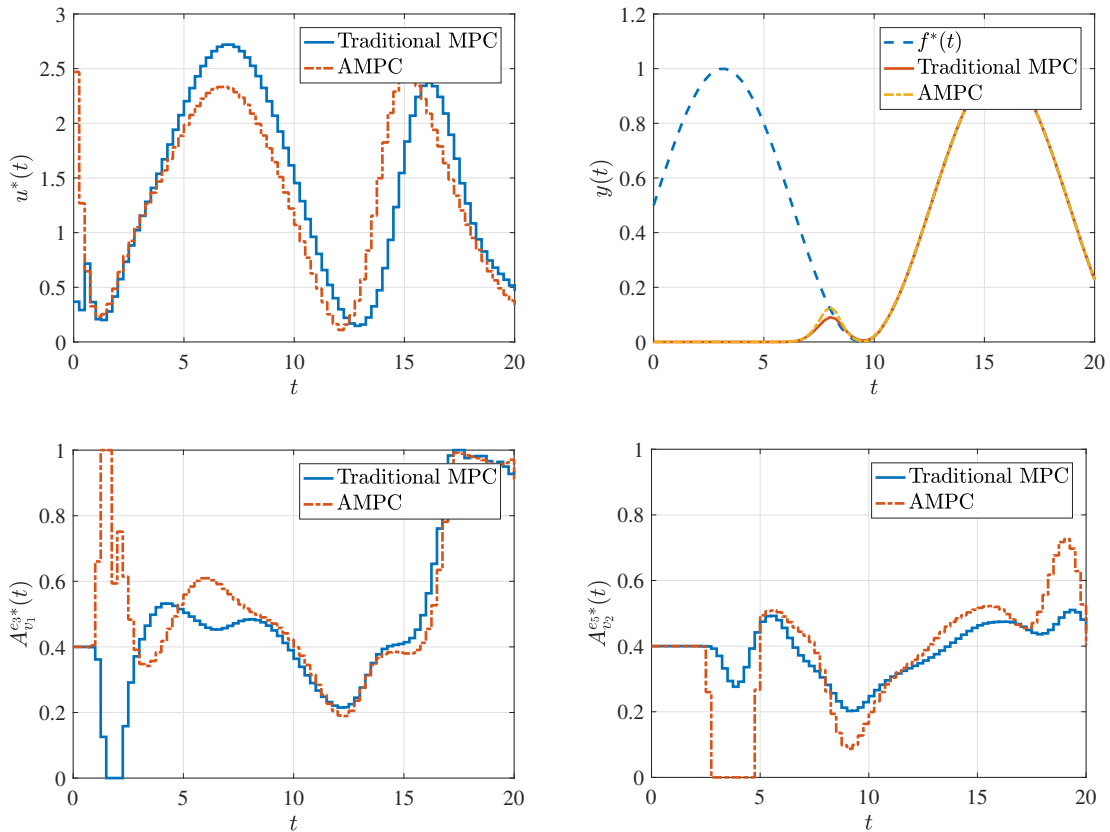
The control parameter C is chosen to become a fixed value to evaluate the AMPC performance by changing only the value of the prediction P . In general, the control horizon is picked due to the appearance of the perturbations, thus reducing the computational time. As shown from Fig. 5.4, the lower value of P obtains the worst performance of AMPC. The reason for this is due to that the prediction horizon does not capture the whole system dynamics. Furthermore, the value of P is still in the transient region because of the system delay. The higher the prediction P the performance gets better. Starting from the prediction horizon equals 17.5 h, and the performance to follow the desired demand trajectory is not changing anymore compared to the larger prediction horizons. To summarize, the best selection of the prediction horizon is when the performance does not vary, which reduces the computational time compared to choosing a larger prediction horizon.

5.5.2 Performance Analysis of AMPC

The performance of the AMPC is investigated for both the demand tracking and the backlog problems. The outcomes are compared to the traditional (slandered) MPC. When there is a disturbance, the AMPC's performance is compared to that of open-loop optimum control.

Demand Tracking Simulation Results

The inflow to the system at the inlet of arc e_1 is $u(t) = f^{e_1}(0, t)$ and the outflow $y(t) = f^{e_7}(1, t)$ is the outlet of the arc e_7 . The manipulated variables are the inflow and the fractions of the vertices $u(t)$, $A_{v_1}^{e_3}(t)$, $A_{v_2}^{e_5}(t)$, $A_{v_3}(t)$ and $A_{v_4}(t)$ respectively. The system parameters are chosen as $\kappa = 0.25$, $M^e = 10$, $\mu^{e_1} = 6$ lots/h, $\mu^{e_2} = 4$ lots/h, $\mu^{e_3} = 3$ lots/h, $\mu^{e_4} = 5$ lots/h, $\mu^{e_5} = 3.5$ lots/h, $\mu^{e_6} = 4.5$ lots/h, and $\mu^{e_7} = 6$ lots/h. The final time $t_f = 20$ h. For the numerical settings are picked as, $\Delta x = 0.1$ and $CFL = 0.5$ in each arc e , $\Delta t = 0.25$, $P = 81$, and $C = 1$.



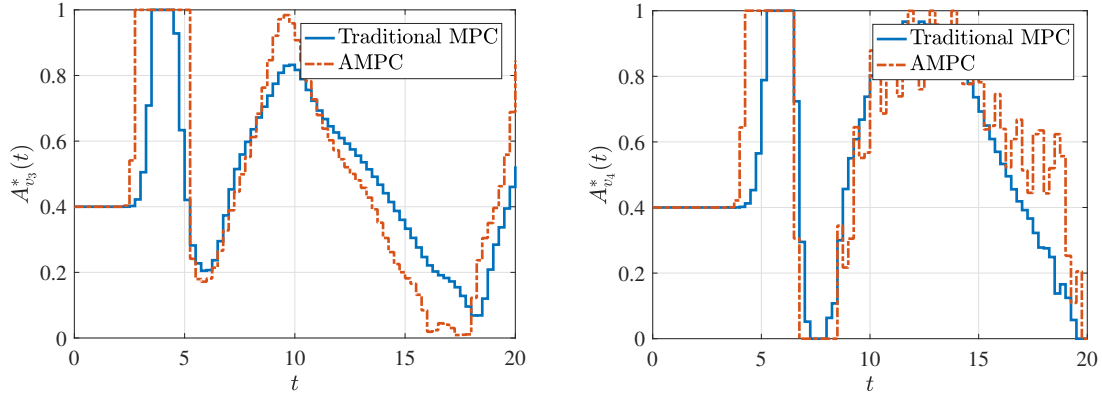


Figure 5.5: The complex network for the demand tracking problem using both AMPC and traditional MPC.

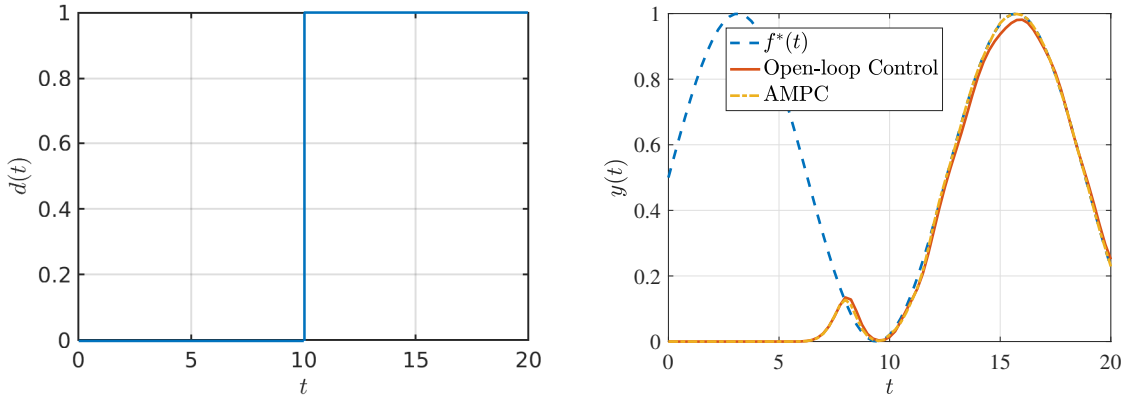


Figure 5.6: The complex network for the demand tracking problem with disturbance.

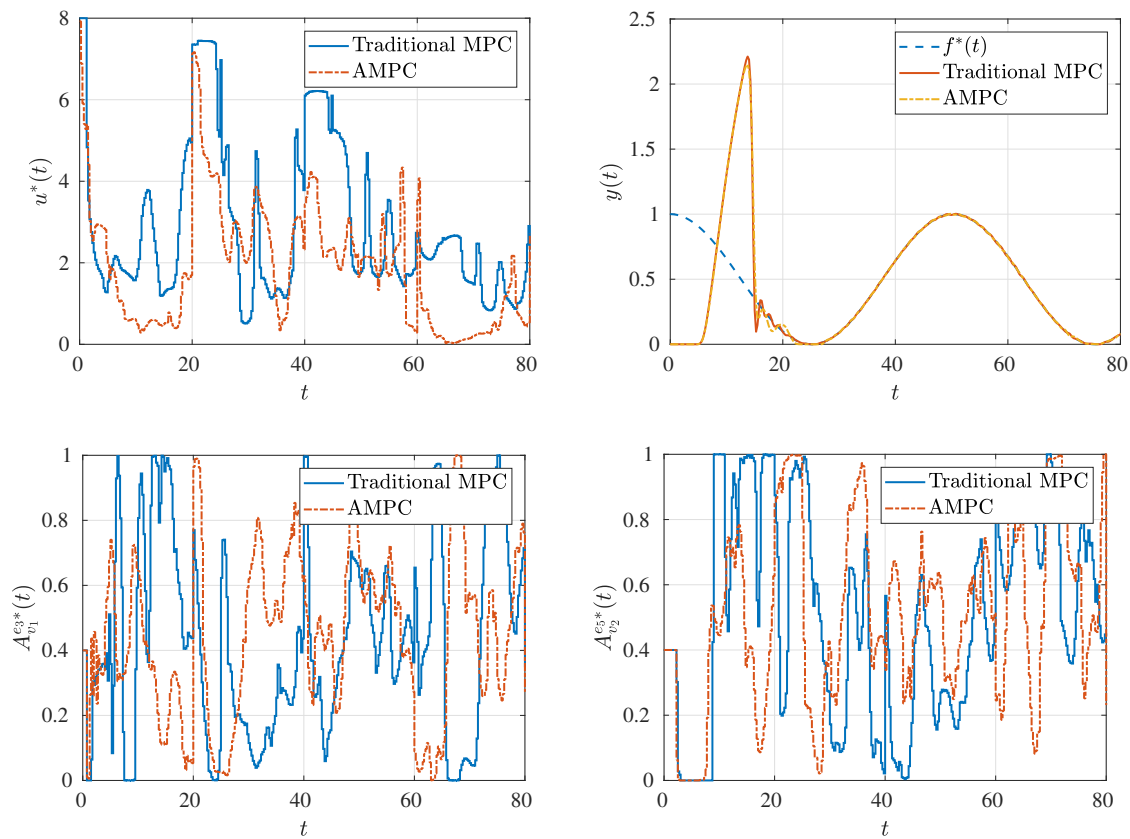
The Fig. 5.5 shows the control variable $u^*(t)$ at the inlet of the arc e_1 and the decision variables $A_{v_1}^*(t)$, $A_{v_2}^*(t)$, $A_{v_3}^*(t)$, and $A_{v_4}^*(t)$ and the outflow $y(t)$ at the outlet of the arc e_7 . The relative computational time is reduced by 72.35% when applying the AMPC compared to the traditional MPC. The outflows $y(t)$ of both approaches are completely converged to the reference trajectory starting from $t = 9$ h. However, the AMPC converges faster than the traditional one where it starts converging to the demand trajectory at $t = 8$ h. When compared to open-loop control, the AMPC results show solvability with impressive convergence to local minima in the context of the disturbance $d(t)$ effect which starts from 10 h and disappeared at 12 h as shown in Fig. 5.6.

Backlog Simulation Results

The system parameters of the complex network are chosen as $\kappa = 0.25$, $M^e = 10$, $\mu^{e_1} = 8$ lots/h, $\mu^{e_2} = 4$ lots/h, $\mu^{e_3} = 5$ lots/h, $\mu^{e_4} = 3.5$ lots/h, $\mu^{e_5} = 4$ lots/h, $\mu^{e_6} = 5$ lots/h, and

$\mu^{e7} = 6$ lots/h. The final time $t_f = 80$ h, $P = 321$, and $C = 80$ where the control horizon is the quarter value of the prediction horizon. For the numerical settings are picked as, $\Delta x = 0.1$ and $CFL = 0.5$ in each arc e , $\Delta t = 0.25$ h.

The final values of the objective functional of both approaches are almost similar. As shown from the Fig. 5.7, the outflows $y(t)$ match the reference after compensating the intractable lots for both approaches. Although $y(t)$ of the traditional MPC converges faster than AMPC, the relative computational time is significantly reduced by 96.26% when applying the AMPC compared to the traditional one. The backlog $B(t)$ in both approaches remains at zero after the compensation of the required lots. In the case of the influence of the disturbance $d(t)$, the AMPC shows satisfactory results to suppress its effect. Subsequently, the open-loop control starts gradually deviating from zero value after the disturbance starts from $t = 35$ h as depicted in Fig. 5.8.



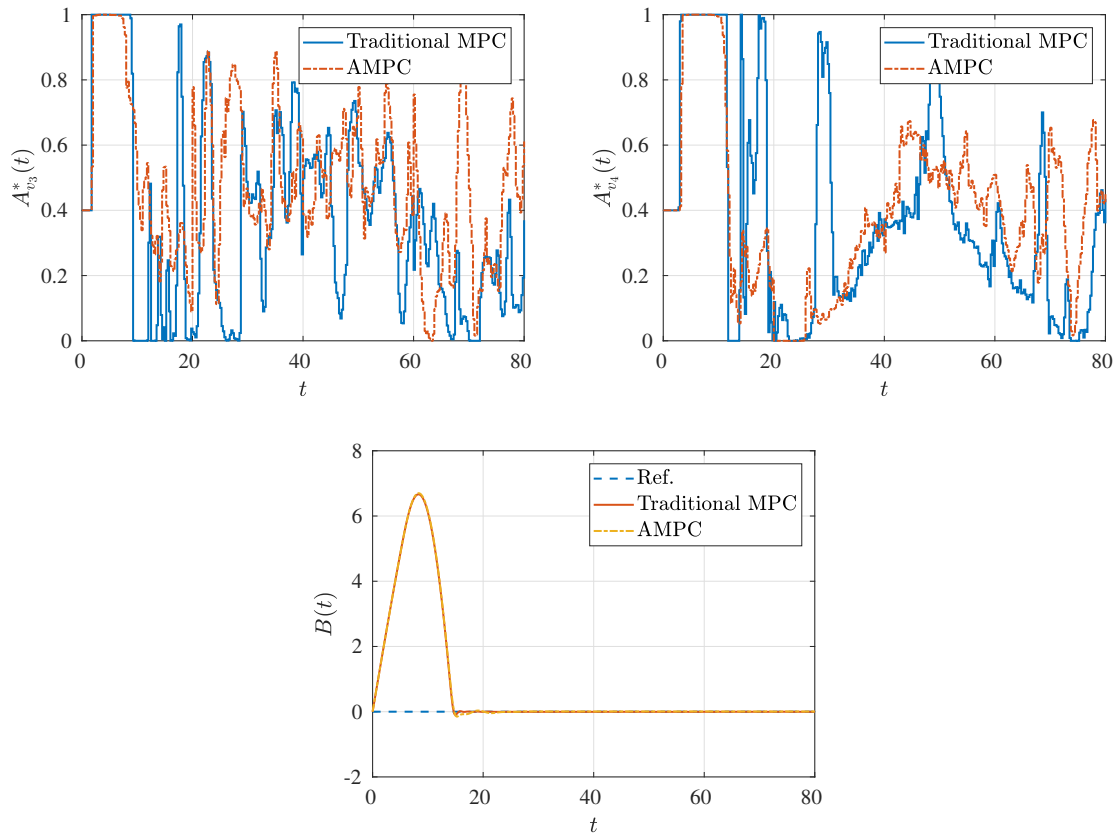


Figure 5.7: The complex network for the backlog problem using MPC.

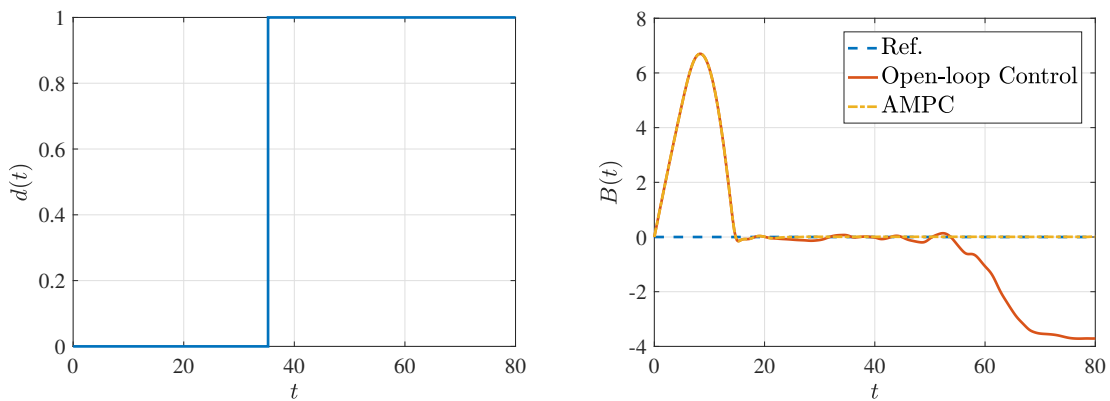


Figure 5.8: The complex network for the backlog problem with disturbance.

5.6 Summary

In this chapter, AMPC was introduced to investigate demand tracking and backlog problems in the context of production systems. By coupling their related PDEs and ODEs, the complex network comprising of arcs and storage spaces has been modelled. The addressed network

includes structures that are dispersing and merging. When choosing the proper control and prediction horizon, the control horizon is picked first to be tuned where it varies between 1 and P . When $C = 1$ is totally feedback control, and $C = P$ is termed open-loop control, it depends on the presence of perturbations. An appropriate selection of the prediction horizon must exceed the system delay. In addition, the performance does not change when selecting a bigger prediction from the required one. This recommended value of the prediction horizon reduces the computational time compared to choosing a larger prediction horizon and is considered the best choice.

The proposed AMPC provides for the solutions of demand tracking and backlog problems. In general, AMPC and traditional MPC attain local minima with close behaviour that leads to steady-state convergence. The performance of the AMPC demonstrates significant reduction in the computational time compared to the traditional MPC. Additionally, the AMPC enables obtaining high accuracy of optimal solutions because it provides a mathematical insight into the structure of the method. Finally, the AMPC is characterized by its robustness in terms of perturbation effects.

Chapter 6

Conclusions and Outlook

This work aims to design boundary control strategies to solve demand tracking and backlog problems for manufacturing systems in terms of conservation laws coupled with ODEs in different network topologies.

In the chapter one, the relevant literature is reviewed to motivate the methods addressed in this thesis. The basis and principles of Little's law and conservation laws are presented in the chapter two. A transformation from a derived discrete event simulation to a continuum limit of conservation law is produced in the microscopic view.

In the chapter three, the proposed PDE model for the single flow line in the manufacturing systems is explored. The dynamic behaviour of the model is studied using ramp-up and ramp-down scenarios. It is also interesting to contrast the manufacturing flow line architecture, which is built up of the M/M/1 PDE model, with setting up a DES in ARENA. The goal is to appropriately describe the transient and steady-state behaviours of a simple manufacturing system which is considered acceptable results for PDE model validation compared to DES. Two alternative topologies are addressed in the context of the manufacturing system network. Conditions for each vertex of the network are defined to design either dispersing or merging networks. It is modelled using a set of both PDEs and ODEs. The influence of the uncontrolled flow evolution across the entire network is demonstrated using arbitrary inflows.

In the chapter four, two different control challenges, demand tracking and backlog are considered in the context of the production system network. The backlog problem is an accumulated error that describes the mismatch between the desired lot accumulation and the total number of lots at the system outlet over a finite time interval that leads to either under- or over-production. The OCPs are investigated in the dispersing and the merging networks. The problems are optimized utilizing open-loop optimal control based on the direct and the indirect approaches. The proposed approaches enable the solution of the OCPs. All of the approaches, in general, reach a local minima with similar behaviour that leads to the steady-state. The

results analysis reveals that each method has its own distinct characteristics. The indirect methodology is characterized by excellent accuracy and minimal processing burden; yet, due to the information necessary to compute the gradient, it is a sensitive method. The ease of use and flexibility to any problem distinguishes the direct method. However, this approach takes substantially longer to achieve a solution when compared to the indirect method.

Finally in the chapter five, AMPC was introduced to investigate demand tracking and backlog problems in the context of the complex network of production systems. The addressed network includes structures that are dispersing and merging. Furthermore, the appropriate way to handle the parameters of the AMPC for both control and prediction horizons is addressed. Moreover, the proposed AMPC provides for the solutions of demand tracking and backlog problems. In general, AMPC and traditional MPC attain local minima with similar behaviour that leads to steady-state convergence. When compared to a typical MPC, the AMPC's performance shows a considerable reduction in computational time. Additionally, because it provides a mathematical insight into the method's structure, the AMPC allows for great accuracy of optimal solutions. Finally, the AMPC is characterized by its robustness according to perturbation effects.

Outlook and Future Work

The study performed for this thesis revealed some concerns and limits that should be applied in future studies. In this section, various proposals for further work are addressed as follows:

- Further investigation and validation are required for generalized PDE models according to G/G/1 processes, where G stands for general distribution or new higher-order PDE models that can completely follow the realistic behaviour of the production systems.
- Explore more complex situations for the production system such as considering that the process rate is controllable and the machines are able to break down.
- Develop suitable control strategies based on the considered PDE models, which comprise a mixture of flatness-based trajectory planning and backstepping-based feedback control for stabilization and tracking control.
- Modifying the optimization algorithms by applying the second-order optimality conditions to get the Hessian, which leads to more accurate results.

Appendix A

Solving the Single Flow PDE Model

The analytical solution of the PDE model is found to be implicit which requires to be solved iteratively. The model can be solved analytically by using the method of characteristics (MOC). The PDE in (3.4) and (3.5) is recalled to get

$$\frac{\partial}{\partial t} \rho^e(x, t) = - \left(\frac{\mu^e M^e}{(M^e + \rho^e(x, t))^2} \right) \frac{\partial}{\partial x} \rho^e(x, t), \quad (\text{A.1a})$$

$$\rho^e(x, 0) = g(x), \quad (\text{A.1b})$$

$$\rho^e(0, t) = \sigma(t), \quad (\text{A.1c})$$

$$0 \leq \sigma(t) \leq \mu^e. \quad (\text{A.1d})$$

The characteristic lines use the parametrization of $x = x(\eta)$, $t = t(\eta)$. Then, the chain rule defines

$$\frac{d\rho^e}{d\eta} = \frac{\partial \rho^e}{\partial t} \frac{dt}{d\eta} + \frac{\partial \rho^e}{\partial x} \frac{dx}{d\eta}, \quad (\text{A.2})$$

by comparing (A.1) to (A.2), $\frac{dt}{d\eta} = 1$, i.e. $dt = d\eta$ and $\frac{dx}{d\eta} = \frac{\mu^e M^e}{(M^e + \rho^e)^2}$. Also, $\frac{d\rho^e}{d\eta} = 0$ which means that the solution of ρ is constant along the characteristic lines. If $x > \frac{\mu^e M^e t}{(M^e + \rho^e)^2}$, the ODE turns into $\frac{dx}{dt} = \frac{\mu^e M^e}{(M^e + \rho^e)^2}$. By integration, it becomes $x_o = x - \frac{\mu^e M^e t}{(M^e + \rho^e)^2}$. While, if $x < \frac{\mu^e M^e t}{(M^e + \rho^e)^2}$, the ODE defines $\frac{dt}{dx} = \frac{(M^e + \rho^e)^2}{\mu^e M^e}$ which gives after integration $t_o = t - \frac{(M^e + \rho^e)^2 x}{\mu^e M^e}$. Substituting x_o and t_o in (A.1b) and (A.1c), respectively, results in

$$\rho^e(x, t) = \begin{cases} g \left(x - \frac{M^e \mu^e t}{(M^e + \rho^e)^2} \right), & x > \frac{M^e \mu^e t}{(M^e + \rho^e)^2} \\ \sigma \left(t - \frac{x(M^e + \rho^e)^2}{M^e \mu^e} \right), & x < \frac{M^e \mu^e t}{(M^e + \rho^e)^2} \end{cases} \quad (\text{A.3})$$

The equation (A.3) is implicit solution which has to be solved numerically for this type of the initial-boundary-value problems (IBVPs).

Appendix B

Derivation of OCPs of a Single Flow Line in the Case of the Indirect Method

B.1 Demand Tracking Problem:

The objective functional of the demand tracking problem is defined as

$$\begin{aligned}
 \min J(u) &= \frac{1}{2} \int_0^{t_f} ((f^*(t) - y(t))^2 dt, \\
 \text{subject to} \\
 \frac{\partial}{\partial t} \rho(x, t) &= -\frac{\partial}{\partial x} f(\rho(x, t)), \\
 f(\rho(x, t)) &= v\rho = \frac{\mu\rho(x, t)}{M + \rho(x, t)}, \\
 \rho(x, 0) &= 0, \quad f(0, t) = u(t), \\
 0 &\leq u(t) < \mu.
 \end{aligned} \tag{B.1}$$

The form of L is obtained as

$$\begin{aligned}
 L &= \frac{1}{2} \int_0^{t_f} ((f^*(t) - y(t))^2 dt \\
 &\quad + \int_0^{t_f} \int_0^1 \lambda(x, t) \left(\frac{\partial \rho}{\partial t} + \frac{\partial}{\partial x} \left(\frac{\mu\rho(x, t)}{M + \rho(x, t)} \right) \right) dx dt.
 \end{aligned}$$

By using the integration by parts one obtains

$$L = \frac{1}{2} \int_0^{t_f} ((f^*(t) - y(t))^2 dt + \int_0^1 \lambda(x, t_f) \rho(x, t_f) dx$$

$$\begin{aligned}
& - \int_0^{t_f} \int_0^1 \frac{\partial \lambda(x, t)}{\partial t} \rho(x, t) dx dt + \int_0^{t_f} \lambda(1, t) \left(\frac{\mu \rho(1, t)}{M + \rho(1, t)} \right) dt \\
& - \int_0^{t_f} \lambda(0, t) \left(\frac{\mu \rho(0, t)}{M + \rho(0, t)} \right) dt - \int_0^{t_f} \int_0^1 \frac{\partial \lambda(x, t)}{\partial x} \left(\frac{\mu \rho(x, t)}{M + \rho(x, t)} \right) dx dt.
\end{aligned}$$

By evaluating the Gateaux derivative of L

$$\begin{aligned}
\delta L &= - \int_0^{t_f} (f^*(t) - y(t)) \delta y(t) dt + \int_0^1 \lambda(x, t_f) \delta \rho(x, t_f) dx \\
& - \int_0^{t_f} \int_0^1 \frac{\partial \lambda(x, t)}{\partial t} \delta \rho(x, t) dx dt + \int_0^{t_f} \lambda(1, t) \delta y(t) dt \\
& - \int_0^{t_f} \lambda(0, t) \delta u dt \\
& - \int_0^{t_f} \int_0^1 \frac{\partial \lambda(x, t)}{\partial x} \left(\frac{\mu M}{(M + \rho(x, t))^2} \right) \delta \rho dx dt \\
& = 0.
\end{aligned}$$

After regrouping, the PDE adjoint equations can be written as

$$\frac{\partial \lambda}{\partial t} = - \left(\frac{\mu M}{(M + \rho(x, t))^2} \right) \frac{\partial \lambda}{\partial x}, \quad (\text{B.2a})$$

$$\lambda(x, t_f) = 0, \quad (\text{B.2b})$$

$$\lambda(1, t) = f^*(t) - y(t), \quad (\text{B.2c})$$

$$\delta_u J(t) = -\lambda(0, t). \quad (\text{B.2d})$$

B.2 Backlog Problem:

The objective functional of the backlog problem is defined as

$$\min J(u) = \frac{1}{2} \int_0^{t_f} (B(t))^2 dt,$$

subject to

$$\frac{\partial}{\partial t} \rho(x, t) = - \frac{\partial}{\partial x} f(\rho(x, t)), \quad (\text{B.3})$$

$$f(\rho(x, t)) = v\rho = \frac{\mu \rho(x, t)}{M + \rho(x, t)},$$

$$\rho(x, 0) = 0, \quad f(0, t) = u(t),$$

$$0 \leq u(t) < \mu.$$

The form of L is obtained as

$$L = \frac{1}{2} \int_0^{t_f} (B(t))^2 dt$$

$$+ \int_0^{t_f} \int_0^1 \lambda(x, t) \left(\frac{\partial \rho}{\partial t} + \frac{\partial}{\partial x} \left(\frac{\mu \rho(x, t)}{M + \rho(x, t)} \right) \right) dx dt.$$

By using the integration by parts one obtains

$$\begin{aligned} L &= \frac{1}{2} \int_0^{t_f} (B(t))^2 dt + \int_0^1 \lambda(x, t_f) \rho(x, t_f) dx \\ &\quad - \int_0^{t_f} \int_0^1 \frac{\partial \lambda(x, t)}{\partial t} \rho(x, t) dx dt + \int_0^{t_f} \lambda(1, t) \left(\frac{\mu \rho(1, t)}{M + \rho(1, t)} \right) dt \\ &\quad - \int_0^{t_f} \lambda(0, t) \left(\frac{\mu \rho(0, t)}{M + \rho(0, t)} \right) dt - \int_0^{t_f} \int_0^1 \frac{\partial \lambda(x, t)}{\partial x} \left(\frac{\mu \rho(x, t)}{M + \rho(x, t)} \right) dx dt. \end{aligned}$$

By evaluating the Gateaux derivative of L

$$\begin{aligned} \delta L &= - \int_0^{t_f} B(t) \int_0^t \delta y(c) dc dt + \int_0^1 \lambda(x, t_f) \delta \rho(x, t_f) dx \\ &\quad - \int_0^{t_f} \int_0^1 \frac{\partial \lambda(x, t)}{\partial t} \delta \rho(x, t) dx dt + \int_0^{t_f} \lambda(1, t) \delta y(t) dt \\ &\quad - \int_0^{t_f} \lambda(0, t) \delta u dt \\ &\quad - \int_0^{t_f} \int_0^1 \frac{\partial \lambda(x, t)}{\partial x} \left(\frac{\mu M}{(M + \rho(x, t))^2} \right) \delta \rho dx dt \\ &= 0. \end{aligned}$$

By substituting

$$\begin{aligned} \delta y(t) &= \delta_d(t - \gamma), \quad \gamma \in (0, t_f), \\ \delta y(c) &= \delta_d(c - \gamma). \end{aligned}$$

$$\begin{aligned} \delta L &= - \int_0^{t_f} B(r) \int_0^r \delta_d(c - \gamma) dc dr + \int_0^1 \lambda(x, t_f) \delta \rho(x, t_f) dx \\ &\quad - \int_0^{t_f} \int_0^1 \frac{\partial \lambda(x, t)}{\partial t} \delta \rho(x, t) dx dt + \int_0^{t_f} \lambda(1, t) \delta_d(t - \gamma) dt \\ &\quad - \int_0^{t_f} \lambda(0, t) \delta u dt \\ &\quad - \int_0^{t_f} \int_0^1 \frac{\partial \lambda(x, t)}{\partial x} \left(\frac{\mu M}{(M + \rho(x, t))^2} \right) \delta \rho dx dt \\ &= 0. \end{aligned}$$

From the shifting property of the delta function δ_d

$$\lambda(1, \gamma) = \int_0^{t_f} \lambda(1, t) \delta_d(t - \gamma) dt,$$

$$\int_{\gamma}^{t_f} B(r)dr = \int_0^{t_f} B(r) \int_0^r \delta_d(c - \gamma)dcdr.$$

Since $\gamma \in (0, t_f)$ is any value in the domain t therefore after regrouping, the PDE adjoint equations can be written as

$$\frac{\partial \lambda}{\partial t} = - \left(\frac{\mu M}{(M + \rho(x, t))^2} \right) \frac{\partial \lambda}{\partial x}, \quad (\text{B.4a})$$

$$\lambda(x, t_f) = 0, \quad (\text{B.4b})$$

$$\lambda(1, t) = \int_t^{t_f} B(r)dr, \quad (\text{B.4c})$$

$$\delta_u J(t) = -\lambda(0, t). \quad (\text{B.4d})$$

Appendix C

Derivation of Distribution Models

This appendix aims to generate a PDE model for a G/G/1 process in a manufacturing flow line. Herein, G/G/1 refers to a general distribution for inter-arrival and processing times. Based on queuing theory, the mean waiting time WT_q for a single workstation is computed according to the coefficient of variation in G/G/1, which is known as Kingman's formula [54]

$$WT_q = \left(\frac{C_a^2 + C_p^2}{2} \right) \left(\frac{\Gamma}{1 - \Gamma} \right) T_p. \quad (\text{C.1})$$

Herein, the parameters $C_p = \frac{\sigma}{T_p}$ and $C_a = \frac{\sigma}{T_a}$ are the coefficient of variation for process time and inter-arrival time, respectively. Besides, σ is the standard deviation of the distribution, T_a is the mean inter-arrival time, T_p is the mean process time and the utilization is denoted by $\Gamma = \frac{u}{\mu}$. In the case of the M/M/1 PDE model for the manufacturing flow line, the coefficient of variations C_p and C_a are equal to one. The mean flow time in steady-state φ is the mean waiting time of the queue and the mean process time in a single workstation

$$\varphi = \left(\frac{C_a^2 + C_p^2}{2} \right) \left(\frac{\Gamma}{1 - \Gamma} \right) T_p + T_p, \quad (\text{C.2a})$$

$$C_d^2 = (1 - \Gamma^2)C_a^2 + \Gamma^2 C_p^2, \quad (\text{C.2b})$$

where C_d is the approximate coefficient of variation of inter-departure by Kuehn's coupling equation [59]. When the load is heavy ($\Gamma \approx 1$), C_d^2 is approximately equal to C_p^2 . When the load is light ($\Gamma \approx 0$), C_d^2 is approximately equal to C_a^2 .

In case of a serial production flow line, workstations are more than one, this parameter is equal to the squared coefficient of variation of inter-arrival time for the next workstation i.e., $C_{a,k+1}^2 = C_{d,k}^2$. For the sake of simplicity, these workstations are assumed to be identical and there is no change in the coefficient of variation of processing time C_p^2 . Thus, the overall coefficient of variations can be stated as follows

$$TC_a = \sum_{k=1}^M C_{a,k}^2, \quad (\text{C.3a})$$

$$TC_p = \sum_{k=1}^M C_{p,k}^2, \quad (\text{C.3b})$$

herein, TC_a and TC_p are the total squared coefficient of variations of both inter-arrival times and processing times respectively.

C.1 M/D/1 Model

In the case of the M/D/1, $TC_p = 0$ and C_a is computed recursively by

$$C_{a,k+1} = \begin{cases} 1, & \text{if } k = 0. \\ \prod_{k=1}^M (1 - \Gamma^2)^{2^{k-1}}, & \text{otherwise.} \end{cases}$$

The total coefficient of variation of the inter-arrival times TC_a is obtained from (C.3) and the flow time becomes

$$\begin{aligned} \varphi &= \left(\frac{TC_a}{2M} \right) \left(\frac{Mf}{\mu - f} \right) T_p + MT_p \\ &= \frac{TC_a \rho}{2\mu M} + \frac{M}{\mu} \\ &= \frac{TC_a \rho + 2M^2}{2\mu M}, \end{aligned}$$

where, the inverse of the process time T_p is the process rate μ . Since the inverse of the flow time is the velocity, then the velocity reads

$$v = \frac{2\mu M}{TC_a \rho + 2M^2},$$

from the adiabatic equation $f = \rho v$, the flow gets

$$f = \rho \left(\frac{2\mu M}{TC_a \rho + 2M^2} \right),$$

after separating ρ from the equation, we obtain

$$\rho = \frac{2M^2 f}{2\mu M - TC_a f},$$

and the partial derivative of ρ with respect to time be

$$\frac{\partial \rho}{\partial t} = \left(\frac{4\mu M^3}{(2\mu M - TC_a f)^2} \right) \frac{\partial f}{\partial t},$$

form the conservation of mass

$$\frac{\partial}{\partial t}\rho(x, t) + \frac{\partial}{\partial x}f(x, t) = 0,$$

the general form of M/D/1 is obtained by

$$\frac{\partial}{\partial t}f(x, t) = -\left(\frac{(2\mu M - TC_a^2 f(x, t))^2}{4\mu M^3}\right) \frac{\partial}{\partial x}f(x, t), \quad (\text{C.5a})$$

$$f_{IC}(x, 0) = g(x), \quad (\text{C.5b})$$

$$f_{BC}(0, t) = u(t). \quad (\text{C.5c})$$

C.2 G/G/1 Model

By considering the parameter $C = \frac{TC_a + TC_p}{2}$ herein, TC_p and TC_a are obtained from (C.3) and the flow time becomes

$$\begin{aligned} \varphi &= \left(\frac{C}{M\mu}\right) \left(\frac{Mf}{\mu - f}\right) + \frac{M}{\mu} \\ &= \frac{C\rho}{\mu M} + \frac{M}{\mu} \\ &= \frac{C\rho + M^2}{\mu M}, \end{aligned}$$

and the velocity reads

$$v = \frac{\mu M}{C\rho + M^2},$$

from the adiabatic equation $f = \rho v$, the flow gets

$$f = \frac{\mu M \rho}{C\rho + M^2},$$

after separating ρ from the equation, we obtain

$$\rho = \frac{M^2 f}{\mu M - C f},$$

and the partial derivative of ρ with respect to time be

$$\frac{\partial \rho}{\partial t} = \left(\frac{\mu M^3}{(\mu M - C f)^2}\right) \frac{\partial f}{\partial t},$$

form the conservation of mass

$$\frac{\partial}{\partial t}\rho(x, t) + \frac{\partial}{\partial x}f(x, t) = 0,$$

and the general form becomes

$$\frac{\partial}{\partial t} f(x, t) = - \left(\frac{(\mu M - C f(x, t))^2}{\mu M^3} \right) \frac{\partial}{\partial x} f(x, t), \quad (\text{C.7a})$$

$$f_{IC}(x, 0) = g(x), \quad (\text{C.7b})$$

$$f_{BC}(0, t) = u(t). \quad (\text{C.7c})$$

Remark C.1. For the cross-check, if C in $G/G/1$ equals $M/D/1$ then $C = \frac{TC_a}{2}$ and the model in (C.7) is converted to $M/D/1$ model in (C.5).

Bibliography

1. Aamo, O. M. and Krstic, M. (2003). *Flow control by feedback: stabilization and mixing*. Springer Science & Business Media.
2. Altioik, T. and Melamed, B. (2010). *Simulation modeling and analysis with Arena*. Elsevier.
3. Ambrosino, G. and Albanese, R. (2005). Magnetic control of plasma current, position, and shape in tokamaks: a survey or modeling and control approaches. *IEEE Control Systems Magazine*, 25(5):76–92.
4. Armbruster, D., Degond, P., and Ringhofer, C. (2006a). A model for the dynamics of large queuing networks and supply chains. *SIAM Journal on Applied Mathematics*, 66(3):896–920.
5. Armbruster, D., Marthaler, D., and Ringhofer, C. (2002). Efficient simulations of supply chains. In *Proceedings of the winter simulation conference*, volume 2, pages 1345–1348. IEEE.
6. Armbruster, D., Marthaler, D. E., Ringhofer, C., Kempf, K., and Jo, T.-C. (2006b). A continuum model for a re-entrant factory. *Operations research*, 54(5):933–950.
7. Baehr, H. D. and Stephan, K. (2011). *Heat and mass transfer*. Springer Science & Business Media.
8. Balas, M. J. (1978). Active control of flexible systems. *Journal of Optimization theory and Applications*, 25(3):415–436.
9. Ballard, G. and Howell, G. (1998). Shielding production: essential step in production control. *Journal of Construction Engineering and management*, 124(1):11–17.
10. Ballard, H. G. (2000). *The last planner system of production control*. PhD thesis, University of Birmingham.
11. Banks, H. T., Smith, R. C., and Wang, Y. (1996). Smart material structures- modeling, estimation and control. *Chichester, United Kingdom and New York/Paris: John Wiley & Sons/Masson, 1996*.
12. Baumgärtner, V., Göttlich, S., and Knapp, S. (2020). Feedback stabilization for a coupled PDE-ODE production system. *Mathematical Control & Related Fields*, 10(2):405.
13. Bewley, T. R. (2001). Flow control: new challenges for a new renaissance. *Progress in Aerospace sciences*, 37(1):21–58.
14. Boyd, S., Boyd, S. P., and Vandenberghe, L. (2004). *Convex optimization*. Cambridge university press.

15. Bozdağ, C. E., Kahraman, C., and Ruan, D. (2003). Fuzzy group decision making for selection among computer integrated manufacturing systems. *Computers in Industry*, 51(1):13–29.
16. Bozza, A., Cavone, G., Carli, R., Mazzoccoli, L., and Dotoli, M. (2021). An mpc-based approach for the feedback control of the cold sheet metal forming process. In *2021 IEEE 17th International Conference on Automation Science and Engineering (CASE)*, pages 286–291. IEEE.
17. Brauer, F. and Nohel, J. A. (1989). *The qualitative theory of ordinary differential equations: an introduction*. Courier Corporation.
18. Bressan, A. (2000). *Hyperbolic systems of conservation laws: the one-dimensional Cauchy problem*, volume 20. Oxford University Press on Demand.
19. Bressan, A., Crasta, G., and Piccoli, B. (2000). *Well-posedness of the Cauchy problem for $n \times n$ systems of conservation laws*, volume 694. American Mathematical Soc.
20. Chew, S. F. and Lawley, M. A. (2006). Robust supervisory control for production systems with multiple resource failures. *IEEE Transactions on Automation Science and Engineering*, 3(3):309–323.
21. Colledani, M., Tolio, T., Fischer, A., Iung, B., Lanza, G., Schmitt, R., and Váncza, J. (2014). Design and management of manufacturing systems for production quality. *Cirp Annals*, 63(2):773–796.
22. Cooper, R. B. (1981). Queueing theory. In *Proceedings of the ACM’81 conference*, pages 119–122.
23. Coron, J. M., Kawski, M., and Wang, Z. (2010). Analysis of a conservation law modeling a highly re-entrant manufacturing system. *Discrete and Continuous Dynamical Systems-Series B*, 14(4):1337–1359.
24. Dafermos, C. M. (2005). *Hyperbolic conservation laws in continuum physics*, volume 3. Springer.
25. d’Apice, C., Gottlich, S., Herty, M., and Piccoli, B. (2010). *Modeling, simulation, and optimization of supply chains: a continuous approach*, volume 121. SIAM.
26. D’Apice, C., Kogut, P. I., and Manzo, R. (2014). On relaxation of state constrained optimal control problem for a PDE-ODE model of supply chains. *Networks & Heterogeneous Media*, 9(3):501.
27. Davidrajuh, R. (2018). *Modeling discrete-event systems with gpensim: An introduction*. Springer.
28. Deif, A. M. (2011). A system model for green manufacturing. *Journal of Cleaner Production*, 19(14):1553–1559.
29. Dmitruk, A. V. and Kaganovich, A. (2011). Maximum principle for optimal control problems with intermediate constraints. *Computational Mathematics and Modeling*, 22(2):180–215.
30. Dong, M. and He, F. (2012). A new continuous model for multiple re-entrant manufacturing systems. *European journal of operational research*, 223(3):659–668.

31. Ekaputri, C. and Syaichu-Rohman, A. (2013). Model predictive control (mpc) design and implementation using algorithm-3 on board spartan 6 fpga sp605 evaluation kit. In *2013 3rd International Conference on Instrumentation Control and Automation (ICA)*, pages 115–120. IEEE.
32. Ferrari, S., Foderaro, G., Zhu, P., and Wettergren, T. A. (2016). Distributed optimal control of multiscale dynamical systems: a tutorial. *IEEE Control Systems Magazine*, 36(2):102–116.
33. Fishwick, P. A. (2007). *Handbook of dynamic system modeling*. CRC Press.
34. Freitag, M. and Hildebrandt, T. (2016). Automatic design of scheduling rules for complex manufacturing systems by multi-objective simulation-based optimization. *CIRP annals*, 65(1):433–436.
35. González-Gaxiola, O. (2009). A note on the derivation of fréchet and gâteaux. *Applied Mathematical Sciences*, 3(19):941–947.
36. Göttlich, S., Herty, M., Klar, A., et al. (2006). Modelling and optimization of supply chains on complex networks. *Communications in Mathematical Sciences*, 4(2):315–330.
37. Gray, M. A. (2007). Discrete event simulation: A review of simevents. *Computing in Science & Engineering*, 9(6):62–66.
38. Grigoriev, S., Sinopalnikov, V., Tereshin, M., and Gurin, V. (2012). Control of parameters of the cutting process on the basis of diagnostics of the machine tool and workpiece. *Measurement techniques*, 55(5):555–558.
39. Grüne, L. (2009). Analysis and design of unconstrained nonlinear mpc schemes for finite and infinite dimensional systems. *SIAM Journal on Control and Optimization*, 48(2):1206–1228.
40. Gu, W. and Wang, C.-Y. (2000). Thermal-electrochemical modeling of battery systems. *Journal of The Electrochemical Society*, 147(8):2910.
41. Gustavsson, M. and Wänström, C. (2009). Assessing information quality in manufacturing planning and control processes. *International Journal of Quality & Reliability Management*.
42. He, F., Armbruster, D., Herty, M., and Dong, M. (2015). Feedback control for priority rules in re-entrant semiconductor manufacturing. *Applied Mathematical Modelling*, 39(16):4655–4664.
43. Helbing, D. (2001). Traffic and related self-driven many-particle systems. *Reviews of modern physics*, 73(4):1067.
44. Herty, M., Michailidis, L., and Ziegler, M. (2015). Kinetic part-feeding models for assembly lines in automotive industries. *Mathematical Models and Methods in Applied Sciences*, 25(02):283–308.
45. Herty, M. and Ringhofer, C. (2011). Feedback controls for continuous priority models in supply chain management. *Computational Methods in Applied Mathematics Comput. Methods Appl. Math.*, 11(2):206–213.
46. Hillen, T. and Hadeler, K. (2005). Hyperbolic systems and transport equations in mathematical biology. In *Analysis and numerics for conservation laws*, pages 257–279. Springer.

47. Hittle, B. and Leonard, K. M. (2011). Decision making in advance of a supply chain crisis. *Management Decision*.
48. Holden, H. and Risebro, N. H. (2015). *Front tracking for hyperbolic conservation laws*, volume 152. Springer.
49. Hopp, W. J. and Spearman, M. L. (2011). *Factory physics*. Waveland Press.
50. Ito, K. and Kunisch, K. (2006). Reduced order control based on approximate inertial manifolds. *Linear Algebra and its Applications*, 415(2-3):531–541.
51. Ivanov, D. (2021). Supply chain viability and the covid-19 pandemic: A conceptual and formal generalisation of four major adaptation strategies. *International Journal of Production Research*, 59(12):3535–3552.
52. Jakobsen, H. (2008). *Chemical reactor modeling: Multiphase reactive flows*, springer.
53. King, R., Seibold, M., Lehmann, O., Noack, B., Morzyński, M., Tadmor, G., et al. (2005). Non-linear flow control based on a low dimensional model of fluid flow. In *Control and Observer Design for Nonlinear Finite and Infinite Dimensional Systems*, pages 369–386. Springer.
54. Kingman, J. (1961). The single server queue in heavy traffic. In *Mathematical Proceedings of the Cambridge Philosophical Society*, volume 57, pages 902–904. Cambridge University Press.
55. Kirchner, C., Herty, M., Göttlich, S., and Klar, A. (2006). Optimal control for continuous supply network models. *NHM*, 1(4):675–688.
56. Koga, S., Krstic, M., and Beaman, J. (2020). Laser sintering control for metal additive manufacturing by pde backstepping. *IEEE Transactions on Control Systems Technology*, 28(5):1928–1939.
57. Kreyszig, E. (1991). *Introductory functional analysis with applications*, volume 17. John Wiley & Sons.
58. Krstic, M., Guo, B.-Z., Balogh, A., and Smyshlyaev, A. (2008). Output-feedback stabilization of an unstable wave equation. *Automatica*, 44(1):63–74.
59. Kuehn, P. (1979). Approximate analysis of general queuing networks by decomposition. *IEEE Transactions on communications*, 27(1):113–126.
60. La Marca, M., Armbruster, D., Herty, M., and Ringhofer, C. (2010). Control of continuum models of production systems. *IEEE Transactions on Automatic Control*, 55(11):2511–2526.
61. Lauzon, S., Ma, A., Mills, J., and Benhabib, B. (1996). Application of discrete-event-system theory to flexible manufacturing. *IEEE Control Systems Magazine*, 16(1):41–48.
62. Law, A. M. (2019). How to build valid and credible simulation models. In *2019 Winter Simulation Conference (WSC)*, pages 1402–1414. IEEE.
63. Li, X. and Yong, J. (2012). *Optimal control theory for infinite dimensional systems*. Springer Science & Business Media.

64. Lighthill, M. J. and Whitham, G. B. (1955). On kinematic waves. ii. a theory of traffic flow on long crowded roads. In *Proceedings of the Royal Society of London A: Mathematical, Physical and Engineering Sciences*, volume 229, pages 317–345. The Royal Society.
65. Little, J. D. (1961). A proof for the queuing formula: $L = \lambda w$. *Operations research*, 9(3):383–387.
66. Liu, Z. and Zheng, S. (1999). *Semigroups associated with dissipative systems*, volume 398. CRC Press.
67. Loganathan, M. and Gandhi, O. (2016). Maintenance cost minimization of manufacturing systems using pso under reliability constraint. *International Journal of System Assurance Engineering and Management*, 7(1):47–61.
68. Luo, B. and Wu, H.-N. (2012). Approximate optimal control design for nonlinear one-dimensional parabolic pde systems using empirical eigenfunctions and neural network. *IEEE Transactions on Systems, Man, and Cybernetics, Part B (Cybernetics)*, 42(6):1538–1549.
69. Luo, B., Wu, H.-N., and Li, H.-X. (2014). Adaptive optimal control of highly dissipative nonlinear spatially distributed processes with neuro-dynamic programming. *IEEE transactions on neural networks and learning systems*, 26(4):684–696.
70. Luo, Z.-H., Guo, B.-Z., and Morgül, Ö. (2012). *Stability and stabilization of infinite dimensional systems with applications*. Springer Science & Business Media.
71. Manassero, G., Semeraro, Q., and Tolio, T. (2004). A new method to cope with decision makers' uncertainty in the equipment selection process. *CIRP Annals*, 53(1):389–392.
72. Meirovitch, L. (1991). *Dynamics and control of structures*. John Wiley & Sons.
73. Meurer, T. (2012). *Control of higher-dimensional PDEs: Flatness and backstepping designs*. Springer Science & Business Media.
74. Meurer, T. (2017). Some perspectives in pde control. In *Proc. 20th IFAC World Congress*, pages 09–14.
75. Meurer, T. and Kugi, A. (2009). Tracking control for boundary controlled parabolic pdes with varying parameters: Combining backstepping and differential flatness. *Automatica*, 45(5):1182–1194.
76. Meurer, T., Thull, D., and Kugi, A. (2008). Flatness-based tracking control of a piezoactuated euler-bernoulli beam with non-collocated output feedback: theory and experiments. *International Journal of Control*, 81(3):475–493.
77. Meurer, T. and Zeitz, M. (2005). Feedforward and feedback tracking control of nonlinear diffusion-convection- reaction systems using summability methods. *Industrial & engineering chemistry research*, 44(8):2532–2548.
78. Newell, G. F. (1993). A simplified theory of kinematic waves in highway traffic, part ii: Queueing at freeway bottlenecks. *Transportation Research Part B: Methodological*, 27(4).

79. Othman, K. A. and Gomma, H. W. (2011). Reducing the bullwhip effect in supply chains using genetic algorithm and control engineering. In *2011 IEEE International Conference on Systems, Man, and Cybernetics*, pages 440–445. IEEE.
80. Othman, K. A. and Meurer, T. (2020). Demand tracking control in manufacturing systems. *IFAC-PapersOnLine*, 53(2):11219–11224.
81. Othman, K. A. and Meurer, T. (2022). Optimal boundary control for the backlog problem in production systems. In *Proceedings of the 10th Vienna International Conference on Mathematical Modelling Vienna, Austria, July 27-29*, pages 591–596. IFAC.
82. Panayiotou, C. and Cassandras, C. G. (2006). Infinitesimal perturbation analysis and optimization for make-to-stock manufacturing systems based on stochastic fluid models. *Discrete Event Dynamic Systems*, 16(1):109–142.
83. Panayiotou, C. G., Cassandras, C. G., and Zhang, P. (2002). On-line inventory cost minimization for make-to-stock manufacturing systems. In *Proceedings of the 2002 American Control Conference (IEEE Cat. No. CH37301)*, volume 6, pages 4469–4474. IEEE.
84. Papadopoulos, H. and Heavey, C. (1996). Queueing theory in manufacturing systems analysis and design: A classification of models for production and transfer lines. *European Journal of Operational Research*, 92(1):1–27.
85. Potočník, P. and Grabec, I. (2002). Nonlinear model predictive control of a cutting process. *Neurocomputing*, 43(1-4):107–126.
86. Preumont, A. (2018). *Vibration control of active structures: an introduction*, volume 246. Springer.
87. Rashidinejad, A., Reniers, M., and Fabian, M. (2019). Supervisory control of discrete-event systems in an asynchronous setting. In *2019 IEEE 15th International Conference on Automation Science and Engineering (CASE)*, pages 494–501. IEEE.
88. Richards, P. I. (1956). Shock waves on the highway. *Operations Research*, 4(1):42–51.
89. Rockwell Automation, Inc. (2005). Arena simulation. See <http://www.arenasimulation.com>.
90. Rosseel, E. and Wells, G. N. (2012). Optimal control with stochastic pde constraints and uncertain controls. *Computer Methods in Applied Mechanics and Engineering*, 213:152–167.
91. Rossetti, M. D. (2015). *Simulation modeling and Arena*. John Wiley & Sons.
92. Shang, H., Forbes, J. F., and Guay, M. (2004). Model predictive control for quasilinear hyperbolic distributed parameter systems. *Industrial & engineering chemistry research*, 43(9):2140–2149.
93. Shaw, J. (2004). *Mathematical principles of optical fiber communications*. SIAM.
94. Singler, J. R. and Batten, B. A. (2009). A proper orthogonal decomposition approach to approximate balanced truncation of infinite dimensional linear systems. *International Journal of Computer Mathematics*, 86(2):355–371.

95. Stanewsky, E. (2001). Adaptive wing and flow control technology. *Progress in Aerospace Sciences*, 37(7):583–667.
96. Summers, S. and Bewley, T. R. (2007). Mpdopt: A versatile toolbox for adjoint-based model predictive control of smooth and switched nonlinear dynamic systems. In *2007 46th IEEE Conference on Decision and Control*, pages 4785–4790. IEEE.
97. Sundmacher, K., Kienle, A., Pesch, H. J., Berndt, J. F., and Huppmann, G. (2007). *Molten carbonate fuel cells*. Wiley Online Library.
98. Taylor, T. (1997). Physics of advanced tokamaks. *Plasma Physics and Controlled Fusion*, 39(12B):B47.
99. Tröltzsch, F. (2010). *Optimal control of partial differential equations: theory, methods, and applications*, volume 112. American Mathematical Soc.
100. Tucsnak, M. and Weiss, G. (2009). *Observation and control for operator semigroups*. Springer Science & Business Media.
101. Unger, A. and Tröltzsch, F. (2001). Fast solution of optimal control problems in the selective cooling of steel. *ZAMM-Journal of Applied Mathematics and Mechanics/Zeitschrift für Angewandte Mathematik und Mechanik: Applied Mathematics and Mechanics*, 81(7):447–456.
102. Unver, A. K., Ringhofer, C., and KOKSAL, M. (2016). Parameter extraction of complex production systems via a kinetic approach. *Kinetic & Related Models*, 9(2).
103. Vali, M., Petrović, V., Boersma, S., van Wingerden, J.-W., and Kühn, M. (2017). Adjoint-based model predictive control of wind farms: Beyond the quasi steady-state power maximization. *IFAC-PapersOnLine*, 50(1):4510–4515.
104. Van Beek, D. and Rooda, J. (2000). Languages and applications in hybrid modelling and simulation: Positioning of chi. *Control Engineering Practice*, 8(1):81–91.
105. Van Beek, D. A. and Rooda, J. (1997). Design of discrete controllers for continuous systems using hybrid chi. *IFAC Proceedings Volumes*, 30(4):21–26.
106. van den Berg, R., Lefeber, E., and Rooda, K. (2008). Modeling and control of a manufacturing flow line using partial differential equations. *IEEE Transactions on Control Systems Technology*, 16(1):130–136.
107. Velasco Acosta, A. P., Mascle, C., and Baptiste, P. (2020). Applicability of demand-driven mrp in a complex manufacturing environment. *International Journal of Production Research*, 58(14):4233–4245.
108. Xia, C., Pan, Z., Zhang, S., Polden, J., Wang, L., Li, H., Xu, Y., and Chen, S. (2020). Model predictive control of layer width in wire arc additive manufacturing. *Journal of Manufacturing Processes*, 58:179–186.

109. Xu, C.-Z. and Sallet, G. (1996). On spectrum and riesz basis assignment of infinite-dimensional linear systems by bounded linear feedbacks. *SIAM journal on control and optimization*, 34(2):521–541.
110. Zhao, Z.-Y., Tomizuka, M., and Isaka, S. (1993). Fuzzy gain scheduling of pid controllers. *IEEE transactions on systems, man, and cybernetics*, 23(5):1392–1398.